NOV 9 - 1932

U. S. DEPARTMENT OF COMMERCE

BUREAU OF STANDARDS JOURNAL OF RESEARCH

Vol. 9 JULY, 1932 No. 1

CONTENTS

RP. No.	TITLE AND AUTHOR	Page
453.	The use of α-benzoinoxime in the determination of molybdenum. H. B. Knowles	1
454.	Effect of zinc coatings on the endurance properties of steel. W. H. Swanger and R. D. France	9
455.	Power input and dissipation in the positive column of cæsium discharge. F. L. Mohler	25
456.	Thermal expansion of some silicates of elements in Group II of the periodic system. R. F. Geller and Herbert Insley	35
457.	An automatic reverberation meter for the measurement of sound absorption. W. F. Snyder	47
458.	Note on the probable presence of 2,2-dimethylpentane in a mid-continent petroleum. Johannes H. Bruun and Mildred M. Hicks-Bruun	53
459.	Notes on the orifice meter: The expansion factor for gases. Edgar Buckingham	61
460.	Theory of voltage dividers and their use with cathode ray oscillographs. Melville M. Peters, George F. Blackburn, and Paul T. Hannen	81

BUREAU OF STANDARDS JOURNAL OF RESEARCH

CONTENTS OF RECENT NUMBERS

January, 1932 (Vol. 8, No. 1)

RP396. The preparation of crystalline methyl-*d*-gulosides by means of coordination compounds with calcium chloride. Horace S. Isbell. Price, 5 cents.

RP397. International comparison of X-ray standards. Lauriston S. Taylor. Price, 10 cents.

RP398. Volumetric determination of pentoses and pentosans. G. M. Kline and S. F. Acree. Price, 5 cents.

RP399. A method for determining the volume changes occurring in metals during casting. C. M. Saeger, jr., and Eugene J. Ash. Price, 10 cents.

RP400. Registration of cathode rays by thin films of metals and metal compounds. Warren W. Nicholas and C. G. Malmberg. Price, 5 cents.

RP401. Effect of casting temperature and of additions of iron on bearing bronze (Cu 80 : Sn 10 : Pb 10). C. E. Eggenschwiler.

RP402. Ultrasonic measurements of the compressibility of solutions and of solid particles in suspension. Chester R. Randall. Price, 10 cents.

RP403. On elimination of liquid potentials with potassium chloride and ammonium chloride. G. M. Kline, M. R. Meacham, and S. F. Acree. Price, 5 cents.

RP404. An electrostatic voltmeter. Warren W. Nicholas. Price, 5 cents.

RP405. The heats of combustion of methyl and ethyl alcohols. Frederick D. Rossini. Price, 10 cents.

RP406. A clock-controlled constant-frequency generator. A. B. Lewis. Price, 10 cents.

February, 1932 (Vol. 8, No. 2)

RP407. Deteriorative effect of sulphur dioxide upon paper in an atmosphere of constant humidity and temperature. Arthur E. Kimberly.

RP408. Tensile properties of rail steels at elevated temperatures. G. Willard Quick. Price, 5 cents.

RP409. The resistance to impact of rail steels at elevated temperatures. G. Willard Quick.

RP410. Kaolins; effect of firing temperature on some of their physical properties. R. A. Heindl, W. L. Pendergast, and L. E. Mong. Price, 5 cents.

RP411. Composite-coil electrodynamic instruments. F. B. Silsbee. Price, 10 cents.

RP412. Some studies of radio transmission over long paths made on the Byrd Antarctic expedition. L. V. Berkner. Price, 10 cents.

RP413. Phase equilibra in the system SiO_2-ZnO-Al_2O_3. E. N. Bunting. Price, 5 cents.

RP414. System CaO-Na_2O-Al_2O_3. L. T. Brownmiller and R. H. Bogue. Price, 5 cents.

RP415. Determination of tin in iron and steels. J. A. Scherrer. Price, 5 cents.

March, 1932 (Vol. 8, No. 3)

RP416. Heat of vaporization of water at 50°, 70°, and 90° C. E. F. Fiock and D. C. Ginnings.

RP417. Note on international comparison of X-ray standards. Lauriston S. Taylor.

RP418. The course of the oxidation of the aldose sugars by bromine water. H. S. Isbell and C. S. Hudson.

RP419. Fluctuations of the rate of emissions of α particles for weak sources and large solid angles. L. F. Curtiss.

RP420. Gases obtained from commercial feldspars heated in vacuo. G. R. Shelton and H. H. Holscher.

RP421. Experiments on the emission and absorption of radiation by metallic silver. F. L. Mohler.

RP422. Accelerated weathering tests of soldered and tinned sheet copper. Peter R. Kosting.

RP423. The chromium oxide and the vanadium oxide band spectra. W. F. C. Ferguson.

RP424. Air density corrections for X-ray ionization chambers. Lauriston S. Taylor and George Singer.

RP425. The arc spectrum of phosphorus. C. C. Kiess.

RP426. Some physical properties of levulose and its estimation by copper reduction methods. Richard F. Jackson and Joseph A. Mathews.

Research papers, where price is given, are already available, and others will be available in the near future as separates for purchase from the Superintendent of Documents, United States Government Printing Office, Washington, D. C.

U. S. DEPARTMENT OF COMMERCE
R. P. LAMONT, Secretary
BUREAU OF STANDARDS
GEORGE K. BURGESS, Director

BUREAU OF STANDARDS JOURNAL OF RESEARCH

July, 1932
Vol. 9, No. 1

UNITED STATES
GOVERNMENT PRINTING OFFICE
WASHINGTON : 1932

For sale by the Superintendent of Documents, Washington, D. C. - $3 per year on subscription

For a partial list of previous research papers appearing in BUREAU OF STANDARDS JOURNAL OF RESEARCH see pages 2 and 3 of the cover

RP453

THE USE OF α-BENZOINOXIME IN THE DETERMINATION OF MOLYBDENUM

By H. B. Knowles

ABSTRACT

Present methods for the determination of molybdenum in any considerable amount require a number of tedious and time-consuming operations prior to the actual determination of that element. α-benzoinoxime, advocated as being specific for copper, has been found to precipitate molybdenum quantitatively and to isolate it from most of the more commonly encountered elements. As a result of the present study a procedure has been developed by which molybdenum can be determined in ores, steels, and other products in much less time than by present methods and with all the accuracy of the best methods now in use.

CONTENTS

	Page
I. Introduction	1
II. Experimental	2
1. Preliminary considerations	2
(a) Permissible acidity	2
(b) Temperature of the solution	2
(c) Amount of reagent required	2
(d) Time necessary for complete precipitation	2
(e) Washing the precipitate	3
(f) Final treatment of the precipitate	3
2. Procedure recommended for general use	3
3. Behavior of other elements in recommended procedure	4
4. Applications of the procedure	5
(a) Analysis of steel	5
(b) Analysis of ores and commercial products	6
III. Acknowledgments	7

I. INTRODUCTION

In an investigation of some reagents proposed as being specifics for copper, consideration was given α-benzoinoxime, which has been recommended by Feigl,[1] and for which he has proposed the name "Cupron." Briefly, it is stated by Feigl that complete precipitation of copper results when an alcoholic solution of the reagent is added to a hot, "clear blue" ammoniacal solution of copper. In the presence of iron, aluminum, lead, etc., precipitation is made in an ammoniacal tartrate solution, while in the presence of nickel, a tartaric acid solution buffered with tartrate is recommended. The resulting precipitate is said to be insoluble in water, alcohol, dilute ammonium hydroxide, acetic, and tartaric acids; easily soluble in mineral acids and slightly soluble in concentrated ammonium hydroxide. After appropriate washing it is dried and weighed as

$$Cu\ (C_6H_5—\underset{\displaystyle O}{\underset{|}{CH}}—\overset{\displaystyle NO}{\overset{\|}{C}}—C_6H_5)$$

containing 22.02 per cent of copper.

[1] F. Feigl, Ber., vol. 56, II, p. 2083, 1923.

The desirability of using α-benzoinoxime for the precipitation of copper in the presence of other elements, notably molybdenum, led to a study of the behavior of the reagent toward such elements. Preliminary tests disclosed the fact that while the reagent was not as specific for copper as could be wished, it did present interesting possibilities in its reactions with molybdenum. This element was not only quantitatively precipitated in an acetic acid solution buffered with acetate, but also in cold mineral acid solutions containing as much as 20 per cent by volume of sulphuric acid.

II. EXPERIMENTAL

1. PRELIMINARY CONSIDERATIONS

(a) PERMISSIBLE ACIDITY

Experiments showed that to prevent the interference of certain elements the solution must be distinctly acid with either sulphuric, hydrochloric, or nitric acid. A solution containing 5 per cent by volume of sulphuric acid is preferable, although good precipitations were also obtained from solutions containing as much as 20 per cent by volume of sulphuric acid. Solutions containing 5 per cent of hydrochloric or nitric acid gave excellent results in instances, in which sulphuric acid was objectionable, such as in the presence of tin or lead. Successful precipitations were also obtained in solutions containing 5 per cent by volume of phosphoric acid. Precipitations made in the presence of tartaric acid were not quite complete, while those made in solutions containing hydrofluoric acid indicated that this acid must be absent.

(b) TEMPERATURE OF THE SOLUTION

Precipitations at 80° to 90° C., as well as those performed at room temperature showed that there was danger of reducing sexivalent molybedenum before it was precipitated. Experiments showed that this condition was avoided best by working with a cold solution and adding sufficient bromine water to faintly tinge the solution after the addition of the reagent.

(c) AMOUNT OF REAGENT REQUIRED

When slightly more than the theoretical quantity of the reagent was used, as determined by the relation 1 Mo to 3 $C_6H_5{\cdot}CH(OH){\cdot}C{:}(NOH){\cdot}C_6H_5$, incomplete precipitation resulted. Similar unsatisfactory results prevailed when ten times the theoretical quantity of reagent was employed. This effect may have been caused, in part, by the large quantity of alcohol added with the reagent. It was found that from two to five times the theoretical amount of reagent provided an adequate excess.

(d) TIME NECESSARY FOR COMPLETE PRECIPITATION

Experiments to determine the time necessary for complete precipitation showed that although filtration could be begun almost immediately following the final addition of the reagent, equally satisfactory results were obtained when filtrations were made at the end of 10 minutes, during which time ample opportunity was afforded to permit intermittent thorough stirring. Low results were obtained when the precipitates were allowed to remain in contact with the solutions for 30 minutes.

(e) WASHING THE PRECIPITATE

It was found that water, absolute ethyl alcohol, and various mixtures of diluted alcohol containing a little sulphuric acid were not suitable for washing the precipitate. The most promising wash solution was found to be a cold, diluted sulphuric acid (1 per cent by volume) containing a small amount of α-benzoinoxime.

(f) FINAL TREATMENT OF THE PRECIPITATE

Experiments in which it was sought to weigh or titrate the molybdenum precipitate, after appropriate washing and drying, gave no immediate indication of success, and further attempts were abandoned. Difficulties, such as are experienced in the direct ignition of some organic compounds, were not encountered, for it was found that the precipitate could be ignited directly to molybdic oxide after a short drying.

2. PROCEDURE RECOMMENDED FOR GENERAL USE

Prepare a solution containing 10 ml of sulphuric acid (specific gravity 1.84) in a volume of 200 ml and not more than 0.15 g of sexivalent molybdenum. If vanadates or chromates are present add sufficient freshly prepared sulphurous acid to reduce them and heat to boiling. Continue the boiling until the odor of sulphur dioxide can no longer be detected. Chill the solution to a temperature of 5° to 10° C. Stir and slowly add 10 ml of a solution of 2 g of α-benzoinoxime in 100 ml of alcohol and 5 ml extra for each 0.01 g of molybdenum present. Continue to stir the solution, add just sufficient bromine water to tint the solution a pale yellow and then add a few milliliters of the reagent. Allow the beaker and contents to remain in the cooling mixture 10 to 15 minutes with occasional stirring, stir in a little macerated filter pulp and filter through a paper of close texture, such as S. & S. No. 589 Blue Band. Filtration can be greatly facilitated by using a coarser filter, such as S. & S. No. 589 Black Band, but it is then requisite that the filtrate be very carefully examined and the first portions refiltered if they are not absolutely clear. Wash the precipitate with 200 ml of a cold, freshly prepared solution containing 25 to 50 ml of the prepared reagent and 10 ml of sulphuric acid in 1,000 ml. On standing, the filtrate will deposit needlelike crystals if sufficient reagent has been employed.

Transfer the washed precipitate to a weighed platinum crucible, cautiously dry; char, without flaming, over a very low gas flame and then ignite to constant weight in an electric muffle at 500° to 525° C. In umpire analyses of materials containing silica it is best to remove that constituent before proceeding with the precipitation of molybdenum rather than to treat the final precipitate with sulphuric and hydrofluoric acids, because of the uncertainty of completely decomposing molybdenum sulphate at the temperature of ignition. If the oxide contains no impurities, except tungsten, it should dissolve completely in warm dilute ammonium hydroxide. If an insoluble residue remains, it must be separated by filtration, ignited, weighed, and the weight subtracted. If tungsten may be present, the clear ammoniacal solution should be acidified with hydrochloric acid and treated with cinchonine as in II, 4(*b*), "analysis of ores and commercial products."

Results obtained by use of the recommended procedure with pure solutions of molybdenum are given in Table 1.

TABLE 1.—*Determination of molybdenum in pure solution*

Experiment No.	Mo added	Mo found	Difference
	g	*g*	*g*
1	0.0001	0.0001	0.0000
2	.0010	.0009	−.0001
3	.0051	.0051	.0000
4	.0103	.0101	−.0002
5	.0205	.0205	.0000
6	.0513	.0513	.0000
7	.1026	.1027	+.0001

3. BEHAVIOR OF OTHER ELEMENTS IN RECOMMENDED PROCEDURE

In a survey of the behavior of other elements in the procedure recommended in II, 2, the following elements were studied: Silver, lead, mercury, bismuth, copper, cadmium, arsenic, antimony, tin, selenium, tellurium, aluminum, iron, titanium, zirconium, chromium, vanadium, silicon, tungsten, tantalum, columbium, cerium, uranium, rhenium, nickel, cobalt, manganese, zinc, and the members of the platinum group—ruthenium, rhodium, palladium, osmium, iridium, and platinum.

The only elements that give precipitates in mineral acid solutions with α-benzoinoxime are tungsten, palladium, sexivalent chromium, quinquevalent vanadium, and tantalum. The precipitation of tungsten and palladium is seemingly quantitative and the use of α-benzoinoxime in quantitative determinations of these elements is being studied. For example, in a determination of molybenum in the Bureau of Standards standard sample of chrome-vanadium steel No. 72 the result obtained was too high. The error was afterwards found to be caused by tungsten, the presence of which had not been previously noted. The precipitation of sexivalent chromium and quinquevalent vanadium was not studied because satisfactory methods for their determination are available, and it was found that they cause no interference when reduced to lower valences (Cr^{III} and V^{IV}). The precipitate with tantalum appeared more like the hydrated acid than a compound with the reagent, and the reaction was not studied further because tantalum occurs but seldom, and most of it would be removed before precipitation of molybdenum would be attempted.

Silver, lead, mercury, bismuth, copper, cadmium, arsenic, antimony, tin, aluminum, iron, titanium, zirconium, trivalent chromium, quadrivalent vanadium, cerium, uranium, nickel, cobalt, manganese, and zinc are not precipitated either when alone or when associated with molybdenum. Experiments dealing with mixtures of these elements are shown in Table 2. The separation of molybdenum from antimony is of particular interest because good methods for the separation of these elements are lacking.

Selenium, tellurium, rhenium, ruthenium, rhodium, osmium, iridium, and platinum are not precipitated when they occur alone. Their behavior when associated with molybdenum was not studied.

Columbium and silicon, in addition to the already mentioned sexivalent chromium, quinquevalent vanadium, palladium, tungsten,

and tantalum contaminate the precipitate and must be removed before precipitation of molybdenum is attempted, or else determined in the weighed precipitate and deducted.

The results given in Table 2 were obtained when a single precipitation of molybdenum was made in the presence of other elements. With the exception of experiment No. 3, tests of the final precipitates showed no evidence of the presence of contaminating elements. The filtrate and washings from each experiment, after evaporation with nitric and sulphuric acids to destroy organic matter and testing colorimetrically by treating with potassium thiocyanate and stannous chloride [2] showed less than 0.1 mg of molybdenum.

TABLE 2.—*Determination of molybdenum in the presence of other elements*

Experiment No.	Mo added	Mo found	Difference	Remarks
	g	*g*	*g*	
1	0.0103	0.0101	−0.0002	Precipitated in 5 per cent HCl+1 per cent HNO_3.
2	.0103	.0102	−.0001	Precipitated in 5 per cent HCl.
3	.0513	.0632	+.0119	Precipitated in presence of 0.05 g V^{v}.
4	.0513	.0514	+.0001	Precipitated in presence of 0.05 g V^{IV}.
5	.0513	.0514	+.0001	Precipitated in presence of 0.05 g Sn^{IV} in 5 per cent HCl.
6	.0513	.0514	+.0001	Precipitated in presence of 0.05 g each of Ni, Co, Mn, Cr^{III}, Fe^{III}, Zn, Cu.
7	.0513	.0514	+.0001	Precipitated in presence of 0.05 g each of Tl, Zr, Ce^{III}, Al, U.
8	.0513	.0510	−.0003	Precipitated in presence of 0.05 g each of Pb, Sb, As, after removal of Pb as sulphate. $PbSO_4$ not examined for Mo.
9	.0513	.0516	+.0003	Precipitated in presence of 0.05 g each of Ag, Bi, Cd, Hg^{II}.
10	.0513	.0516	+.0003	Precipitated in presence of 0.05 g Sb^{v} in 5 per cent acid (50 per cent H_2SO_4: 50 per cent HCl).

It was found that if correct colorimetric determinations of molybdenum are to be obtained the complete absence of nitric acid and platinum must be assured. The removel of nitric acid is readily accomplished by heating to fuming with an excess of sulphuric acid, while the absence of platinum is best assured by conducting all necessary fusions and evaporations in either silica or porcelain laboratory ware.

4. APPLICATION OF THE PROCEDURE

(a) ANALYSIS OF STEEL

To study the applicability of the procedure to the determination of small amounts of molybdenum in steel, samples of the Bureau of Standards standard sample No. 72 and of No. 11d with small additions of molybdenum were used. One-gram samples of the steel were dissolved in 50 ml of diluted sulphuric acid (1+6) and the solution treated with a minimum amount of nitric acid (specific gravity 1.42) to decompose carbides and oxidize the molybdenum. The solutions were filtered, if not perfectly clear, diluted to 100 ml with water, cooled, treated with sufficient ferrous ammonium sulphate to reduce vanadic and chromic acids, and then cooled to 5° to 10° C. Five to ten milliliters of the α-benzoinoxime reagent was added, followed by the addition of bromine water and a few more milliliters of the reagent. After standing 10 to 15 minutes, the precipitates

[2] Lundell, Hoffman, and Bright, Chemical Analysis of Iron and Steel, p. 323, John Wiley & Sons, New York, 1931.

were filtered, washed, and ignited as in the procedure already described. The ignited oxides were examined for any insoluble residue and tungsten they might have contained.

The results obtained by the above procedure are shown in Table 3.

TABLE 3.—*Determination of molybdenum in steel*

Experiment No.	Material	Percentage of molybdenum		Difference	Remarks
		Added or present	Found		
		Per cent	*Per cent*	*Per cent*	
1	Chrome molybdenum steel No. 72.	0.149	0.166	+0.017	Gravimetric determination.
2	do	.149	.160	+.011	Do.
3	B. O. H. steel No. IId	.0051	.0054	+.0003	Colorimetric determination after solution of the precipitate.
4	do	.0103	.0096	−.0007	Do.
5	do	.51	.52	+.01	Gravimetric determination.
6	do	5.13	5.15	+.02	Do.

(b) ANALYSIS OF ORES AND COMMERCIAL PRODUCTS

To study the applicability of the method to large amounts of molybdenum, determinations were made on the Bureau of Standards standard sample of calcium molybdate No. 71 and samples of wulfenite and molybdenite ore. The procedure adopted in the analysis of these materials consisted of an initial attack of 0.2 to 0.5 g of the material with either hydrochloric acid, nitric acid, or a mixture of both. Molybdenite is perhaps more readily attacked by treating with a mixture of fuming nitric acid (specific gravity 1.49) and bromine. Following the preliminary decomposition the solution was diluted with water, treated with 25 ml of diluted sulphuric acid (1+1) and evaporated until fumes of sulphuric acid appeared. After the addition of 100 ml of water, the solution was heated to dissolve soluble sulphates, filtered, and washed with diluted sulphuric acid (2+100). The insoluble residue obtained at this stage contained a small amount of molybdenum which was determined by fusing the residue with sodium carbonate, extracting with water, and making a colorimetric test of the water extract. The filtrate, at room temperature, was then diluted to 200 ml and treated with a few drops of tenth normal potassium permanganate, enough to produce a permanent pink tinge, to insure complete oxidation of the molybdenum. Freshly prepared sulphurous acid was then added to reduce vanadates and chromates, and the solution boiled until no odor of sulphur dioxide could be detected. After thorough cooling, the solution was treated with an excess of α-benzoinoxime, and the resulting precipitate filtered, washed, dried, ignited, and weighed. The ignited oxide was dissolved in the least possible amount of warm dilute ammonium hydroxide, filtered, washed with warm water, and the filter with its contents ignited and weighed. The ammoniacal extract containing all the molybdenum was acidified with hydrochloric acid, treated with cinchonine, digested overnight, and any precipitate of tungsten was filtered, washed, ignited at 525° C. and weighed. The weight of this residue, together with that of the residue insoluble in ammonium hydroxide, was deducted from the weight of the molybdenum oxide.

Results of the experiments are given in Table 4.

TABLE 4.—*Determinations of molybdenum in ores and commercial products*

Experiment No.	Material	Mo found	Remarks
1	Calcium molybdate	35.22 per cent Mo	Certificate value 35.3 per cent.
2	do	35.26 per cent Mo	
3	Wulfenite ore	18.77 per cent MoO_3	11 analysts reported values between 18.29 and 21.86 per cent by various procedures.
4	do	18.84 percent MoO_3	Do.
5	Molybdenite ore	70.4 per cent MoO_3	13 analysts reported values between 68.62 and 74.79 per cent by various procedures.
6	do	70.1 per cent MoO_3	Do.

In some further tests on the wulfenite ore, a 5 g sample was treated as described, and the solution diluted to exactly 500 ml after decomposition and the removal of the lead as sulphate. Direct precipitation with α-benzoinoxime in 50 ml aliquots indicated 18.73, 18.67, and 18.73 per cent of molybdenum trioxide. Tests on similar aliquots indicated 18.77 and 18.75 per cent after the long and tedious process of eliminating arsenic and vanadium by triple precipitation with ammonium hydroxide in the presence of ferric iron, separation from tungsten by precipitation of the molybdenum as sulphide from an acid solution containing tartaric acid, recovery of the molybdenum which escaped the sulphide precipitation and other time-consuming attendant operations. The removal of copper, which does not interfere in the α-benzoinoxime procedure, is a requisite of the longer procedure before attempting either a gravimetric or volumetric determination of molybdenum.

In connection with the process of removing arsenic and vanadium by precipitating with ammonium hydroxide in the presence of ferric iron, it is to be noted that if lead is present in the original material, and escapes separation as sulphate, it will combine with and retain molybdenum in the precipitate of ferric hydroxide. The amount of molybdenum thus held may be conveniently determined by dissolving the ferric hydroxide in sulphuric acid, treating with potassium thiocyanate and stannous chloride, and comparing the resulting color with that of a standard molybdenum solution by means of a colorimeter.

III. ACKNOWLEDGMENTS

The author desires to express his gratitude to G. E. F. Lundell, under whose direction this investigation has been conducted, and also to R. Gilchrist for helpful assistance in the investigation dealing with the platinum metals.

WASHINGTON, April 29, 1932.

EFFECT OF ZINC COATINGS ON THE ENDURANCE PROPERTIES OF STEEL

By W. H. Swanger and R. D. France

ABSTRACT

The effect of the surface alterations, resulting from the application and presence of hot-dipped galvanized and electroplated zinc coatings, on the endurance properties of 0.02 per cent carbon open-hearth iron and 0.45 and 0.72 per cent carbon steels was determined by fatigue tests made with R. R. Moore rotating beam and Haigh axial loading machines.

Rotating beam tests were made on: (*a*) Polished but uncoated specimens, (*b*) specimens coated by the hot-dip galvanizing process, (*c*) zinc-plated specimens, and (*d*) on specimens acid pickled as for galvanizing. Axial loading tests were made on uncoated and galvanized specimens only.

The open-hearth iron was tested in the "as rolled" condition. The two carbon steels were tested in the normalized and annealed condition, in the quenched condition, and in the tempered condition, except that axial loading tests were not made on quenched specimens.

The results of the fatigue tests are given in conventional S–N diagrams and are summarized in a table, together with the results of tensile strength and hardness determinations. Photomicrographs showing the structures of the heat-treated steels and of the two types of coatings are given.

The endurance ratios (endurance limit : tensile strength) by the rotating beam method of test of the uncoated specimens varied from 0.38 to 0.70; by the axial loading method, from 0.31 to 0.59.

The decrease in fatigue limit from that of the polished uncoated materials caused by the acid pickling was more marked in the quenched steels than in the annealed and the tempered steels. The decrease varied from 0 to 40 per cent.

A still greater decrease, as much as 42.5 per cent, was caused by the presence of the hot-dipped galvanized coatings, The quenched and the tempered steels were affected more adversely than the annealed steels.

The fatigue limits of the zinc electroplated specimens were equal to or greater than those of the uncoated specimens.

The difference in the effects of the two types of coating is believed to be caused by the differences in the nature of the bond between zinc and steel and differences in the structure and hardness of the two coatings.

CONTENTS

		Page
I.	Introduction	9
II.	Materials	10
III.	Testing procedure	12
IV.	Results	13
V.	Discussion	15
VI.	Acknowledgment	24
VII.	Selected bibliography	24

I. INTRODUCTION

It is generally agreed that the character of the surface of a metal is an important factor in determining its resistance to repeated stresses. If an endurance limit is accepted as an intrinsic property of a metal, this limit is correctly determined only when smoothly polished specimens with generous fillets are used. The damaging effects of surface

corrosion and of mechanically produced notches have formed the subject of numerous investigations on "fatigue of metals." The information gained from these investigations has shown the necessity for avoiding "notch effects" in highly stressed members subjected to repeated stresses. Careful removal of tool marks, protection from corrosion and use of adequate fillets at abrupt changes of section, aid materially in realizing in practice the normal endurance strength of metals.

Metallic coatings are frequently used on iron and steel to protect against corrosion. It is a matter of considerable interest to know what effect such metallic coatings may have upon the fatigue limit of metals when damage by corrosion is not involved. From a mechanical standpoint the presence of a metallic coating on a specimen of iron or steel introduces factors which complicate this problem. There are two surfaces, the free surface of the coating and that of the underlying steel, the characteristics of which may influence the fatigue limit of the composite specimen. Another factor is the endurance strength of the coating itself. Very little is known about this property of the various protective metallic coatings in general use, but it is probably low in comparison with the endurance strength of steels. The nature of the bond or interface between coating and steel is believed to have a very important influence on the endurance properties of the composite specimen. The nature of the surface of the steel, the kind of coating and the manner in which it is applied largely determine the character of the bond between coating and steel.

This investigation was restricted to a study of the effect of hot-dipped galvanized and electroplated zinc coatings on the endurance properties of low carbon open hearth iron and two carbon steels.

II. MATERIALS

Zinc coatings were chosen because they are the most commonly used protective metallic coatings on ordinary structural grades of iron and steel. Both hot-dipped galvanized and electroplated coatings were used because of the known difference in the nature of the bond between steel and zinc coating of these two types. Sherardized, "galvannealed," and sprayed zinc coatings were not studied. It is believed that the difference in the nature of the bond of hot-dipped galvanized coatings and sherardized or "galvannealed" coatings, and of electrodeposited coatings and sprayed zinc coatings, is one of degree rather than of kind. It is, of course, possible that each of the above-mentioned types of zinc coatings might affect the endurance properties of a given steel to a different degree.

The open-hearth iron and the two carbon steels were purchased from jobbers and were not specially made for this investigation. The chemical compositions of the three materials (ladle analyses) are given in Table 1.

TABLE 1.—*Chemical composition of steels*

	Carbon	Manganese	Phosphorus	Sulphur	Silicon
	Per cent	*Per cent*	*Per cent*	*Per cent*	*Per cent*
Open-hearth iron	0.02	0.03	0.042	0.005	.....
0.45 per cent C steel	.45	.60	.015	.040	0.18
0.72 per cent C steel	.72	.31	.017	.019	.24

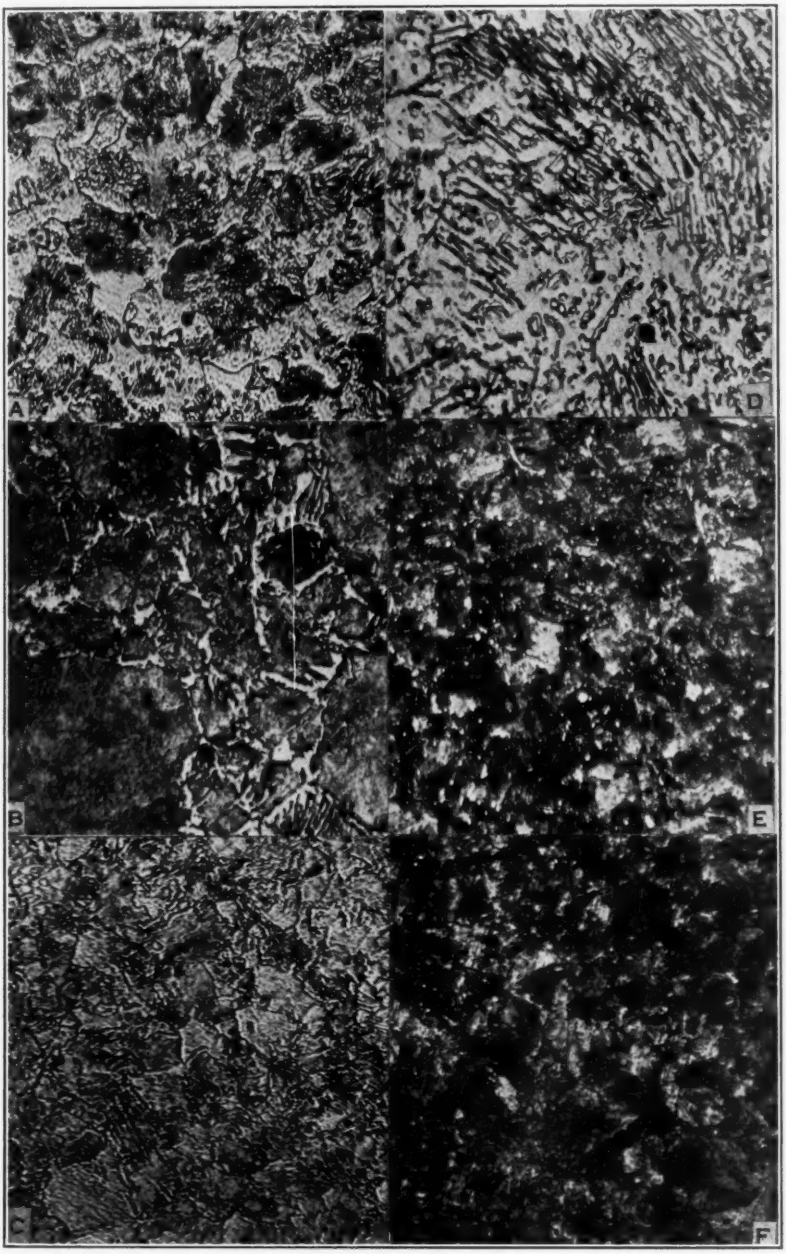

FIGURE 1.—*Structure of the carbon steels. Specimens were etched with nital (alcohol containing 2 per cent nitric acid).* × *450*

a, 0.45 per cent carbon steel, normalized at 875° C., annealed at 800° C.; *b*, 0.45 per cent carbon steel, normalized at 875° C., annealed at 800° C., quenched in oil from 830° C; *c*, 0.45 per cent carbon steel, normalized at 875° C., annealed at 800° C., quenched in oil from 830° C., tempered at 595° C.; *d*, 0.72 per cent carbon steel, normalized at 795° C., annealed at 765° C.; *e*, 0.72 per cent carbon steel, normalized at 795° C., annealed at 765° C., quenched in oil from 775° C.; *f*, 0.72 per cent carbon steel, normalized at 795° C., annealed at 765° C., quenched in oil from 775° C., tempered at 450° C.

UNIV OF MICH.

The open-hearth iron test specimens were machined from the center of 1-inch diameter hot-rolled bars and the specimens of the two carbon steels from the center of corresponding bars of three-quarter inch diameter.

All of the specimens were carefully machined on a lathe and finish ground to size. They were then polished longitudinally until all traces of circumferential tool marks were eliminated with emery papers of successively finer grit, ending with 0000 paper.

Endurance limits of the two carbon steels, coated and uncoated, were determined with the steels in the normalized and annealed condition, in the oil-quenched condition, and in the tempered condition. The details of the heat treatments are given in Table 2.

To minimize any decarburization effect, an atmosphere of illuminating gas was maintained in the furnace during the heat treatments. As a further precaution the hardened specimens were machined oversize and a layer 0.005 inch thick was ground off the test length after the heat treatments.

The open-hearth iron was used in the "as rolled" condition. The microstructures of the two carbon steels in the three conditions of heat treatment are shown in Figure 1.

TABLE 2.—*Heat treatment of carbon steels*

	Temperature for—							
	Normalizing [1]		Annealing [2]		Quenching [3]		Tempering [4]	
0.45 per cent carbon steel:	°F.	°C.	°F.	°C.	°F.	°C.	°F.	°C.
Annealed	1,607	875	1,472	800	-----	---	-----	---
Quenched	1,607	875	1,472	800	1,526	830	-----	---
Tempered	1,607	875	1,472	800	1,526	830	1,103	595
0.72 per cent carbon steel:								
Annealed	1,463	795	1,409	765	-----	---	-----	---
Quenched	1,463	795	1,409	765	1,427	775	-----	---
Tempered	1,463	795	1,409	765	1,427	775	842	450

[1] ¾-inch rods, heated with furnace, held 20 minutes, air cooled.
[2] ¾-inch rods, heated with furnace, held 40 minutes, cooled with furnace.
[3] Machined test bars, heated with furnace, held 20 minutes, quenched in oil.
[4] Machined test bars, heated with furnace, held 60 minutes, cooled with furnace.

The galvanized coatings were applied by the research division of the New Jersey Zinc Co. (of Pa.) by a method approximating commercial practice for hot-dip galvanizing. The specimens to be galvanized were first polished to the same degree as the specimens tested in the uncoated condition. They were then dipped in a hydrochloric acid solution (2 parts water to 1 part hydrochloric acid, specific gravity 1.19) for two minutes and immediately into the zinc bath held at 440° C. (824° F.). A high-grade zinc (containing 99.94+ per cent Zn) was used. The weight of coating obtained varied from 1.6 to 2.0 oz./ft.^{2} The galvanized coatings varied from 0.0017 to 0.0035 inch in thickness. This variation in thickness was probably caused by the fact that some of the specimens had to be dipped more than once to obtain a complete coating. The length of time in the zinc bath, accordingly, varied from 45 to 100 seconds.

In order to distinguish between the effect of the acid pickling and the combined effect of pickling and galvanizing, fatigue tests were

made on specimens of each material which, after final polishing, had been dipped for two minutes into hydrochloric acid of the same strength used for the galvanized specimens.

The specimens of the quenched 0.45 and 0.72 per cent carbon steels which were not galvanized were dipped into a lead bath for 45 seconds at 440° C. (824° F.) so that they had the same heat treatment as the corresponding hot-dipped galvanized specimens. A final polish with 0000 emery paper was given to the lead-dipped specimens before they were dipped into the acid or tested.

The electroplated zinc coatings were applied at the Bureau of Standards.[1] The procedure was as follows: (*a*) cathode-electrolytic cleaning, two minutes, at 90° C.; (*b*) hot-water rinse; (*c*) cold-water rinse; (*d*) pickled in sulphuric acid (2 *N*), two minutes at 50° C.; (*e*) hot-water rinse; (*f*) hot alkali dip without current, two minutes; (*g*) scrubbed with cleaning solution, bristle brush; and (*h*) plated in acid zinc bath, 24 minutes 1.5 amperes, 35° C.

The electrolytic cleaner was made up as follows: Sodium carbonate, 30 g per liter; trisodium phosphate, 30 g per liter; and sodium hydroxide, 7.5 g per liter.

The zinc anodes for the electroplating process were of the same order of purity as the zinc used for the hot-dipped coatings. The thickness of the electrodeposited coatings varied from 0.0021 to 0.0031 inch, which is roughly equivalent to a 2-ounce coating.

III. TESTING PROCEDURE

The endurance limit determinations were made by both the rotating beam and the axial loading methods of stressing. The rotating beam tests were made on R. R. Moore machines and the axial loading tests were made on Haigh alternating stress testing machines, in which the specimens were subjected to alternating equal tensile and compressive stresses. The form of the specimens, methods of calibration of the testing machines, and testing procedure followed have been described previously by one of the authors.[2]

Axial loading tests were not made on zinc-plated specimens as it was believed that the effect of the electrodeposited coating on the endurance limit determined by this method, would be of the same order as was found for the rotating beam tests. As a further economy in number of specimens, axial loading tests were not made on the 0.45 and 0.72 per cent carbon steels in the quenched condition because these steels are seldom used in this condition. Rotating beam tests of electroplated specimens of the 0.72 per cent carbon steels in the quenched condition and of the 0.45 per cent carbon steel in the annealed and in the quenched conditions were also omitted.

Usually nine specimens were used in the determination of each endurance limit. One specimen of each series, except the pickled specimens, tested on the Moore machines was subjected to 25,000,000 cycles of reversed stress at the endurance limit and then restressed at a value 5,000 lbs./in.^{2} above the endurance limit. An annealed, a quenched, and a tempered specimen of the 0.45 per cent carbon steel and an annealed and a tempered specimen of the 0.72 per cent carbon

[1] The plating was done by the electrochemistry laboratory under the supervision of Dr. W. Blum.
[2] R. D. France, Endurance Testing of Steel: Comparison of Results Obtained with Rotating-Beam versus Axially-Loaded Specimens, Proc., Am. Soc. Testing Materials, vol. 31, pt. 2, p. 176, 1931.

steel were stripped of their galvanized coatings, after which they were tested at a stress just under the fatigue limit determined on the acid-pickled specimens of the corresponding materials.

The stresses applied to the acid pickled and the coated specimens were calculated on the diameter of the polished specimen before it was pickled or coated. The diameters were measured with a special micrometer capable of a precision of plus or minus 0.0001 inch. The change in diameter caused by either the acid treatment alone or the acid treatment and the application of the zinc coating was in all cases less than 0.0002 inch.

The tensile strengths of the three materials were determined on standard 0.505 inch diameter test bars, heat treated in the same way as the endurance specimens. Hardness determinations were made on the ends of the tensile and endurance test bars.

IV. RESULTS

The results of the fatigue limit determinations are given in Table 3, together with the tensile strength and hardness of the steels and the per cent change in fatigue limits caused by the pickling, by the pickling and galvanizing, and by the electroplating. The fatigue limits are also shown graphically in Figure 2.

Conventional S–N diagrams for all of the fatigue limit determinations are given in Figures 3 to 9.

TABLE 3.—*Physical properties and results of endurance tests*

Material (per cent carbon)	Heat treatment	Tensile strength	Hardness		Rotating beam								Axial loading			
					Uncoated		Pickled		Galvanized		Electroplated		Uncoated		Galvanized	
			Brinell hardness number	Rockwell number	Endurance ratio [1]	Endurance limit	Fatigue limit	Change in fatigue limit	Fatigue limit	Change in fatigue limit	Fatigue limit	Change in fatigue limit	Endurance ratio [1]	Endurance limit	Fatigue limit	Change in fatigue limit
		Lbs./in.²				*Lbs./in.²*	*Lbs./in.²*	*Per cent*	*Lbs./in.²*	*Per cent*	*Lbs./in.²*	*Per cent*		*Lbs./in.²*	*Lbs./in.²*	*Per cent*
0.02	Hot rolled	44,000	90	51 B	0.61	27,000	22,000	−18.5	26,000	−4.0	27,500	+1.8	0.59	26,000	22,500	−13.5
.45	Annealed	81,000	153	84 B	.44	36,000	33,000	−8.0	27,000	−25.0			.31	25,500	24,500	−4.0
.45	Quenched	121,500	248	28 C	.65	80,000	60,000	−25.0	46,000	−42.5						
.45	Tempered	102,000	207	98 B	.45	46,500	46,500	0	40,000	−14.0	49,000	+5.5	.45	46,000	30,000	−35.0
.72	Annealed	92,000	192	93 B	.38	35,000	31,500	−10.0	30,500	−13.0	35,000	0	.31	29,000	28,500	−2.0
.72	Quenched	176,000	340	39 C	.70	124,500	75,000	−40.0	75,500	−40.0						
.72	Tempered	168,500	332	37 C	.56	94,000	87,000	−7.5	54,500	−42.0	105,000	+11.0	.37	62,500	47,000	−25.0

[1] Endurance ratio = $\frac{\text{Endurance limit}}{\text{Tensile strength}}$.

V. DISCUSSION

The fatigue limits of the specimens that had been dipped in acid were lower than the fatigue limits of the polished uncoated specimens of the corresponding materials. The decrease was not uniform for the different materials but ranged from zero for the tempered 0.45

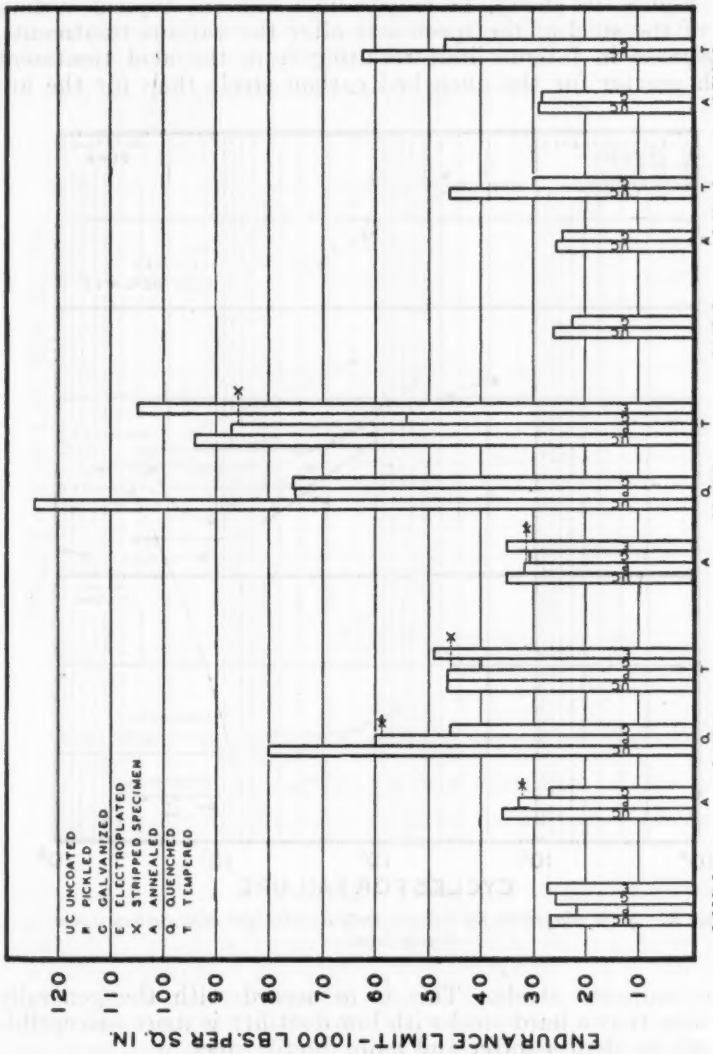

FIGURE 2.—*Fatigue limits determined by rotating beam and axial loading methods for open-hearth iron, 0.45 and 0.72 per cent carbon steels, in the annealed, quenched, and tempered conditions*

per cent carbon steel to 40 per cent for the quenched 0.72 per cent carbon steel. This result was clearly a manifestation of the "notch effect" caused by the acid treatment and was of the same nature as the corrosion effect which has been shown by McAdam (1, 2),[3] to have a pronounced influence on the endurance properties of metals.

[3] The numbers in parentheses here and throughout the text refer to the papers listed in the selected bibliography appended to this paper.

The variations in the effect of the acid treatment on the fatigue limits are undoubtedly associated with different solubility rates of the materials in the three conditions of heat treatment. The difference in the surface contours of the steel in different specimens of any one series was of about the same magnitude as the difference between the three series of specimens (acid pickled, galvanized, and electroplated). Figure 10 shows, in longitudinal section, typical surface contours of the steel of the specimens after the various treatments.

The decrease in fatigue limit resulting from the acid treatment was much greater for the quenched carbon steels than for the an-

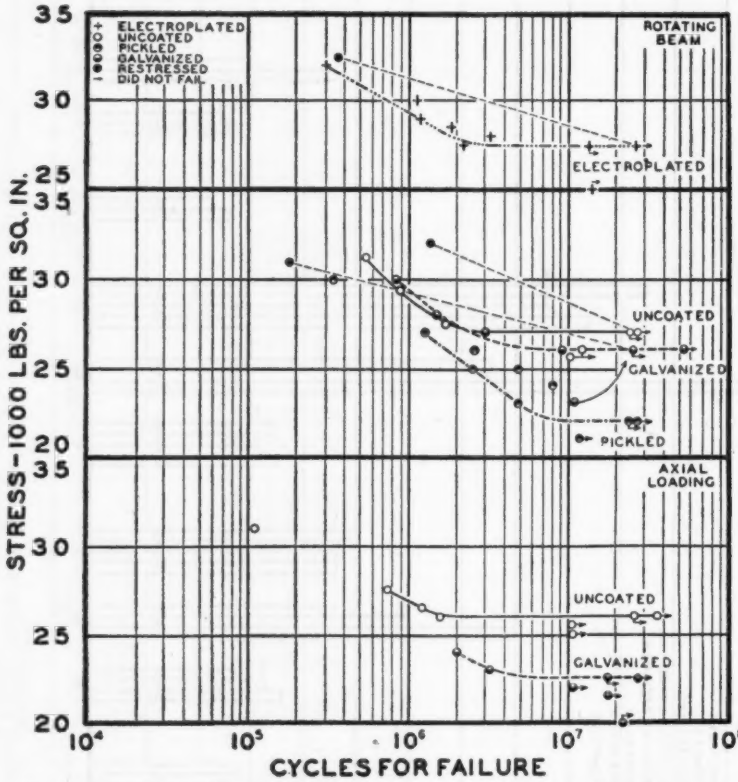

FIGURE 3.—*S–N diagrams for fatigue tests of 0.02 per cent carbon open-hearth iron*

nealed or tempered steels. This is in accord with the generally accepted idea that a hard steel with low ductility is more susceptible to notch effects than a softer and more ductile steel.

There was a marked decrease in the fatigue limit of the galvanized materials as determined by the rotating-beam method except for the open-hearth iron, for which there was little if any difference (4.0 per cent). For the carbon steels the decrease ranged from 13 to 42.5 per cent, and was greater for the quenched and the tempered steels than for the annealed steels. By the axial loading method of test the decrease for the open-hearth iron was 13.5 per cent and for the carbon

steels the decrease was much greater in the tempered steels than in the annealed steels.

Except for the open-hearth iron and the quenched 0.72 per cent carbon steel, the decrease in fatigue limit was greater for the galvanized than for the acid-pickled material. It might be considered that this further decrease was caused by an increased pitting or notch effect on the surface of the steel by the action of the zinc in the galvanizing process. That this was not the only cause is indicated by the fact that galvanized specimens of the annealed and the

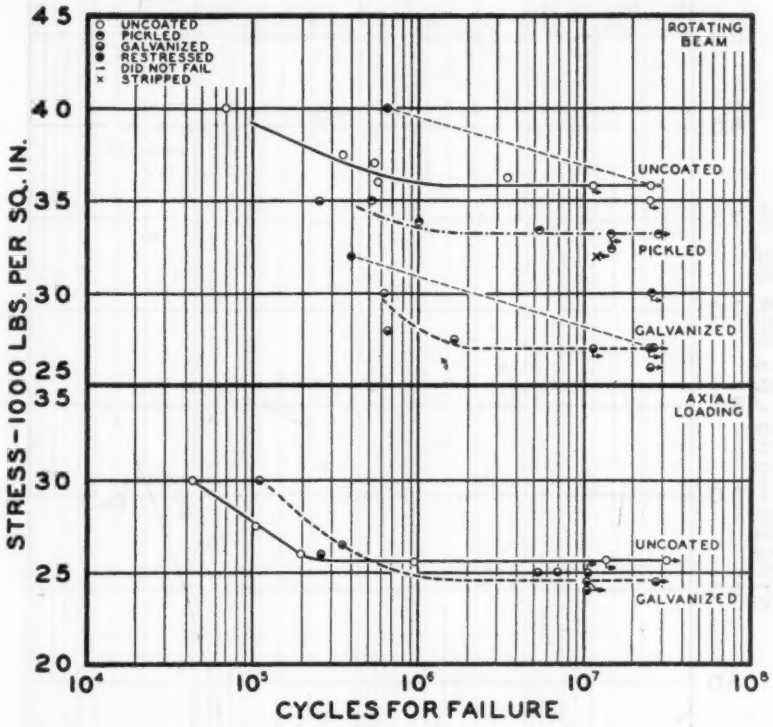

FIGURE 4.—*S–N diagrams for fatigue tests of 0.45 per cent carbon steel, annealed*

quenched 0.45 per cent carbon steels, and of the annealed 0.72 per cent carbon steels, when stripped of the zinc coating[4] did not fail in 10,000,000 cycles in the rotating beam machines at stresses just under the fatigue limits of the acid-pickled materials. The stripped specimen of the tempered 0.45 per cent carbon steel failed after 3,500,000 cycles which indicated that its fatigue limit was not much lower than the stress at which it failed. The stripped specimen of the tempered 0.72 per cent carbon steel failed after 300,000 cycles, but at a stress 32,000 lbs./in.^{2} higher than the fatigue limit of the galvanized material.

Hence it is believed that the conclusion is warranted that the presence of a hot-dip galvanized coating causes a serious lowering

[4] The zinc coatings were dissolved in hydrochloric acid (specific gravity 1.19) containing 1 ml of antimony chloride solution [32 g of $SbCl_3$ in 1,000 ml HCl (specific gravity 1.19)] to 100 ml of acid. A. S. T. M. specification A 90-30.

of the fatigue limit of carbon steels below that which would be obtained in the same steels in the polished but uncoated condition.

A similar conclusion can be drawn from the results of investigations by Harvey (3, 4), Haigh (5), and Fuller (6) of the protection against corrosion fatigue afforded to steels by galvanized or other types of metallic coatings. Although their results showed that the endur-

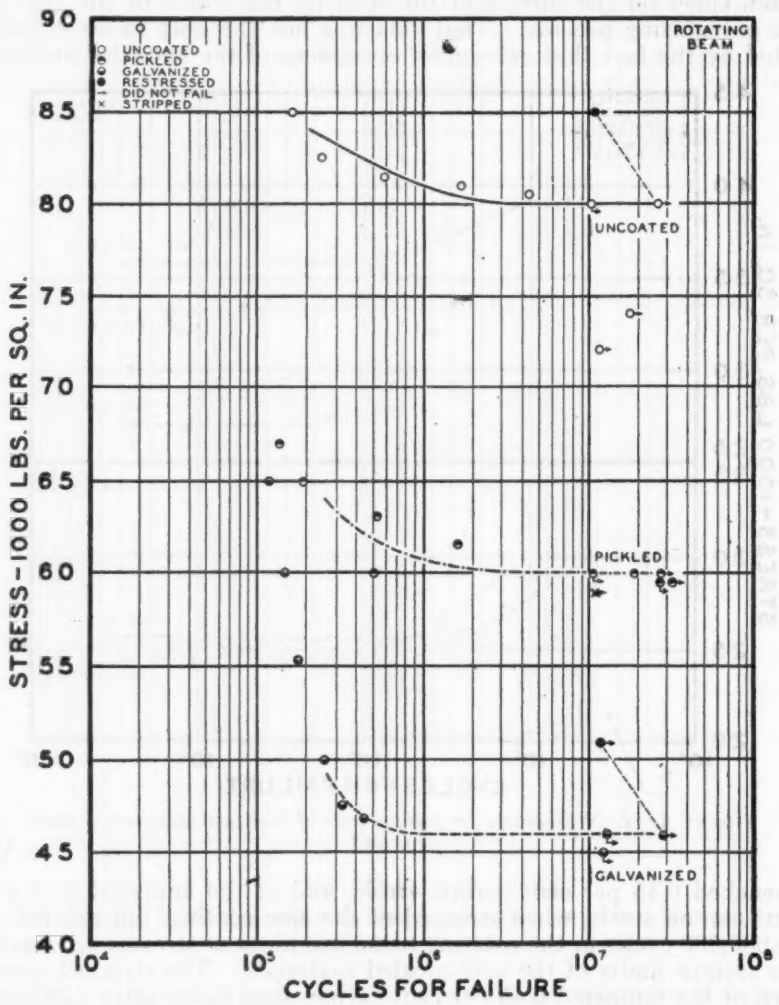

FIGURE 5.—*S–N diagrams for fatigue tests on 0.45 per cent carbon steel, quenched*

ance properties of the coated metals were definitely better than for the uncoated metals, when subjected to simultaneous stress and corrosion, the corrosion-fatigue limits of the galvanized materials were at the same time lower than the endurance limits of the uncoated materials not subjected to corrosion.

In marked contrast to the lower fatigue limit of the galvanized specimens, the fatigue limits of the zinc-plated specimens of the softer

steels were equal to those of the corresponding uncoated specimens. The fatigue limits of the zinc-plated specimens of the tempered steels were higher than those of the corresponding uncoated specimens by 5.5 per cent for the medium carbon and 11 per cent for the higher carbon steel.

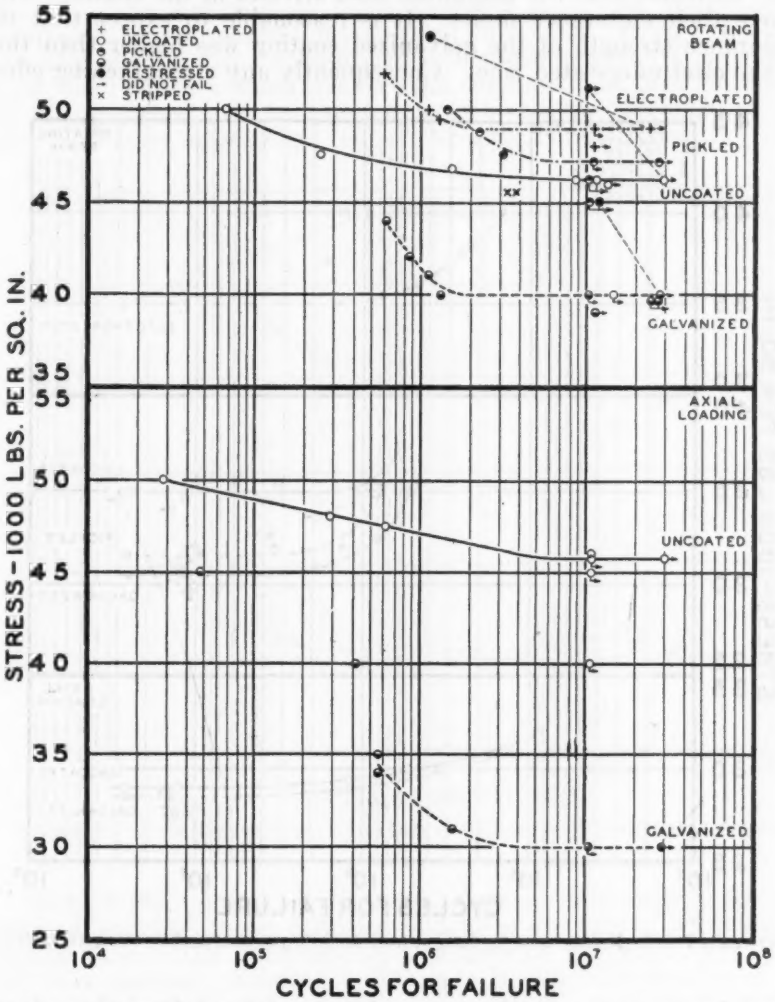

FIGURE 6.—*S–N diagrams for fatigue tests on 0.45 per cent carbon steel, tempered*

Both the hot-dip galvanized and the electroplated specimens had been subjected to comparable acid treatments before the coatings were applied. Furthermore, the steels of each series were identical in composition and had received the same heat treatments. Hence any differences in fatigue properties of the galvanized and electroplated specimens of the same series can not be ascribed to differences in the steels themselves, particularly to any suspected differences in

rate of notch propagation. It is believed that the increased fatigue limits of the electroplated coatings were not the result of a strengthening effect of the zinc coating. Numerous cracks were found in both types of coatings in the more highly stressed portions of the specimens after they were removed from the testing machines. This indicates that the maximum fiber stresses in the coatings were above their endurance limits. It is reasonable to expect that the endurance strength of the galvanized coating was higher than that of the electrodeposited zinc. Consequently any strengthening effect

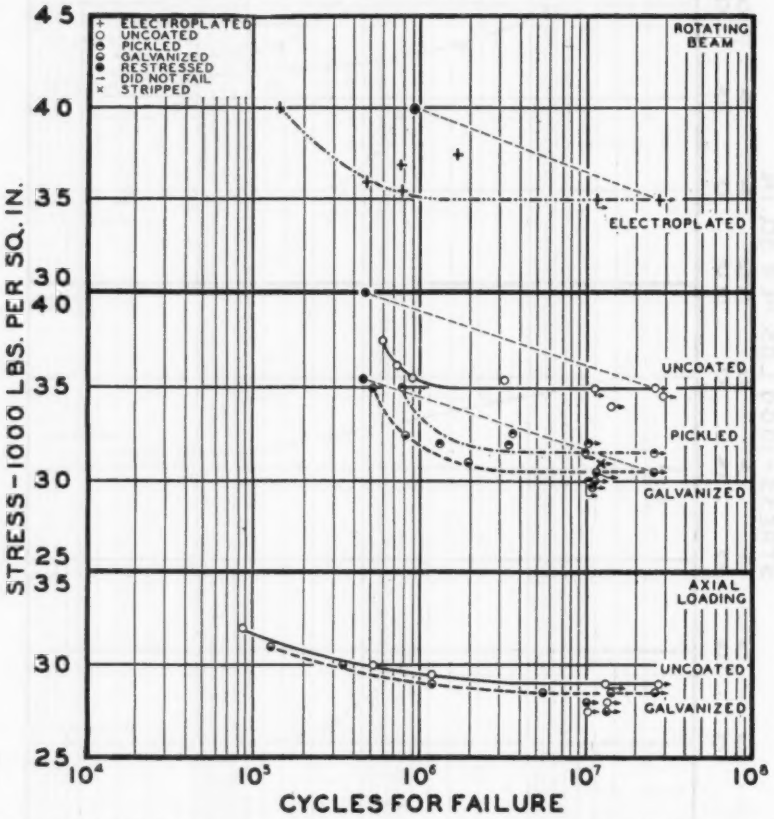

FIGURE 7.—*S–N diagrams for fatigue tests on 0.72 per cent carbon steel, annealed*

from the coating would be expected to be derived from the galvanized rather than from the electrodeposited coating.

The two types of coating are different in many respects. The electrodeposited coatings, as would be expected, were homogeneous throughout. The bond between zinc and steel may have been a "molecular bond," but at the interface there was little, if any, diffusion of iron into the zinc. Figure 11 (*a*) shows a typical cross section of the electroplated steel specimen.

The structure of hot-dipped galvanized coatings on steel has been studied by a number of investigators (7, 8, 9). Without going into

a detailed discussion of the composition of the layers it suffices at this time to state that the galvanized coatings on the specimens used in this investigation consisted of at least three layers. The outer layer was predominantly pure zinc, the innermost layer consisted largely of the more or less well-known iron-zinc intermetallic compounds. The intermediate layer consisted largely of intermetallic compound or compounds interspersed in a zinc matrix. On the annealed steel and the open-hearth iron specimens the intermediate layer was relatively much thicker than the innermost layer, whereas, on the quenched and on the tempered steels the thickness of the innermost layer approached that of the intermediate layer.

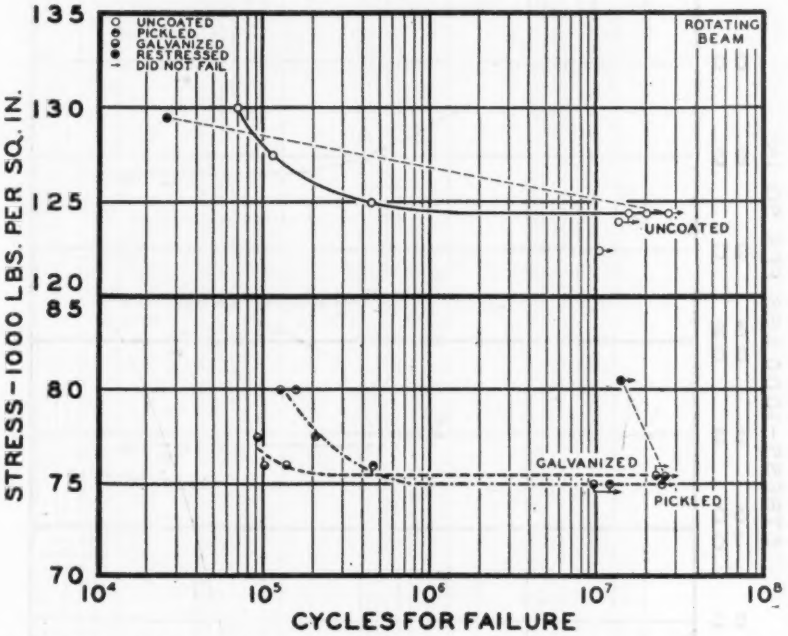

FIGURE 8.—*S–N diagrams for fatigue tests on 0.72 per cent carbon steel, quenched*

Micrographs (*c*) and (*d*) Figure 11 show in cross-section the galvanized coatings on an annealed and on a quenched 0.45 per cent carbon steel. The difference in thickness of the inner, iron rich, layers is marked. Possibly a difference in solubility in zinc of the heat-treated steel, and the annealed steel or open-hearth iron is responsible for the difference in thickness of the alloy layers.

The scratch hardness of the two types of coating indicated that the outer layer of the galvanized coatings was of the same order of hardness as the electrodeposited coatings. The intermediate and innermost layers of the galvanized coatings were increasingly harder as the steel surface was approached. This is illustrated in the micrographs (*e*) and (*f*) of Figure 11. The alloy layer adjacent to the steel (*e*) appears to be even harder than the steel itself.

As stated before, there were numerous cracks in both types of coating of the tested specimens. In the electrodeposited coatings

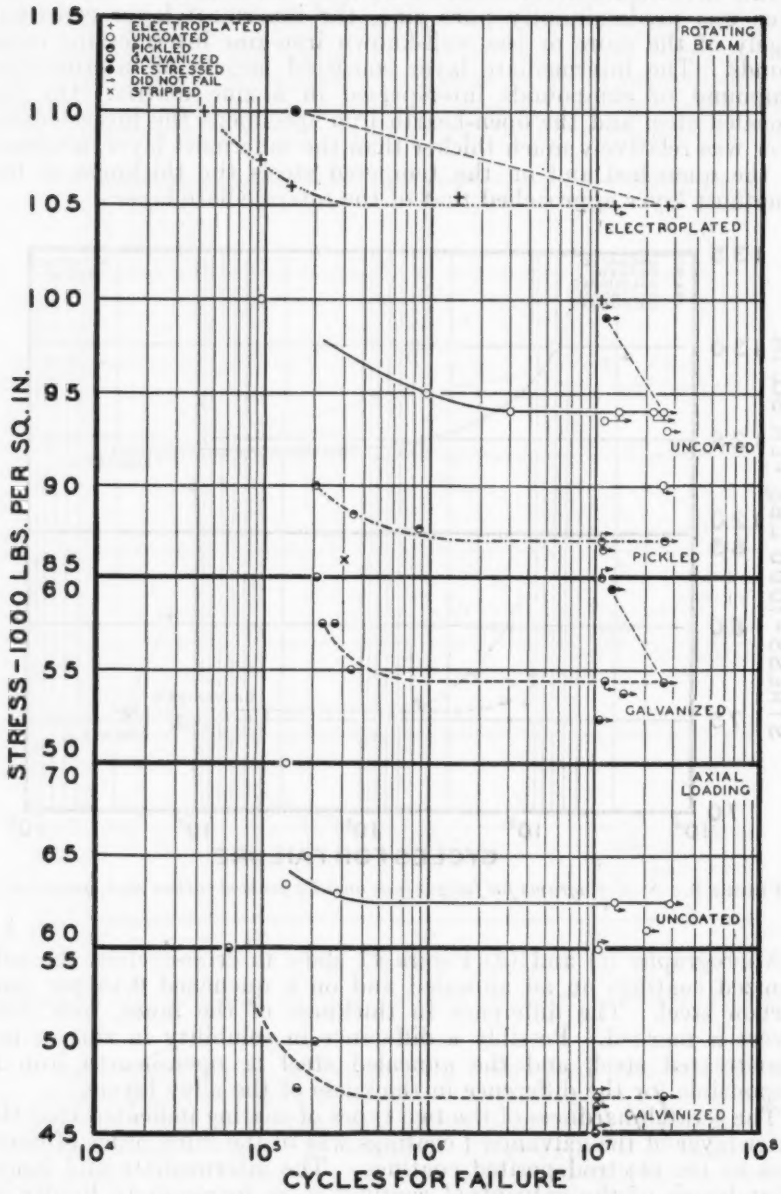

FIGURE 9.—*S–N diagrams for fatigue tests on 0.72 per cent carbon steel, tempered*

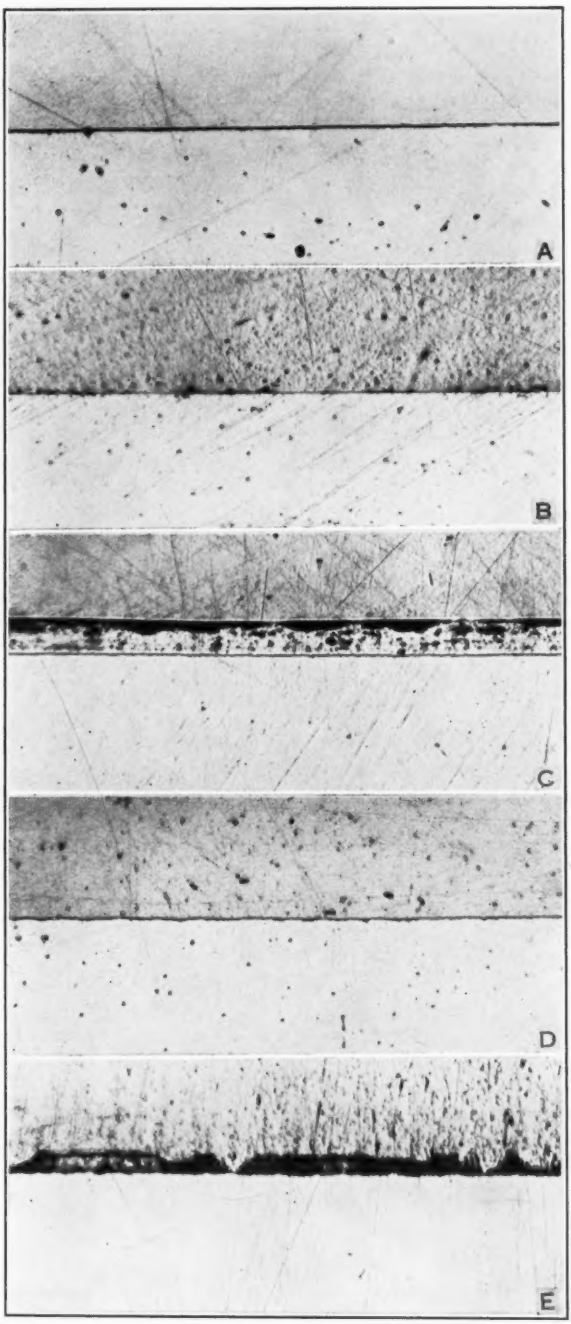

FIGURE 10.—*Typical contours of the steel surface of specimens unetched.* × *50*

a, Polished; *b*, polished and then acid pickled; *c*, polished, acid pickled, and then galvanized; *d*, polished, acid pickled, galvanized, and then stripped; and *e*, polished and then electroplated.

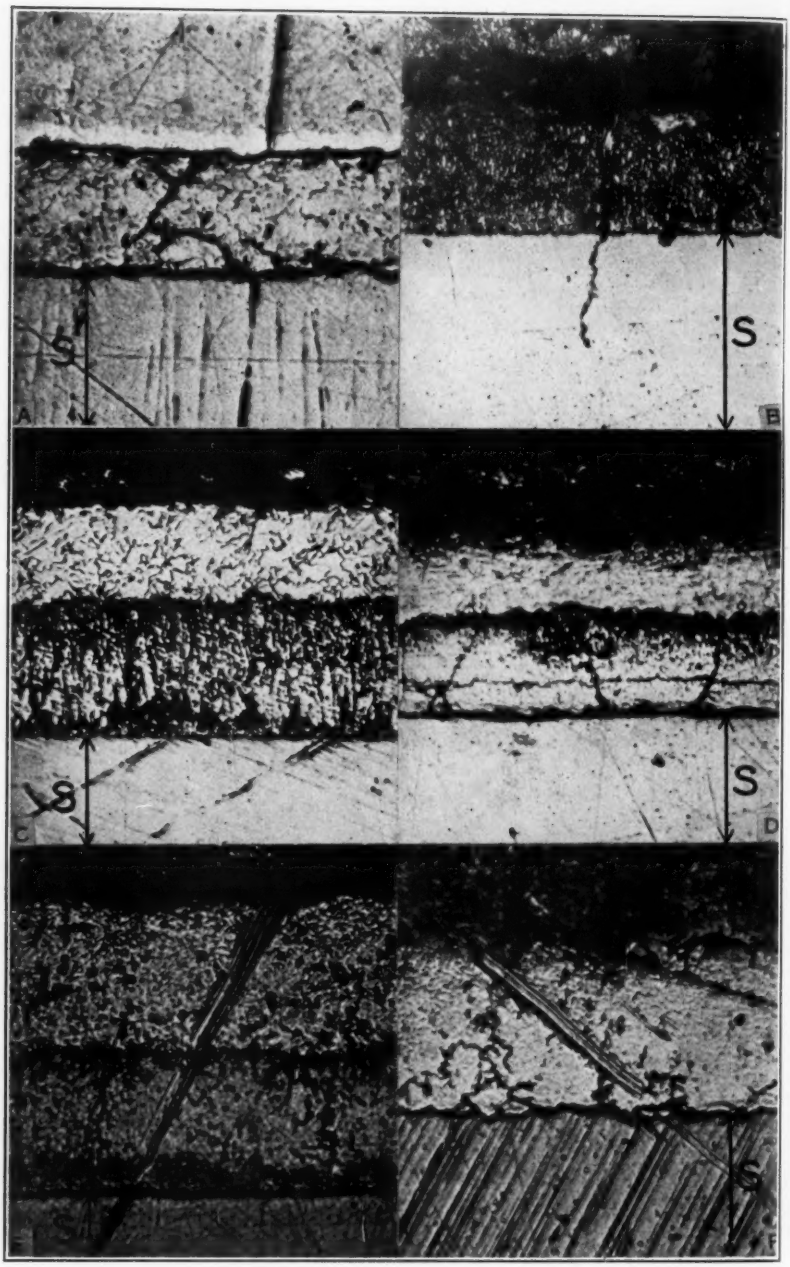

FIGURE 11

a, Structure of electrodeposited zinc coating on 0.72 per cent carbon steel, annealed; *b*, crack in galvanized coating extending into steel, 0.45 per cent carbon, annealed; *c*, structure of galvanized coating on 0.45 per cent carbon steel, annealed. Note the relatively thick intermediate layer, the thin innermost layer, and the light colored outer layer of relatively pure zinc; *d*, galvanized coating on 0.45 per cent carbon steel tempered. Note the thickness of the inner, hard, brittle layer adjacent to the hardened steel as compared with the thin layer of similar composition next to the softer steel of photograph *c*; *e*, scratch made with Bierbaum microcharacter across galvanized coating on tempered 0.45 per cent carbon steel. Note differences in width of scratch in the outer zinc layer and the intermediate and innermost iron-zinc alloy layers. Note that the innermost alloy layer appears to be harder than the steel; *f*, scratch made with Bierbaum microcharacter across electrodeposited zinc coating on tempered 0.72 per cent carbon steel. Discontinuity of scratch between zinc and steel was caused by difference in elevation between zinc and steel. Etched with chromic acid solution containing sodium sulphate (20 g CrO_3, 1.5 g Na_2SO_4 in 100 ml H_2O). × 275. Arrows indicate steel base.

the cracks were irregular (*a*) Figure 11, and appeared to be intergranular. In the galvanized coatings there were many more cracks in the intermediate and innermost layers than in the outer layer. Many of the cracks appeared to have started in the layer adjacent to the steel and to have progressed toward the outer surface, and in some instances the surface was not quite reached. In many instances the cracks undoubtedly originated at the surface and progressed inwardly toward the steel.

Of the broken specimens which were sectioned for examination under the microscope, two were found in which there was a crack in the steel which was a continuation of a crack in the innermost layer of the galvanized coatings. One of these is shown in (*b*) Figure 11. Although there were many cracks in the galvanized coatings, the evidence indicated that only a few had advanced into the steel. The probability is that none of the cracks in the electrodeposited coatings had extended into the steel, and that the cracks which caused failure of the electroplated specimens in the fatigue test originated in the steel itself.

The explanation of the lower fatigue limits of the galvanized specimens as compared with the uncoated or electroplated specimens is believed to lie: (*a*) In the difference in the stress conditions at the bottom of a crack in the inner, relatively hard, layers of the galvanized coating and those in a similar crack in the softer electrodeposited zinc; and (*b*) in the difference in the nature of the bond between zinc and steel in the two types of coatings.

It has been shown (10) that in relatively soft and ductile metals subjected to repeated stresses, slip lines form either previously to, or subsequently to, the appearance of cracks and that the cracks advance in the direction of the slip lines. The slip lines are an indication of plastic deformation under an applied stress which decreases when the deformation occurs. It is believed that the zinc of the electrodeposited coatings had sufficient ductility to deform around the bottom of an advancing crack, and that the resulting decrease in stress concentration when the crack had advanced to the steel was sufficient to stop the crack at that point. The discontinuity between zinc and steel was an additional aid in halting further advance of the crack. Consequently, the normal endurance limit of the steel was attained.

In the case of the galvanized specimens, a crack advancing into the relatively hard and very brittle inner layers did not meet with any conditions conducive to a decrease of stress concentration. The crack progressed to the outer steel fibers with undiminished stress. The intimate bond between coating and steel offered no obstacle to the advance of the crack into the steel. Naturally not every crack produced in the coating in the course of the fatigue test penetrated into the steel. A fortuitous combination of maximum stress concentration and conditions at the surface of the steel most favorable to the propagation of the stress, determined the location of the crack which led to failure of the specimen. Consequently since the presence of a hot-dipped galvanized coating promotes stress concentrations, the fatigue limit of such a coated specimen was appreciably lower than the normal endurance limit of the steels.

The data obtained on the specimens which were restressed at 5,000 lbs./in.^{2} above the fatigue limit, after they had been subjected to 25,000,000 cycles of stress at the fatigue limit, indicated that only the

quenched and the tempered steels were appreciably strengthened by the previous understressing. All of the annealed carbon steel and open-hearth iron specimens tested failed to "run" at the higher stress. The 0.72 per cent carbon steel specimen, uncoated and the two electroplated specimens of the 0.72 and the 0.45 per cent carbon steel, in the tempered condition, also failed to run.

The interesting observation was made that distinct spangles were developed on the surface of the zinc of the galvanized specimens shortly after they were placed in operation in the rotating beam machines.

VI. ACKNOWLEDGMENT

Grateful acknowledgment is made by the authors to P. R. Kosting for his aid in the preparation of the micrographs of the zinc coatings and of the scratch hardness tests.

VII. SELECTED BIBLIOGRAPHY

1. D. J. McAdam, jr., Influence of Water Composition on Stress Corrosion, Proc., Am. Soc. Testing Materials, vol. 31, pt. 2, p. 259, 1931; and additional papers by McAdam listed at the end of this paper.
2. D. J. McAdam, jr., Stress Corrosion of Metals, Proc., Zurich Congress of the New International Association for the Testing of Materials, 1931.
3. W. E. Harvey, Zinc as a Protective Coating Against Corrosion-Fatigue of Steel, Metals, and Alloys, vol. 1, p. 458, April, 1930.
4. W. E. Harvey, Cadmium Plating *v.* Corrosion-Fatigue. Pickling *v.* Corrosion-Fatigue, Metals and Alloys, vol. 3, p. 69, March, 1932.
5. B. P. Haigh, Chemical Action in Relation to Fatigue of Metals, Trans. Inst. Chem. Engrs., vol. 7, p. 29, 1929.
6. T. S. Fuller, Some Aspects of Corrosion Fatigue, Trans. Inst. of Metals Division, A. I. M. E., p. 47, 1929.
7. H. S. Rawdon, Structure of Commercial Zinc Coatings, Proc., Am. Soc. Testing Materials, vol. 18, pt. 1, p. 216, 1921.
8. W. H. Finkeldey, The Microstructure of Zinc Coatings, Proc., Am. Soc. Testing Materials, vol. 26, pt. 2, p. 304, 1926.
9. W. Guertler, Structure of Galvanized Iron, Zeitschrift für Metallographie, vol. 1, p. 353, 1911.
10. H. F. Moore and Tibor Ver, A Study of Slip Lines, Strain Lines, and Cracks in Metals under Repeated Stress, Bull. No. 208, Eng. Expt. Sta., Univ. Illinois, June 3, 1930.
11. H. W. Gillett, The Need for Information on Notch Propagation, Correlated Abstracts, Metals and Alloys, vol. 1, p. 114, September, 1929.
12. H. W. Gillett, What is This Thing Called Fatigue? Metals and Alloys, vol. 2, p. 71, February, 1931.

WASHINGTON, April 30, 1932.

RP455

POWER INPUT AND DISSIPATION IN THE POSITIVE COLUMN OF A CÆSIUM DISCHARGE

By F. L. Mohler

ABSTRACT

The power input per centimeter is equal to the voltage gradient times the current. Two recognized sources of power dissipation are the recombination of ions on the tube walls and the atomic radiation.

The voltage gradient is measured between two probes at the axis of the discharge tube. The flow of ions to the walls is measured by a disk probe at the wall. The recombination energy is the kinetic energies of the ions and electrons, which can be evaluated from the probe current-voltage curves, plus the ionization energy.

The total radiation was measured by a thermopile while transmission corrections were determined by a photo-electric cell. The first doublet of the principal series at 8,521 and 8,944 A contributes most of the radiation.

Results show that with low currents and pressures the radiation and recombination losses account for nearly the entire power input. With increasing currents and pressures there is an increasing balance of power which is unaccounted for. All the power terms change very slowly with pressure. The recombination loss is negligible at low currents and the most important factor at high currents.

CONTENTS

		Page
I.	Introduction	25
II.	Electrical measurements	27
III.	Radiation measurements	30
IV.	Results	31
V.	Conclusion	32

I. INTRODUCTION

Conditions in the positive column are determined by the nature of the gas in the tube, the density of the gas, the size of the tube and the current. This applies to all types of direct current discharge; cold cathode glow discharges, thermionic discharges and arcs when they operate under current and pressure conditions in which a true column exists. In the uniform or unstriated column the voltage gradient, electron and ion concentrations, electron speed, and, indeed, all the dependent variables remain nearly constant along the length of the column. For this reason it is the simplest part of the discharge to study, and it should be the simplest to understand though there is no general theory relating all dependent and independent variables.[1]

The power input per centimeter of a uniform column is equal to the voltage gradient times the current, and it follows from the nature of the column that the power dissipated in each element of length is equal to the input. The dissipation of power appears as heating of the tube walls, either directly or by conduction and radiation from

[1] Tonks and Langmuir, Phys. Rev., vol. 34, p. 876, 1929.

the gas, and as selective radiation of the atoms which is transmitted by the tube walls. The general statement is made in the Handbuch der Physik that the total radiation is a small fraction of the power input, but the experiments cited deal with gases which have their strongest radiation in the far ultra-violet and this is completely absorbed by the tube walls. Thus Crew and Hulburt [2] find that the total radiation emitted by a hydrogen discharge is about 1 per cent of the input, but they point out that about nine times the observed radiation is in the first Lyman line alone.

The alkali vapor spectra are the only spectra in which all the strong lines are transmitted by glass. The possibility of obtaining a high radiant efficiency is utilized in the Osram sodium lamp.[3] Under normal operating conditions (current density 1 amp. per cm^2) the lamp radiates about 9 per cent of the power input. This radiation is predominantly *D* lines and the luminous efficiency is probably higher than any other light source, though the figure for radiation efficiency is certainly not impressive. The fact is that the lamp has to be overloaded to a point of low efficiency to maintain a high tube temperature and vaporize the sodium. With one-tenth of the normal current and external heating a radiation efficiency of 70 per cent is observed.

There is no published work in which radiation measurements have been combined with detailed electrical measurements in the study of a discharge. Other phases of power dissipation have been treated by Langmuir and his associates in their comprehensive theoretical [4] and experimental [5] studies of the mercury positive column. An important factor is the flow of ions to the walls and their recombination on the walls. The fraction of the power dissipated in this way depends on the current and is small for low currents. Elastic collisions between electrons and atoms will give some energy to the atoms, but Killian has evaluated this loss and finds it negligibly small for the mercury arc. He concludes that power dissipated in inelastic collisions between electrons and atoms and radiated by the atoms must account for the balance of the power loss not accounted for by recombination on the walls. The conclusion seems entirely reasonable, though there is a possibility that the excited atoms dissipate some energy by collisions with normal atoms. The probability of dissipation of energy by collision (quenching) during the life of an excited state is undoubtedly small under most discharge conditions; but since the resonance radiation is very strongly absorbed, the radiation diffuses slowly through the gas by repeated absorption and emission. For this reason the small probability of quenching during the radiation life must be multiplied by a large and unknown factor to give the probability of quenching during the diffusion time.

This paper reports measurements of power input, radiation loss, and wall recombination loss in the positive column of a cæsium discharge. Tubes of one diameter 1.8 cm have been used, and the effect of the two remaining independent variables, vapor density, and current, have been studied. This work has been done in conjunction with a study of collision processes in the positive column which will be reported in another paper.

---

[2] Crew and Hulburt, Phys. Rev., vol. 29, p. 843, 1927.
[3] Kreft, Pirani, and Rompe, Tech. Wissenschaft Abhandl aus dem Osram Konzern, vol 2, p. 24, 1931.
[4] Tonks and Langmuir, General Theory of the Plasma of an Arc, Phys. Rev., vol. 34, p. 876, 1929.
[5] Killian, Uniform Positive Column of an Electric Discharge in Mercury Vapor, Phys. Rev., vol. 35, p. 1238, 1930.

II. ELECTRICAL MEASUREMENTS

Figure 1 illustrates the type of discharge tube used. A thermionic discharge from an oxide-coated platinum strip cathode was employed. Vapor pressure was controlled by a separate heater around the side tube containing the cæsium. Tubes were outgassed by baking and by running a discharge for four or five hours before sealing off from the pumps.

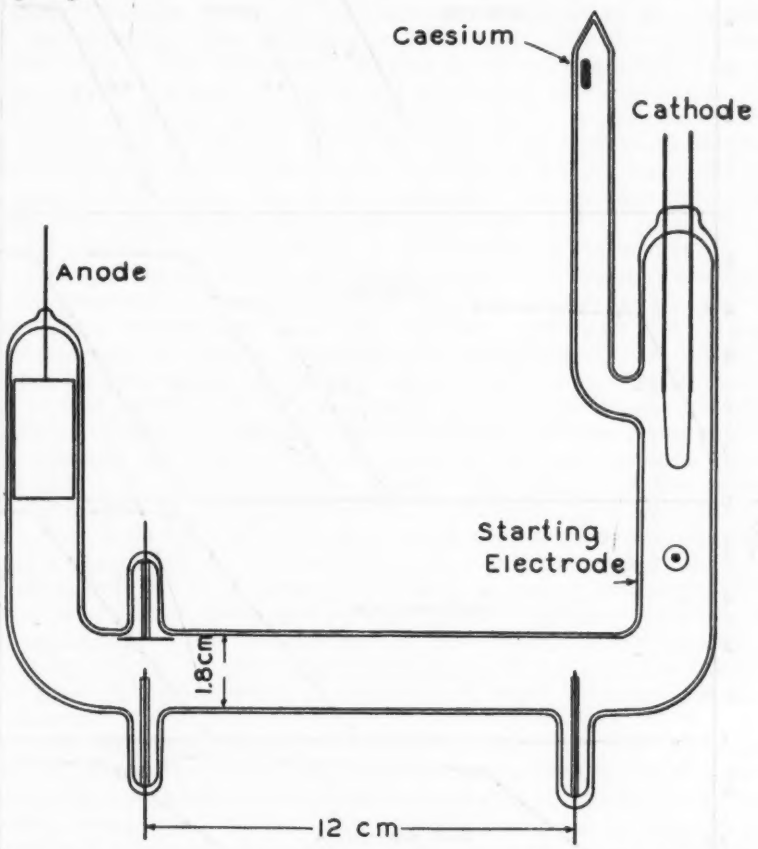

FIGURE 1.—*Discharge tube used in making power input and dissipation measurements*

The voltage gradient was measured between two small probes near the axis of the tube and 12 cm apart. For the lower pressure and current conditions the probes were platinum wires 0.4 mm in diameter and 2 mm long. For the higher currents the platinum wires were cut off flush with the insulating tube. In cæsium vapor difficulty is encountered from leakage over the insulating surfaces, and this was greatly reduced by avoiding a close fit between the insulating tube and the wire. Melting off of the small probes by the striking of an arc was a source of trouble. If a probe is too large the current may rise to a destructive value even at potentials negative to the space potential. The random space current becomes so large that

an electrode less than 0.01 cm² in area may rob the discharge and suddenly become the anode. The ion current to the walls was measured by a disk of platinum 1 cm in diameter which was bent to fit against the wall.

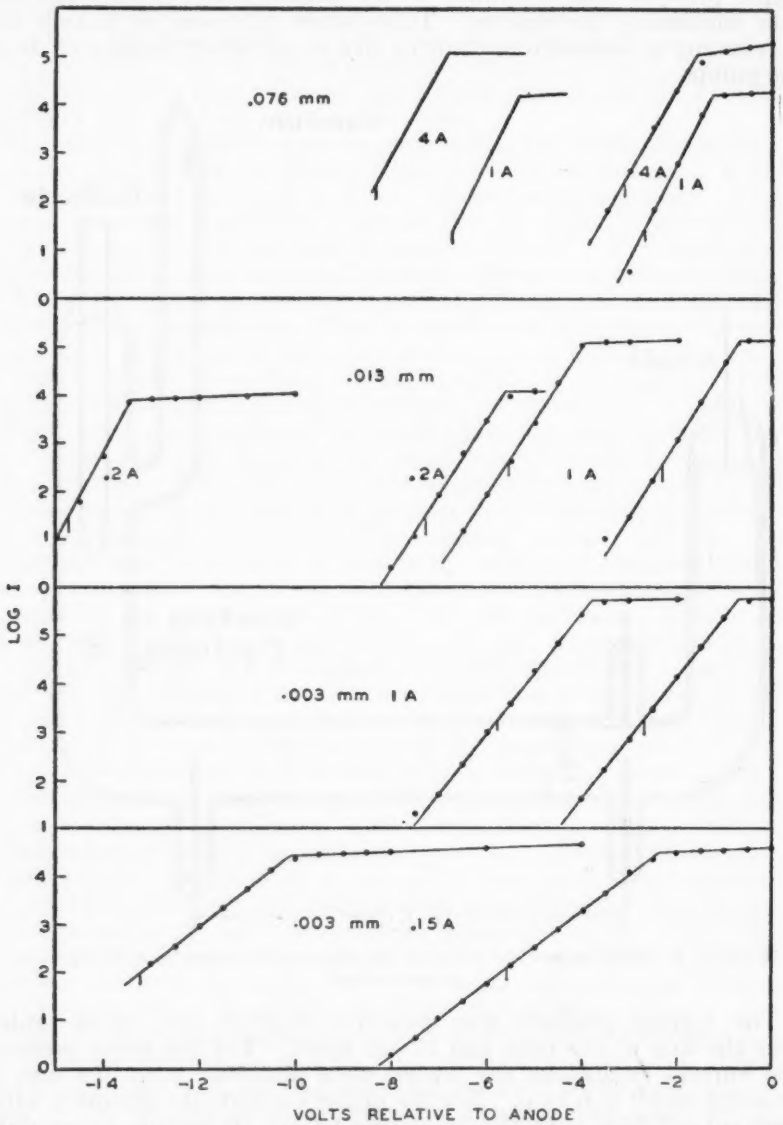

FIGURE 2.—*Log current voltage curves for the two small probes at the axis of the tube and 12 cm apart*

Vertical dashes mark the potentials of zero current.

Figure 2 gives plots of the log of the electron current to the small probes versus potential relative to the anode for several typical conditions. The plots are accurately linear for all conditions. The slope

of the left branch measures the electron energy; the intersection of the two branches measures the space potential. The slopes as measured by the two probes are equal within experimental error. The electron current to the disk also rises at the same rate, showing that the electron energy is the same at the center and at the wall. This has been shown before by Killian.[6]

The voltage difference between the probes can be obtained from the difference between the space potentials, or since the curves are parallel, it can be measured between the potentials of zero current. The two intervals agree within about 0.1 volt, while the difference is several volts. This difference, divided by 12 and multiplied by the current, gives the input in watts per centimeter of the column.

The power dissipated by flow of ions to the tube walls is equal to the ion current in amperes times the sum of the ionization potential (3.9 volts) plus the potential drop through which the ions fall, plus the energy in electron volts of the electrons. The leakage to the disk at negative potentials was always measurable, but in general small enough so that an extrapolation of the current voltage curve to the wall potential should involve no serious error. This current multiplied by the geometrical factor, 7.2, gives the ion current to 1 cm of the tube. The assumption that the current, corrected for leakage, measures pure ion current requires some justification. In many discharges the electron emission from negative electrodes is an important part of the current. This emission comes from photo-electric effect and from collision of excited atoms with the metal surface and in either case depends on whether the energy of the excited states is greater than the work function of the metal. The energy of the cæsium resonance state is 1.45 electron volts. Ives and Olpin [7] find that the minimum work function of a pure metal surface in cæsium is about equal to this, while the results of Boeckner and the author [8] on probe radiation indicate that platinum probes in a cæsium discharge have a high work function compared to other metals (well above 2 volts, but not measured). The consistency of the present measurements of power input and loss gives further evidence that no serious error has been made in interpreting the current at negative potentials as an ion current.

In the discharge space the random electron current is about a thousand times the ion current, and the insulating wall must take up a potential which draws the full ion current to it and limits the electron current to an equal value. The potential difference is limited to a thin sheath a fraction of a millimeter thick over the surface of the tube. There is also a small potential difference in the same direction between the space potential near the wall and at the center of the tube. Since the electrons have a Maxwell distribution of velocity, the small fraction of fast electrons which pass through the retarding field will reach the wall with the same distribution of velocity as the electrons in the field free space. The contribution of the electorn kinetic energy in electron volts (0.2 to 0.3 volt) is obtained from the semilog. plot.

$$V_0 = (V_2 - V_1)/(lnI_1 - lnI_2)$$

A rigorous measurement of the potential through which the ions fall

[6] Killian, Phys. Rev., vol. 35, p. 1238, 1930.
[7] Ives and Olpin, Phys. Rev., vol. 34, p. 117, 1929.
[8] Mohler and Boeckner, B. S. Jour. Research, vol. 7, p. 751, 1931.

would require a small probe at the wall which could be brought to the space potential. (The disk is much too big for this.) Then the difference between the potential of zero current and the space potential would give the potential drop in the sheath (about 2 volts). The average ion also falls through a potential drop somewhat less than the difference in space potentials near the walls and at the center of the tube, a matter of a few tenths of a volt. From a consideration of Killian's measurements it was evident that the difference between the space potential and potential of zero current at the center of the the tube was slightly larger than the potential drop across the wall sheath and less than the drop between the center of the tube and the wall. The error in using this potential drop instead of the true potential difference can only be 0.1 or 0.2 volt; and as the recombination energy is 6 or 7 electron volts, the use of another probe at the wall seemed unnecessary.

III. RADIATION MEASUREMENTS

The predominant lines in an alkali metal spectrum are the first doublet in the principal series, and in cæsium these lines fall in the near infra-red at 8,521 and 8,944 A. Nearly all other lines fall in a range transmitted by glass and water except the first doublet of the diffuse series near 36,000 and 35,000 A. As the tube is operated in a furnace at 250° to 300° C., the use of a water cell in making thermopile measurements was unavoidable and this far infra-red doublet was completely filtered out. The G. E. cæsium-oxygen-silver photo-electric cell is very sensitive to the resonance lines, and it was useful in evaluating the transmission of the water cell, tube walls, etc. A disk thermopile 0.5 cm in diameter was used.

The procedure was as follows: The thermopile was calibrated without the water cell or any window against a radiation standard. It was then exposed through a water cell and furnace window to the cæsium radiation from the full width and a 10 cm length of the positive column. The galvanometer deflection of 3 or 4 cm could be measured with sufficient precision by averaging many observations. It was inconveniently small for routine measurements, so the deflection of the direct radiation was compared with the deflection produced when the radiation from a 1 cm length of the tube was focused by a short focus lens so that the entire image fell on the thermopile. The transmission of the tube wall, furnace window, and water cell for the cæsium radiation were measured by the photo-electric cell. It was assumed that the radiation from the discharge was equal in all directions. Two independent calibrations before and after the series of experiments gave values of 2.13×10^{-2} and 2.18×10^{-2} watts per centimeter galvanometer deflection per centimeter of the column for the total radiation.

An experiment was made on the absorption of the cæsium radiation by a 4 cm cell of cæsium vapor. With the discharge vapor pressure 0.004 mm, the cell containing vapor at about ten times that pressure reduced the photo-electric effect to less than one-tenth. As the vapor is perfectly transparent to all lines except the principal series lines, this shows that most of the energy is in the resonance lines. Photographs of the spectrum indicate that these lines remain predominant at all pressures. Radiation measurements were made before and after

a series of electrical measurements with no evidence of any error appreciable in comparison with the electrical measurements or with the error in optical adjustments when tubes were changed.

IV. RESULTS

Discharges operated with a voltage drop ranging from 5 to 15 volts. It was found that a large change in the battery voltage with a compensating change in the series resistance to give equal current did not change the radiation by 0.1 per cent. Also a change in the voltage drop in the tube produced by changing the cathode temperature had no effect. Currents ranged from 0.15 to 4 amperes; pressures from 0.001 to 0.3 mm. The low pressure limit was set by the dark space approaching the probe nearest the cathode.

Figures 3 and 4 show the power input; P, the power dissipated by recombination; W, the radiation; R, and P-W as functions of the pressure and the current. With currents of 0.2 amp. practically all the power input is radiated. With currents of 1 amp. or less and pressures less than 0.03 mm, P-W is nearly equal to R; that is, the power input is nearly all accounted for. The mean value for all measurements in this range gives

$$R/(P\text{-}W) = 0.95 \pm 0.04$$

where 0.04 is the mean error and does not include the calibration error. With increasing current and pressure there is a rapidly increasing difference between P-W and R. A plot of this unexplained residual is given as a function of the current for various pressures in Figure 5. Up to 0.013 mm the residual is independent of the pressure, but above this point increases roughly in proportion to the pressure. The experimental uncertainty is relatively large for this residual.

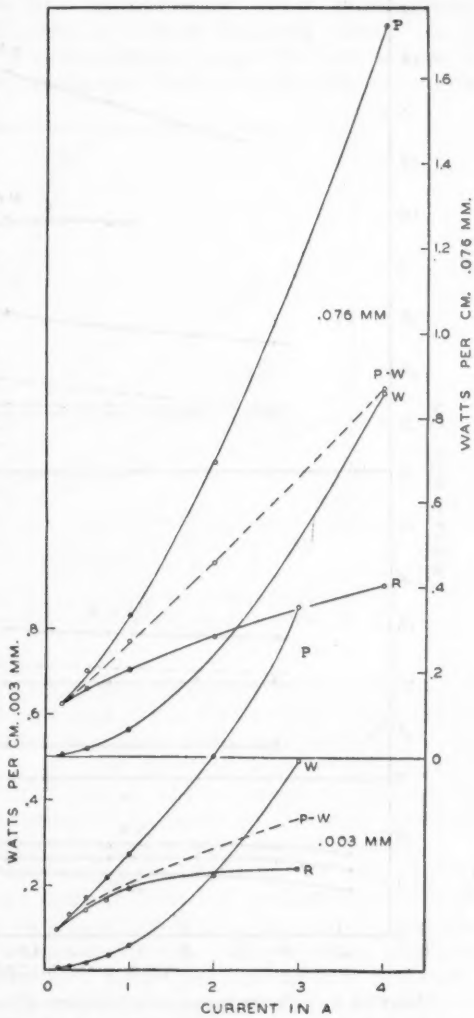

FIGURE 3.—*Power terms as a function of current*

(*P*, input; *W*, recombination; *R*, radiation.)

V. CONCLUSIONS

Little can be said as yet about the factors determining the form of the curves of Figures 3, 4, and 5. With increasing current the gradient at first decreases and then increases and correspondingly the input curve of Figure 3 changes. The rapid increase at higher currents

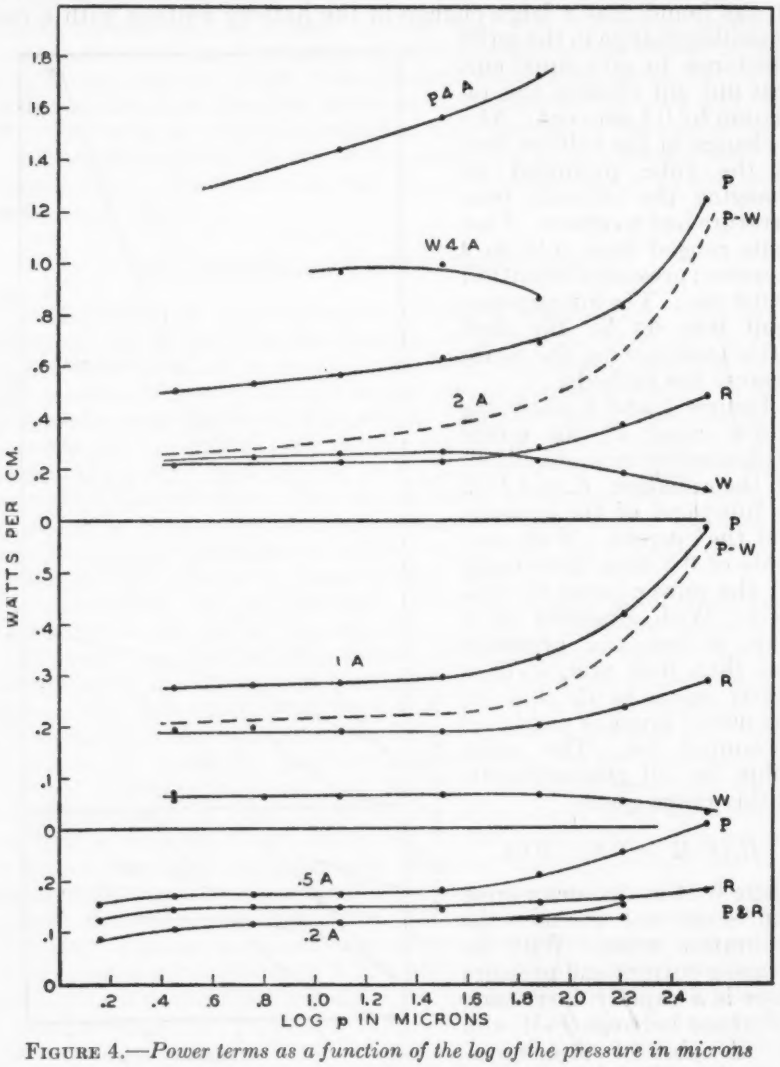

FIGURE 4.—*Power terms as a function of the log of the pressure in microns*

comes in part from the recombination loss and in part from the unknown residual. The variation in recombination loss, W, depends largely on the ion current, for the energy per ion changes very slowly. The ion current is roughly proportional to the electron concentration. The striking feature of Figure 4 is the very slow variation of all power terms with pressure. The measurements cover a 300-fold range of

pressure, and over half of this range the variation is scarcely more than the experimental error. An appreciable variation is evident with high pressures and high currents, and the unknown residual effect is an important factor in this. The fact that there is an unexplained balance in the power equation is not surprising. We have mentioned in the introduction several other sources of power loss; the unmeasured far infra-red radiation, the dissipation of energy by elastic collisions, and the quenching of resonance radiation by interatomic collisions, and there are undoubtedly other possibilities. The evidence is as yet insufficient to choose between them. It is reassuring to find that over a considerable range the power loss is predominantly radiation of the resonance lines and recombination on

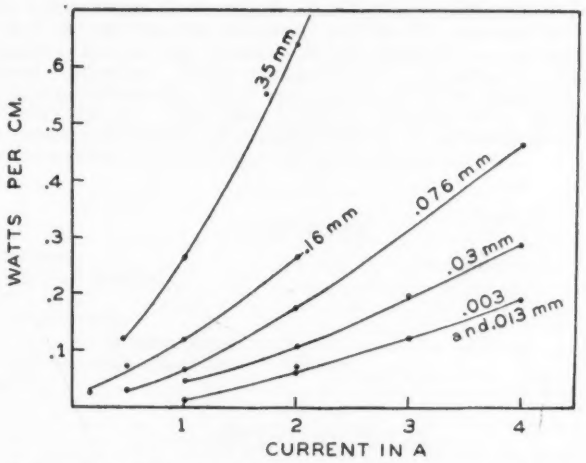

FIGURE 5.—*Balance of the power loss not accounted for by recombination and radiation (P-W-R) as a function of the current*

the walls. It suggests that an approximate theory can be developed which considers production of ions and of the first excited state exclusively and that other phenomena can be treated independently. In this connection it is of interest to note that the visible spectrum of cæsium involving higher excited states shows large variations in intensity and intensity distribution in contrast to the very gradual change of the total radiation which is largely resonance radiation.

The published figures on the radiation efficiency of the Osram sodium lamp referred to in the introduction are consistent with our results, though the data refer to the entire discharge rather than the positive column, so that the values are lower. The cæsium positive column, with a current density of 1 amp. per cm^2 at low pressure, radiates 28 per cent of the power and at 0.1 amp. per cm^2 the radiation is 96 per cent as compared with the overall efficiencies of 9 and 70 per cent for the sodium discharge. Evidently the alkali discharges are qualitatively similar in their characteristics.

Alkali vapor discharges of the type used in this work may have useful applications as sources of intense monochromatic radiation. The intensity of this radiation is insensitive to pressure and current

variations, so that a very accurate control of intensity is possible. The fact that the efficiency of production of radiation can be made almost unity is of little practical value, since the high efficiency is attained only by keeping the power input and brightness low.

WASHINGTON, April 11, 1932.

RP456

THERMAL EXPANSION OF SOME SILICATES OF ELEMENTS IN GROUP II OF THE PERIODIC SYSTEM

By R. F. Geller and Herbert Insley

ABSTRACT

A ceramic body having the unusually low average coefficient of linear thermal expansion of 0.53×10^{-6} in the range 0° to 200° C., reported by W. M. Cohn, was investigated, and it was found that this material is composed essentially of the mineral cordierite. The investigation was amplified to include thermal expansion determinations for some compounds of other elements in Group II of the periodic system. The data obtained indicate that zinc orthosilicate, celsian and beryl appear worthy of consideration by those interested in the development of bodies having low coefficients of thermal expansion.

CONTENTS

	Page
I. Introduction	35
II. Materials and methods	35
III. Results	40
1. Cordierite	40
(a) General comments	43
2. Compounds other than cordierite	44
IV. Summary	46

I. INTRODUCTION

A ceramic body having the unusually low coefficient of linear therma. expansion of 0.53×10^{-6} in the temperature range 0° to 200° [1] has been reported by W. M. Cohn.[2] Science and industry are searching continually for compositions of low thermal dilatation, and applications of otherwise satisfactory materials may be hindered by their comparatively large volume changes when heated and cooled. For this reason, the ceramic body reported by Cohn is of particular interest.

The present report contains the results of a short study in which Cohn's findings are duplicated. The study was amplified to include linear thermal expansion determinations for some silicates of other elements in Group II of the Periodic Table.

II. MATERIALS AND METHODS

The specimens of series A (Table 1) were made of a body composed of 43 per cent talc (approximately 95 per cent $3MgO\cdot4SiO_2\cdot H_2O$), 35 per cent Florida kaolin (93 to 95 per cent kaolinite), and 22 per cent electric furnace corundum (99 per cent Al_2O_3) dry sieved through a No. 200 sieve. This body was intended as a duplicate of

[1] Temperatures are given in °C., throughout this report.
[2] Ber. der Deut. Ker. Gesell., vol. 10, p. 271, June, 1929, and vol. 11, p. 62, February, 1930, and Ann. Physik, vol. 4, p. 493, 1930.

the body described by Singer [3] as typical of those investigated by Cohn.

The specimens of series B (Table 1) were made of a body composed of 39.5 per cent talc, 47.2 per cent Georgia kaolin (96 to 98 per cent kaolinite), and 13.3 per cent anhydrous Al_2O_3 obtained by heating reagent quality aluminum nitrate.

The specimens of series C (Table 1) were made of a wet ground mixture of 24 per cent of reagent quality basic magnesium carbonate ($Mg(OH)_2 \cdot (MgCO_3)_4$), 45 per cent of potters' flint less than 10μ in size, and 31 per cent of Al_2O_3 obtained as described for series B.

No attempt was made to produce specimens containing only one crystal phase. Specimens containing a minimum of 90 per cent of the crystalline compound investigated, as determined by petrographic examination, were considered of sufficient purity to establish the approximate thermal expansion of that compound.

Unless otherwise stated, the various heat treatments described in Tables 1 and 2 and in the text were made in electrically heated furnaces, the resistors being 80 per cent platinum-20 per cent rhodium wire.

Expansion determinations were made by the interferometer method.[4] The specimens of series A and B (Table 1) were molded and heated in the form of disks about 2 cm in diameter, 0.3 cm in thickness, and with a hole through the center about 0.7 cm in diameter. Three small cones or "feet" protruded from opposite points on each side. The over-all height varied between 0.50 and 0.75 cm. Irregularly shaped pieces, approximately pyramidal in form and from 0.50 to 0.75 cm in height, were used for expansion determinations of the other materials investigated; three such pieces were used for each determination. The rate of temperature change during both heating and cooling tests did not as a rule exceed 3° per minute, and for most of the tests was maintained at from 1° to 2° per minute.

[3] Ber. der Deut. Ker. Gesell., vol. 10, p. 269, June, 1929.
[4] Fizeau, Ann. d. Phys., vol. 128, p. 564, 1866. C. G. Peters and C. H. Cragoe, B. S. Sci. Paper No. 393, 1920. G. E. Merritt, B. S. Sci. Paper No. 485, 1924.

TABLE 1.—*Thermal expansion determinations of bodies composed essentially of "cordierite," $2MgO \cdot 2Al_2O_3 \cdot 5SiO_2$*

[All temperatures in ° C.]

Specimen No.	Composition, determined petrographically	Preparation	Test No.	Linear thermal expansion, expressed as average coefficient [1]			
				R. T.[2] to 100°	R. T.[2] to 200°	Miscellaneous	
						R. T. to—	Coefficient
				$\times 10^{-6}$	$\times 10^{-6}$	°C.	$\times 10^{-6}$
A–1[3]	A, corundum, inclusions in phase C B, crystalline grains with tendency to elongated forms and corroded surfaces. Index between 1.60 and 1.65; probably forsterite. C, cordierite, $2MgO \cdot 2Al_2O_3 \cdot 5SiO_2$. Constitutes the ground mass of the body; low double refraction, twinning common; mean index about 1.53.	Body A. Held at 1,350° for 1 hour	1	0.7	1.1	560	1.9
A–15	Measurably less corundum than in A–1; it occurs as inclusions in the cordierite which constitutes the balance of the body.	Body A. Held at 1,350° for 16 hours	1	.5	.8	660	1.6
A–15a	do	Specimen A–15. Reheated at 950° to 960° for 13 days. Maximum temperatures reached in preceding tests: 310°; 203°; 313°; 505°.	5	.4	.8	400	1.3
A–17	do	Body A. Held at 1,300 to 1,350° for 67 hours. Maximum temperatures reached in preceding tests: 323°; 538°.	3	.2	.5	365	.9
A–3	Approximately 90 per cent cordierite and 10 per cent inclusions, largely corundum.	Body A. Heated in a gas-fired kiln at approximately 1,350° for 3 days and permitted to cool in the kiln.	1			75	−.2
						400	+.9
						75–400	1.0
A–3a [4]	do	Rods approximately 1¼ cm in diameter and 30 cm long. Preparation same as A–3.	1			75	−.3
						400	+.8
						75–400	1.0
B–2	90 per cent or more cordierite, balance corundum and a small amount of what appears to be enstatite.	Body B. Heated at 1,345° for 45 hours	1	.5	.9	308	1.1
B–2a	A, cordierite 85 to 90 per cent of total; index 1.53+. Present as well developed grains, larger than in preceding sample. B, spinel occurring as inclusions in phase A C, very small amount of mullite as groups of fine needles in phase A.	Specimen B–2. Reheated at 1,410° for 17 hours. Maximum temperature reached in test No. 1, 211°.	2		.5	55	−.1
						55–100	+.2
						604	1.3

[1] Values derived from observations on heating.
[2] R. T.=Room temperature; varied from 20° to 28°.
[3] Chemical analysis by J. F. Klekotka showed SiO_2, 40.7 per cent; R_2O_3, 43.1 per cent; MgO, 15.2 per cent; CaO, 0.05 per cent; ignition loss, 0.15 per cent.
[4] Expansion determined by P. Hidnert using the apparatus and method described in Bureau of Standards Scientific Paper No 524 (1926) by W. Souder and P. Hidnert. R. T.=25°.

TABLE 1.—*Thermal expansion determinations of bodies composed essentially of "cordierite," $2MgO \cdot 2Al_2O_3 \cdot 5SiO_2$*—Continued

[All temperatures in °C.]

Specimen No.	Composition, determined petrographically	Preparation	Test No.	Linear thermal expansion, expressed as average coefficient [1]			
				R. T. to 100°	R. T. to 200°	Miscellaneous	
						R. T. to—	Coefficient
				$\times 10^{-6}$	$\times 10^{-6}$	°C.	$\times 10^{-6}$
C-1	Composed of at least 90 per cent cordierite; index 1.53. The balance is made up of forsterite in irregular, partly dissolved crystals and of corundum in minute rounded grains.	Reagent quality materials. Heated at 1,425° for 20 minutes, ground to pass 80 mesh and reheated at 1,425° for 2 hours.	1	0.5	0.9	400	1.3
C-1a	do	Portion of C-1. Reheated at 750° to 800° for 2 weeks	1		.9		
C-1b	do	Portion of C-1. Reheated at 950° for 4 days. Maximum temperature of test No. 1, 215°.	2		2.4		
C-2a	do	Portion of C-1. Reheated at 890° to 920° for 24 hours	1		1.6		
C-2b	do	Specimen C-2a. Reheated at 1,025° to 1,050° for 3 days	1		1.9		
C-2c	do	Specimen C-2b. Reheated at 1,120° to 1,150° for 2 days	1		2.0		
C-2d	do	Specimen C-2c. Reheated at 1,300° to 1,380° for 3 days	1		1.0		
C-3	Composed of cordierite of index 1.52+ and approximately 20 per cent of an undetermined constituent of index above 1.56 present as fibrous bundles (mullite?) growing from nuclei (corundum?) and always occurring as inclusions in the cordierite.	C-1. Melted at, and quenched from, 1,550° C. Devitrified at 1,100°, time 54 hours. Maximum temperature of test No. 1, 252°.	2	.6	1.0	265	1.1
C-4	Similar to C-3 except that the fibrous crystals appear to be somewhat better developed.	Portion of glass from C-3 devitrified at 1,355°, time 70 hours. Maximum temperatures of preceding test, 392°; 231°; and 440°.	4	−.5		100–200 100–330	.3 .6
C-5	Practically complete devitrification to "unstable" $2MgO \cdot 2Al_2O_3 \cdot 5SiO_2$ of index 1.54+. The ternary compound constitutes 90 to 95 per cent of the total; balance fibrous growths similar to those in C-3.	Portion of glass from C-3 devitrified at 900°; time 4½ days.	1	3.4	4.0	317	4.0
D	Some mineral matter other than cordierite present. Occurs as extremely minute prismatic crystals of relatively high index, frequently concentrated along runlets.	Mineral from Orijerfoi, Finland. Supplied by U. S. National Museum, specimen No. 78238. Material is not uniform. Values reported were selected from three duplicate tests.	1	.5	.9	300	1.2

TABLE 2.—*Thermal expansion determinations of some compounds containing elements in Group II (periodic table), including compounds of*

TABLE 2.—*Thermal expansion determinations of some compounds containing elements in Group II (periodic table), including compounds of magnesium other than cordierite*

[All temperatures in ° C.]

Specimen No.	Composition, determined petrographically	Preparation	Test No.	Linear thermal expansion, expressed as average coefficient [1]			
				R. T.[2] to 100°	R. T.[2] to 200°	Miscellaneous	
						R. T. to—	Coefficient
				$\times 10^{-6}$	$\times 10^{-6}$	°C.	$\times 10^{-6}$
E	Forsterite, 80 to 85 per cent $2MgO \cdot SiO_2$	Fusion in electric arc of talc and magnesium carbonate. Maximum temperature of test No. 1, 138°.	2	7.2	8.0	304	8.3
F	Spinel, at least 90 per cent $MgO \cdot Al_2O_3$, balance glass and birefracting material, probably clinostatite or forsterite.	Specimen cut from commercial brick and twice reheated to 1,800° C. Expansion determined by R. A. Heindl (B. S. Technical News Bulletin No. 152, December, 1929).				1,400	8.6
G [3]	Beryl, indices, ω, 1.580; ϵ, 1.573 ($3BeO \cdot Al_2O_3 \cdot 6SiO_2$).	Mineral from San Jose de Bujauba, Minas Geraes, Brazil. U. S. National Museum specimen No. 94218. Maximum temperature of test No. 1, 460°.	2			53 225	−.2 +.5
G-a [4]	do	Mineral from San Jose de Bujauba, Minas Geraes, Brazil. U. S. National Museum specimen No. 94218. Maximum temperatures of preceding tests, 460°, 225°.	3	1.6		225 300	2.1 2.3
H [3]	do	Mineral from Royalston, Mass. U. S. National Museum specimen No. 16626. Maximum temperature of test No. 1, 196°.	2	.3	.7	260	.9
I [3]	do	Mineral from Brazil. U. S. National Museum specimen No. 44586. Maximum temperature of test No. 1, 185°.	2	.3	.7	265	1.0
J [3]	Beryl, indices, ω, 1.588; ϵ, 1.580	Mineral from San Diego County, Calif. U. S. National Museum specimen No. 93926.	1	.9	1.3		
J-a [4]	do	Mineral from San Diego County, Calif. U. S. National Museum specimen No. 93926. Maximum temperature of preceding test, 200°.	2	1.6		225 300	2.2 2.2
K	Zinc orthosilicate, approximately 95 per cent $2ZnO \cdot SiO_2$, balance glass.	Prepared by E. N. Bunting (B. S. Jour. Research, vol. 8 (2) (R. P. 413), p. 279, 1932), and obtained by devitrification. Melting point, 1,510° C.	1	.8	1.2	350	1.6
L	Zinc aluminate, 38 per cent ZnO, 55 per cent Al_2O_3, balance mostly oxides of iron.	Mineral supplied by U. S. National Museum. Maximum temperature of test No. 1, 240°.	2	6.4	7.3	525	7.7
M	Celsian, approximately 90 per cent $BaO \cdot Al_2O_3 \cdot 2SiO_2$.	$BaCO_3$ and kaolin heated for 2½ hours at from 1, 550° to 1,580° C.	1	2.7	3.1	400	3.4
N	Anorthite, approximately 95 to 97 per cent $CaO \cdot Al_2O_3 \cdot 2SiO_2$.	Repeated heating of reagent quality materials (at temperatures about 50° below the melting point of anorthite) and regrinding. Prepared in the cement section of the Bureau of Standards.	1	3.5	4.0	300	4.3
O	Dicalcium aluminum silicate, approximately 95 per cent $2CaO \cdot Al_2O_3 \cdot SiO_2$ in well-formed crystals.	Reagent quality materials wet ground. Reheated twice, maximum temperatures 1,300° and 1,570°, respectively. Prepared by H. Insley.	1	7.3	8.0	400	8.1
P	Calcium metasilicate, >95 per cent α $CaO \cdot SiO_2$	Same as specimen N	1	10.9	11.7		
Q	Corundum, over 99 per cent Al_2O_3	Commercial electric furnace product	1	5.9	7.1	600	7.9
R	Mullite, almost entirely $3Al_2O_3 \cdot 2SiO_2$; a small per centage of glass and corundum present.	Fusion of alumina and silica. Expansion determined by R. A. Heindl (B. S. Tech. News Bull. No. 139, November, 1928).				1,100	5.3

[1] Derived from observations on heating. [2] R. T. = Room temperature; varied from 20° to 28°. [3] Parallel to c axis. [4] Perpendicular to c axis.

TABLE 3.—*Values indicating reproducibility of results*

Values given are the total expansion in μ per meter from room temperature to t_o

Specimen No.	t_o °C.	First test	Second test	Third test	Fourth test
		μ	μ	μ	μ
A-17	100	5	15	15	15
	155	60	60	50	45
	255	170	150	140	----

t_o °C.	A-1[1]		A-3[1]		C-1[1]	
	(a)	(b)	(a)	(b)	(a)	(b)
100	50	45	10	5	40	40
200	200	195	80	90	150	160
300	365	380	180	190	295	305
400	590	610	----	----	480	500
560	1,000	1,020	----	----	----	----

[1] Duplicate specimens.

The reproducibility of results is indicated by the data in Table 3.

III. RESULTS

1. CORDIERITE

The first expansion determinations were made on specimens of body A. Results are summarized in Table 1 and shown graphically in Figure 1. Since cordierite ($2MgO \cdot 2Al_2O_3 \cdot 5SiO_2$)[5] was the predominant phase in all of the specimens of the A series, the next series (B and C, Table 1) were prepared of mixtures in the proper proportions to produce this compound. However, in no case did the product contain more than approximately 90 to 95 per cent of cordierite. When heated at about 1,350° the principal impurities in the talc bodies (A–3, Table 1) were corundum (Al_2O_3) and forsterite ($2MgO.\ SiO_2$), while heating at higher temperatures for long periods of time (B–2a) evidently produced some decomposition of the ternary compound with the resultant formation of small amounts of spinel ($MgO \cdot Al_2O_3$) and mullite ($3Al_2O_3 \cdot 2SiO_2$). Prolonged heating of the specimens of series C also promoted the growth of bundles of fibrous crystals, apparently mullite, which originated from minute rounded grains of corundum.

Thermal expansions of the minor constitutents (forsterite, spinel, corundum, and mullite) were determined by test or taken from values given in the literature (Table 2). Their expansions are all considerably higher than the expansions of the specimens which are composed predominantly of "cordierite" (as distinguished from the "unstable" forms of $2MgO \cdot 2Al_2O_3 \cdot 5SiO_2$ by refractive indices and other optical properties)[6] and there was no indication of contraction during heating below 100° for these materials. It is believed that the low expansions observed are characteristic of bodies composed essentially of cordierite.

[5] G. A. Rankin and H. E. Merwin, Am. J. of Sci., vol. 45, p. 301, 1918. E. A. Wulfing and L. Oppenheimer, Ber. der Heidl. Akad. der Wissen, No. 10, 1914.

[6] See footnote 5.

The difference in expansion of specimens A–3 and C–1 (Table 1), both of which contain about 90 per cent cordierite, can not be explained satisfactorily as due to the effect of the impurities alone. That there may be undetermined differences in the crystal structure

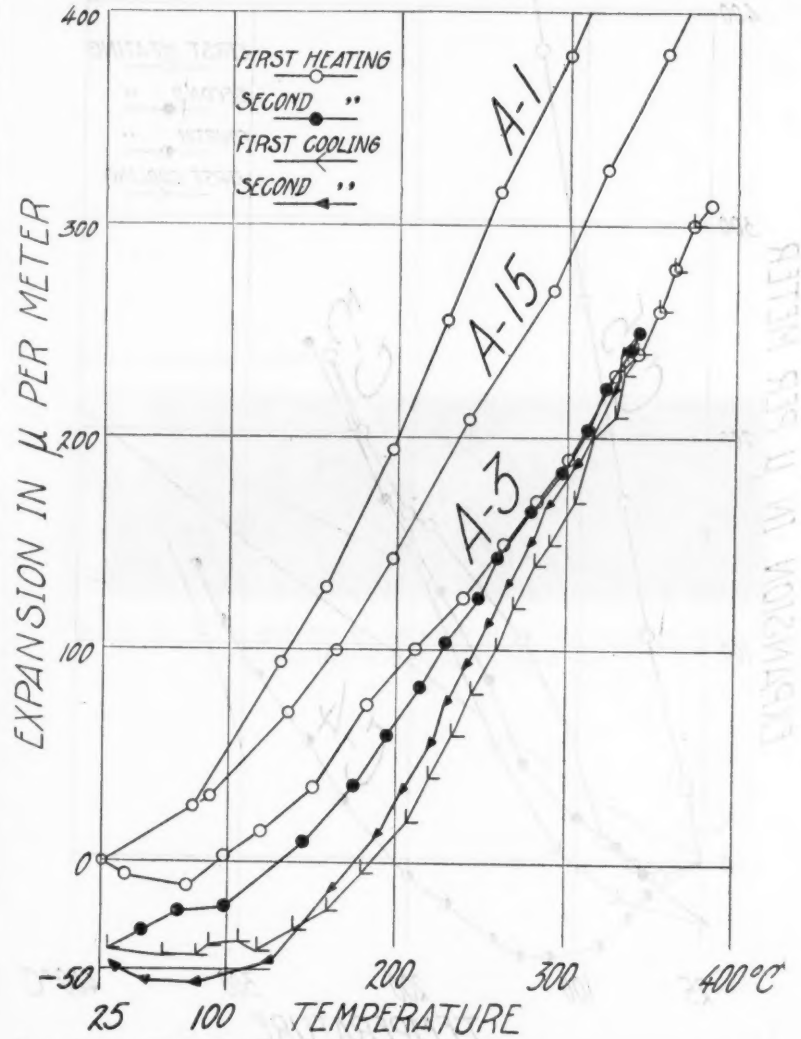

FIGURE 1.—*Thermal expansion curves for cordierite specimens of series A heated at 1,350° C. for one hour (A–1), 16 hours (A–15), and for 3 days (A–3)*

or composition of the cordierite is indicated by Rankin and Merwin,[7] who have observed considerable difference in indices of refraction of the cordierite from samples which appear optically homogeneous, but which vary somewhat in composition. This they attribute to solid solution of SiO_2 in the cordierite. Slight difference in the indices

[7] See footnote 5, p. 40.

of refraction were observed in some of the samples of cordierite used in this investigation, as is evidenced by B–2a and C–3.

The "unstable" form (C–5) with the composition $2MgO \cdot 2Al_2O_3 \cdot 5SiO_2$ was obtained by the method used by Rankin and Merwin;[8] that is,

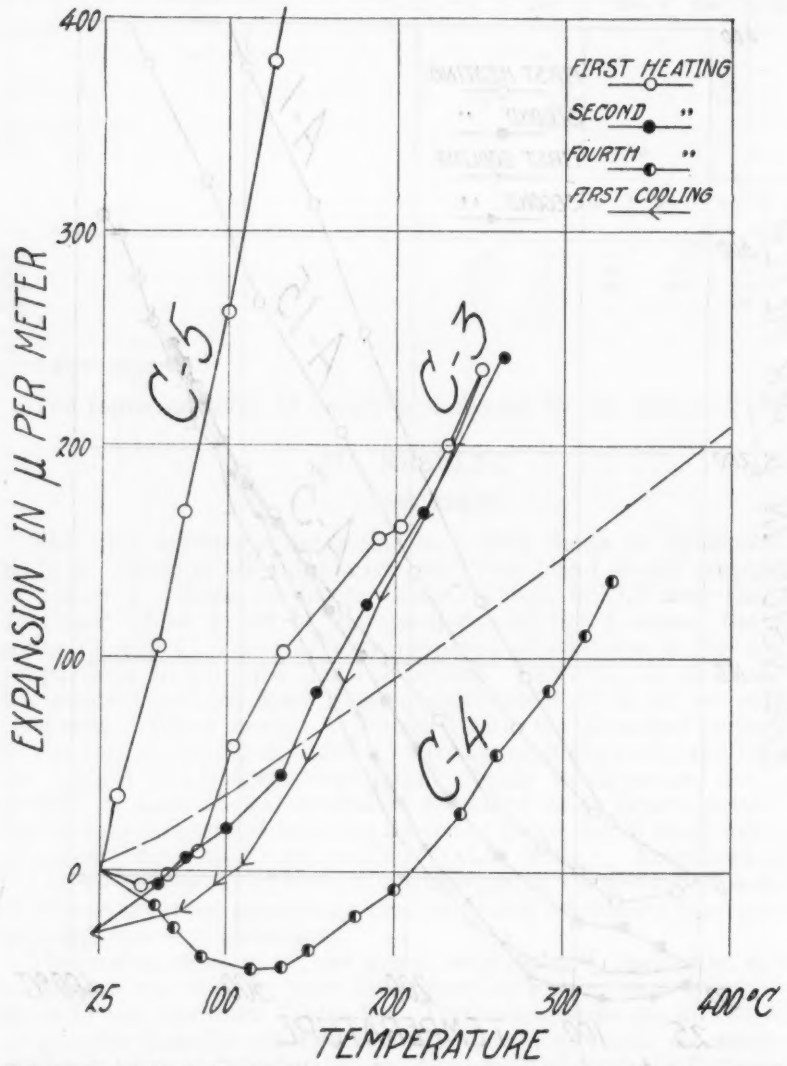

FIGURE 2.—*Thermal expansion curves for cordierite specimens of series C prepared from the glass by devitrification at 900° C. (C–5), 1,100° C. (C–3, and 1,355° C. (C–4)*

The dashed line is for fused quartz and is drawn from data in B. S. Sci. Paper No. 524.

by heating a glass of the same composition at about 900° for a considerable time. The product obtained corresponds in indices of refraction and other optical properties to that described by them. Its

[8] See footnote 5, p. 40.

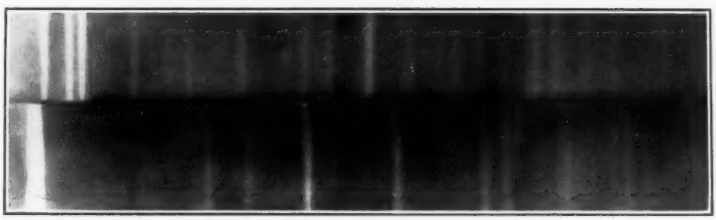

FIGURE 3.—*X-ray patterns of the stable (top) and unstable (bottom) forms of* $2MgO \cdot 2Al_2O_3 \cdot 5SiO_2$ *(cordierite)*

UNIV OF MICH

thermal expansion (C–5, Table 1 and fig. 2) is unquestionably considerably higher than that of cordierite. The increased expansion of specimens C–1b and C–2c after reheating at from 900° to 1,150° could not be duplicated with the talc body A–15. This increased expansion can not be attributed to the unstable form of the 2:2:5 compound, because neither petrographic examinations nor X–ray patterns of the reheated specimens C–1b and C–2c showed its presence. That the X–ray photograph would have shown the pattern of the unstable compound, if present in sufficient quantity to affect the expansion, seems probable from the marked difference in the two patterns. (Fig. 3.)

The small permanent contraction of about 40μ per meter evidently caused by the first heating (specimen C–3 in fig. 1) is characteristic of this form and in one case was noted to a lesser degree (5μ to 10μ per meter) after a specimen (A–17) had been heated and cooled four times. It was also noted that the cordierite specimens may have a slightly higher rate of contraction during cooling than of expansion during heating, in the temperature range above 100°, even though there is no measurable permanent length change. This is typified by the second heating and second cooling curves for A–3. (Fig. 1.)

The results do not permit the presentation of thermal expansion curves, or of coefficients, as correct for a compound of the definitely determined composition $2MgO{\cdot}2Al_2O_3{\cdot}5SiO_2$. It is fairly evident, however, that (*a*) the crystalline phase observed as constituting the bulk of the specimens of series A, B, and C is the same as the stable form of the ternary compound identified by Rankin and Merwin [9] having the approximate composition 2:2:5; (*b*) the thermal dilatation of this stable form of the ternary compound is remarkably low; it may contract slightly during heating from about 20° to 80°; and the average linear expansion, when heated from 20° to 400°, is about 1 μ per meter per °C. (equivalent to a coefficient of 0.000001); (*c*) the average linear change for the temperature range of 20° to 100° is much lower than for any other equivalent range; and (*d*) the expansion of the specimen of the unstable form tested is unmistakably higher than that of the stable.

(a) GENERAL COMMENTS

The specimens of series A and B were uniformly light buff to gray in color and of a firm but open texture. The gain in weight (water absorption) of an A–3a specimen (Table 1) resulting from autoclaving it in water for one and one-half hours at a steam pressure of 150 lbs./in.^{2} was 25.8 per cent; there was no measurable length change or "moisture expansion" over a 10 cm length. The specimens of series C prepared either by devitrification, or by heating at 1,425°, resembled opaque white glass which was very difficult to pulverize with mortar and pestle, and pieces could be heated to a red heat and plunged into cold water without being visibly affected. Specimens of the glass (series C) heated at 900° for five hours or less showed no devitrification. Heating at 900° for four and one-half days produced the unstable, or high expanding, form (C–5, fig. 2) and heating at 950° for two days (or at higher temperatures, C–3 and C–4, fig. 2) produced the stable form. At 1,380° the glass devitrified completely to the stable form in 15 minutes.

[9] See footnote 5, p. 40.

2. COMPOUNDS OTHER THAN CORDIERITE

Of the other compounds investigated (Table 2 and figs. 4 and 5) the three having the lowest average expansion are beryl (*G*, *H*, *I*, and *J*), zinc orthosilicate (*K*), and celsian (*M*). The data for the four specimens of beryl are presented in some detail, partly because of their very low expansions and partly because beryl has received some attention, as a material of low thermal expansion, from previous investigators.[10] Both cordierite and beryl may contract slightly when heated from 20° to 100° and their average coefficients are not greatly different. However, on first heating and cooling beryl it is likely to show a permanent expansion of 30 to 40 μ per meter. The expansion

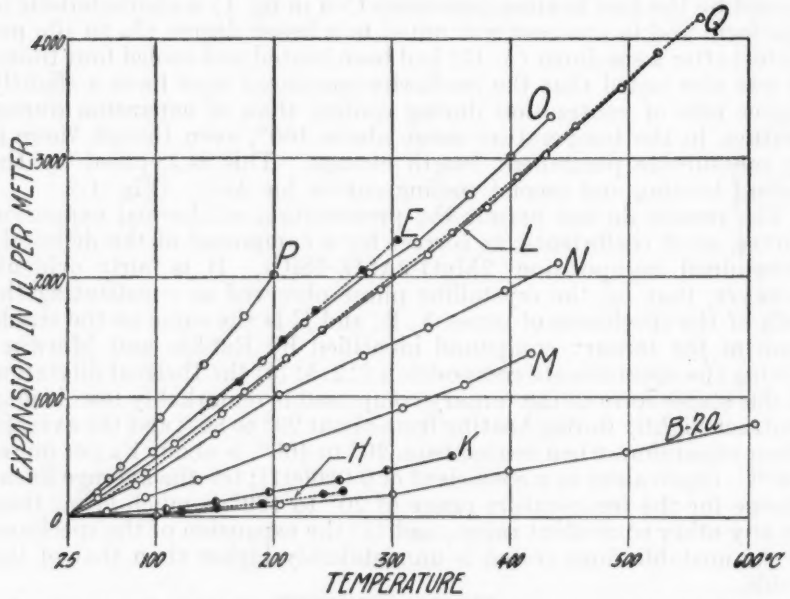

FIGURE 4.—*Thermal expansion curves of some of the materials described in Table 2, E, forsterite; K, zinc orthosilicate; L, zinc aluminate; M, celsian; N, anorthite; O, dicalcium aluminum silicate; P, calcium metasilicate*

Curves for a cordierite specimen (B–2a, Table 1) and for a beryl specimen (*H*) are included for comparative purposes.

curves for the "stabilized" specimens (that is, curves obtained after two or more tests) are given in Figure 5. Worthy of note are (*a*) the similarity in behavior of specimens *G*, *H*, and *I*, which have the same indices (Table 2); (*b*) the somewhat higher rate of expansion of J, which has higher indices; and (*c*) the fact that the expansion perpendicular to the *C* axis is relatively much higher than the expansion parallel to the same axis and is practically identical for both *G* and *J* specimens.

Several attempts to produce a specimen composed chiefly of some one crystalline silicate of cadmium (which has the same crystal habits as zinc, magnesium, and beryllium) were unsuccessful. The proper

[10] H. Fizeau, Compt. rend., T. LXVI, p. 1005, 1868. A. V. Bleininger and F. H. Riddle, J. Am. Ceram. Soc., vol. 2, p. 564, 1919. Robert Twells, jr., J. Am. Ceram. Soc., vol. 5, p. 228, 1922.

mixture of CdO and SiO_2 to form $CdO \cdot SiO_2$, when heated at 1,425° showed no evidence of reaction; after heating at 1,550° there was evidence of reaction, but the material rapidly fell to a powder when removed from the furnace. A mix to form $2CdO \cdot SiO_2$ was heated to a

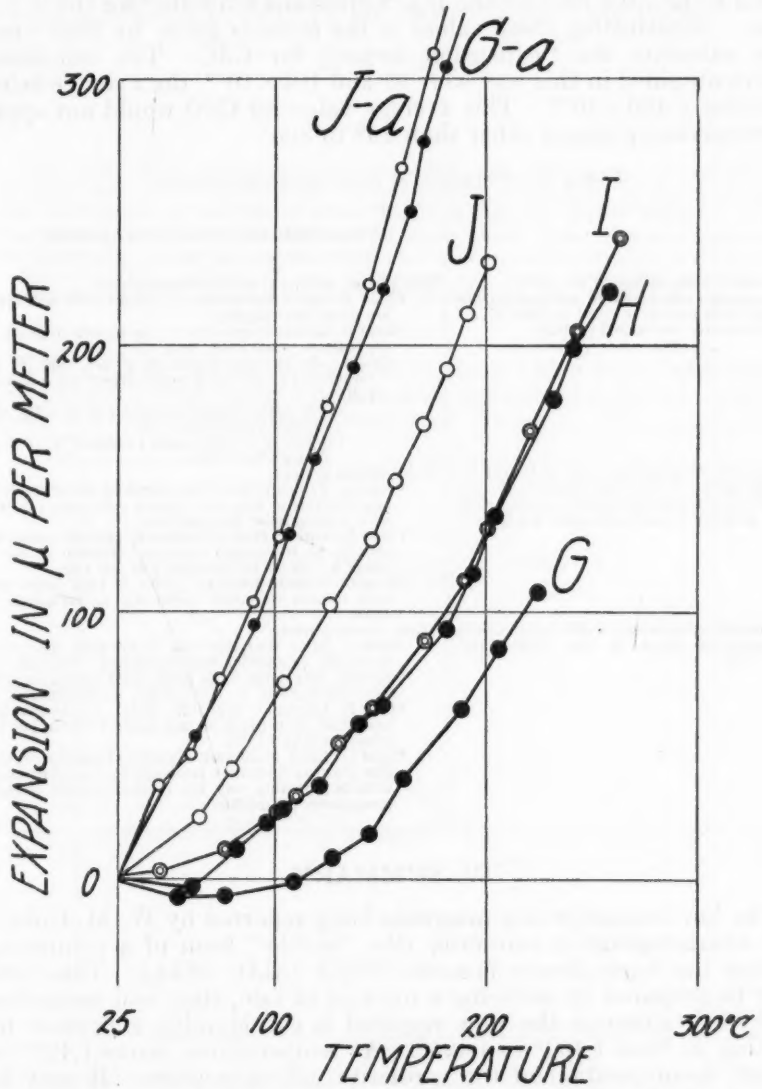

FIGURE 5.—*Thermal expansion curves for specimens of beryl described in Table 2*

J-a and *G*-a were determined perpendicular, the others were determined parallel, to the *C* axis.

maximum temperature of 1,600°. The product is described in Table 4. This material, even when quenched in water from 1,600°, also fell to a powder and no thermal expansion observations were attempted. Glasses having the calculated compositions $CdO \cdot Al_2O_3 \cdot 2SiO_2$ and

$2CdO \cdot 2Al_2O_3 \cdot 5SiO_2$ were obtained when the respective mixtures were heated at 1,450°. They were devitrified at approximately 1,250° and the products are described in Table 4. The average coefficient of expansion for the temperature range 25° to 300° was found to be 7.0×10^{-6} for the 1:1:2 glass and 6.5×10^{-6} for the 2:2:5 glass. Substituting these values in the formula given by Hall [11] one may calculate the "expansion factor" for CdO. The calculated values obtained in this way were 97 and 104×10^{-9}, the average being practically 100×10^{-9}. This average value for CdO would not apply to temperature ranges other than 25° to 300°.

TABLE 4.—*Properties of some cadmium silicates*

	Composition, determined petrographically
Calculated composition, $2CdO \cdot SiO_2$..... *Preparation*—Wet ground mixture of CdO and SiO_2 heated at 1,550° to 1,600° C. for 45 minutes and cooled rapidly.	Two phases, neither of which predominates: Phase A. Index just above 1.7 (about 1.71) with very low or no birefringence. Phase B. Isotropic and occurs as inclusions in phase A; the index is much lower than 1.7. (NOTE.—In Sprechsaal, vol. 52, p. 256, 1919, F. M. Jaeger and H. S. van Klooster report the following values: $2CdO \cdot SiO_2$, melting point 1,243° to 1,252° C.; indices N_1 and $N_2 > 1.739$. $CdO \cdot SiO_2$, melting point 1,242±0.5° C.; indices N_1 and $N_2 > 1.739$)
Calculated composition, $CdO \cdot Al_2O_3 \cdot 2SiO_2$.. *Preparation*—Wet ground mixture of CdO and Georgia kaolin melted to a clear glass at 1,450° C. and devitrified at 1,250° C.	Three phases present: Phase A. Probably the most abundant, occurs as irregular crystals of very low double refraction (<0.005) with a mean index of about 1.65. Phase B. Either glass or isotropic crystals occurring usually as interstitial material between grains of phase A. Index lies between 1.61 and 1.62. Phase C. Minute rounded grains of high index and high double refraction occurring as inclusions in phase A.
Calculated composition, $2CdO \cdot 2Al_2O_3 \cdot 5SiO_2$.. *Preparation*—Same as for $CdO \cdot Al_2O_3 \cdot 2\ SiO_2$.	Three phases present: Phase A. Most abundant and occurs with some faces (probably prismatic) well developed. Crystals are biaxial, very large optic axial angle (approximately 90°) and indices: $a = 1.575 \pm 0.003$, $\gamma = 1.590 \pm 0.003$. Phase B. Isotropic, probably glass. Somewhat less abundant than phase A and index variable but between 1.615 and 1.620. Phase C. Least abundant; occurs as irregular crystalline growths showing a tendency to dendritic forms. Double refraction very low (probably 0.005 or less), mean index 1.65 ± 0.005.

IV. SUMMARY

The low expansion of a magnesia body reported by W. M. Cohn [12] is a characteristic of cordierite (the "stable" form of a compound having the approximate formula $2MgO \cdot 2Al_2O_3 \cdot 5SiO_2$). This form may be prepared by sintering a mixture of talc, clay, and corundum at 1,350°, although the time required is considerably shortened by heating at from 1,400° to 1,425°. At temperatures above 1,425° to 1,450° decomposition of the cordierite will take place. It may be formed also by devitrification of a glass of the proper composition at temperatures above 950° and below about 1,425°.

Zinc orthosilicate, celsian or barium feldspar, and beryl also appear worthy of further consideration by those interested in the development of bodies having low coefficients of thermal expansion.

WASHINGTON, February 19, 1932.

[11] J. Am. Ceram. Soc., vol. 13 (3), p. 182, March, 1930. [12] See footnote 2, p. 35.

AN AUTOMATIC REVERBERATION METER FOR THE MEASUREMENT OF SOUND ABSORPTION

By W. F. Snyder

ABSTRACT

The usual electrical recording method for measuring sound absorption in a reverberation room requires the determination of the rate of decay of sound. The automatic reverberation meter described in this paper works through a range of about 70 decibels, the rate of decay being measured over intervals as short as desired through the whole range.

An automatic control of the apparatus has been developed which allows measurements to be made with but little attention on the part of the observer.

The working ranges of the four methods [1] that have been used at the Bureau of Standards for measuring the rate of decay of sound in a room are shown diagrammatically in Figure 1. The approximate

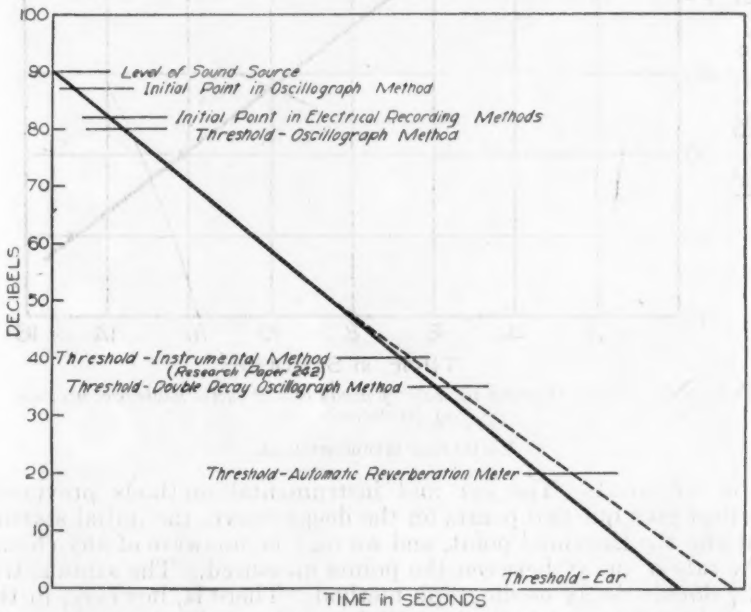

FIGURE 1.—*Working ranges of various methods used at the Bureau of Standards to measure reverberation time*

range through which the rate of decay is measured by each method is indicated by the difference in decibels between the initial point and the final threshold. The ordinary oscillograph method is very limited in range, being about 7 decibels. The other methods described were

[1] See reference 6 in the bibliography.

used through ranges of 40 to 50 decibels. The present automatic reverberation meter works through a range of about 70 decibels. The ear, of course, covers even a greater range since in reverberation measurements the ear must start at the initial sound level in the room and must follow the decay to the threshold of hearing.

More important, however, than a measurement over a wide range of intensity, is the accurate determination of the rate of decay of the sound energy throughout the measured range. Such a procedure is essential when measuring highly absorbent materials in a reverberation room or whenever "two-room" conditions exist.[2] Under these conditions a double rate of decay may exist as shown by the dotted

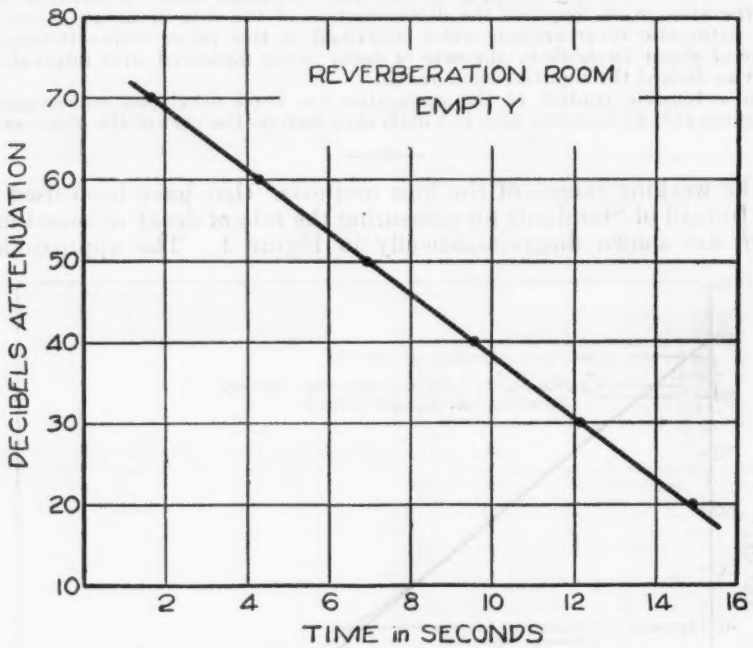

FIGURE 2.—*Curve showing the rate of decay at 512 cycles made over a range of 50 decibels*

It is the result of 60 observations.

line in Figure 1. The ear and instrumental methods previously described give but two points on the decay curve, the initial starting point and the threshold point, and we may be unaware of any change in the rate of decay between the points measured. The same is true in the double-decay oscillograph method. There is, however, in this case a short range at both the initial and threshold points where the rate is accurately known. The two short decay curves photographed on the oscillograms sometimes showed different rates of decay, indicating that the rate was not always uniform through the whole range.

Measurements with a reverberation meter as shown in Figure 2 yield a number of points along the decay curve at definite intervals, and the rate of decay may be determined throughout the working range.

[2] See reference 9 in the bibliography.

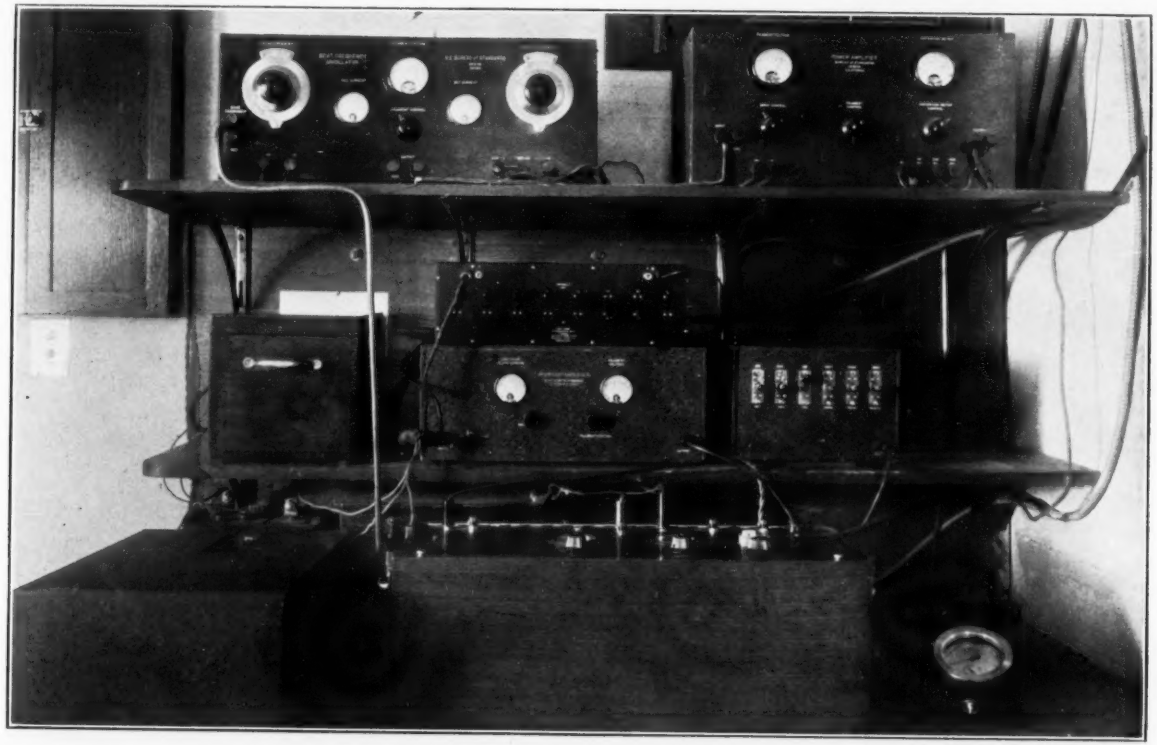

UNIV. OF MICH.

FIGURE 3.—*Equipment used in making absorption measurements with automatic reverberation meter*

Since the decay of sound in a room is of a nonuniform character we must resort to a statistical method of measurement, each measurement being repeated at least ten times. The procedure in making these measurements is as follows: Sound radiated from a source such as a loud speaker is suddenly cut off and a timing mechanism started at the same time. The sound as it dies away is picked up by a microphone and when the sound reaches a certain level in the room an electrical arrangement stops the timer. The timer has then recorded the length of time the sound takes to decay from the initial intensity to the threshold at which the instrument is set. Shifting the threshold of the recording instrument by a definite number of decibels, a different time is measured. Knowing the time it takes the sound to decay through definite ranges of sound levels, a curve can be plotted similar to Figure 2 in which the slope gives the rate of decay. From the rate of decay the absorption of the room can be calculated by the reverberation equation.[3]

Making statistical measurements in such fashion becomes quite laborious. The present design of the reverberation meter used at the Bureau of Standards has made much of the operation automatic.

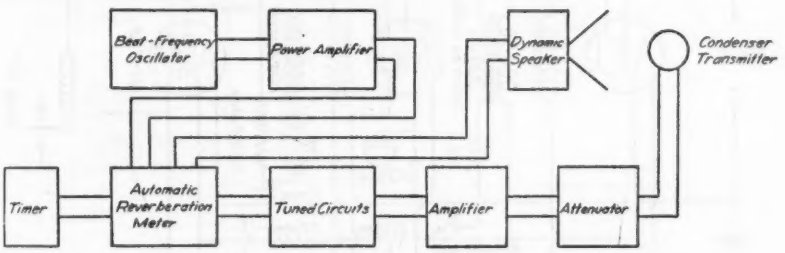

FIGURE 4.—*Schematic diagram of entire apparatus*

Figure 3 shows the recording equipment and Figure 4 is a schematic diagram of the entire apparatus. Alternating current in the audio-frequency range is generated by a beat-frequency oscillator, strengthened by a power amplifier and finally transformed into sound energy by a dynamic speaker. A condenser transmitter transforms the sound back into electrical energy. The weak electrical current is then amplified, the threshold of the instrument being controlled by an attenuator. Immediately following the amplifier is a group of tuned circuits which aid in reducing the level of extraneous noises. These tuned circuits attenuate approximately 15 decibels at the first octave above and below the frequency to which they are tuned. The automatic reverberation meter with its associated timer terminates the recording apparatus.

Figure 5 shows in detail the electrical circuit contained within the reverberation meter which controls the timer. There is one stage of amplification transformer coupled to a screen-grid tube. The screen-grid tube which acts as a rectifier is directly coupled through a 0.5 megohm resistor to a pentode tube. The pentode tube is used as an oscillator and was so chosen because of its high plate current when connected in series with a high resistance relay. Some difficulty has been found in getting a pentode tube to oscillate under the particular

[3] See reference 6 in the bibliography.

circuit requirements which are necessary for the desired operation of the equipment. The frequency of oscillation is about 700 kc per second.

The grid bias of the pentode tube depends upon the potential across the plate resistor of the rectifier tube which in turn is a function of the sound energy picked up by the microphone. When the sound level is high, as at the beginning of the decay, the grid bias on the oscillator is sufficiently negative to prevent it from oscillating and the plate current is nearly zero. As the sound dies away the grid bias becomes more positive. This continues until a sufficiently positive bias sets the tube into oscillation with a sudden increase in plate current. In consequence, a relay in series with the tube opens a set of contacts, stopping the timer. The sudden increase in current

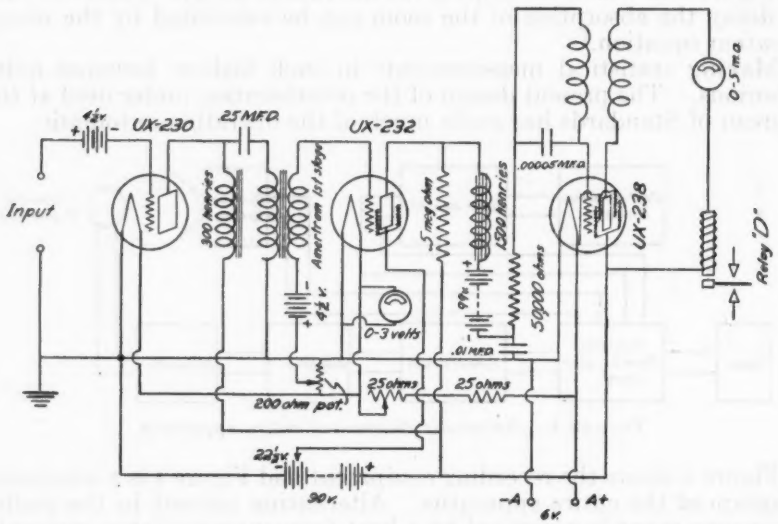

FIGURE 5.—*Electrical circuit diagram of apparatus which stops the electric timer*

through the relay winding gives a positive control to the operation. The point at which this goes into operation, which has been called the threshold of the instrument, depends upon the amount of amplification used and the setting of the attenuator.

The 1,500-henry choke in series with the grid circuit of the pentode tube and the 0.01 μf by-pass condenser serve as a filter for the audio frequencies. This is a necessary precaution to prevent the relay from humming when low frequencies are measured. The circuit is so designed that once the tube goes into oscillation a negative shift in the grid bias caused by an increase in the sound energy amounting to about 4 decibels is necessary to stop oscillations, thereby restarting the timer. This more or less helps to integrate out a variable sound decay and at the same time prevents the timer from following variations less than 4 decibels which would cause excessive starting and stopping of the timer.

Figure 6 shows the arrangement of relays which makes the operation of the reverberation meter almost automatic. The apparatus con-

sists of three relays, a small alternating current motor with a 1,100 to 1 reduction gear coupled by a shaft to a cam operating a 4-pole switch and a self-stopping device. Large condensers across the contacts of the relays prevent sparking and setting up electrical disturbances in the near-by amplifying equipment.

The operation of this device is as follows: A rod connected to the armature of relay *A* is lifted, closing the motor circuit. When no sound is on, the lower contact at relay *D* (fig. 6) is closed, allowing current to flow through the windings of relay *A*, thus holding the armature of relay *A* after it is lifted.

Connected to the same armature is a small pin fitting into cam *B*, which when lifted allows relay *A* to operate properly, since the armature is now close to the pole piece, the pin riding around on top of cam *B*. A 4-pole switch operated by the segments along cam *A* is closed after the cam begins to rotate. This switch closes the loud-speaker circuit and closes a circuit through the winding of relay *A* which

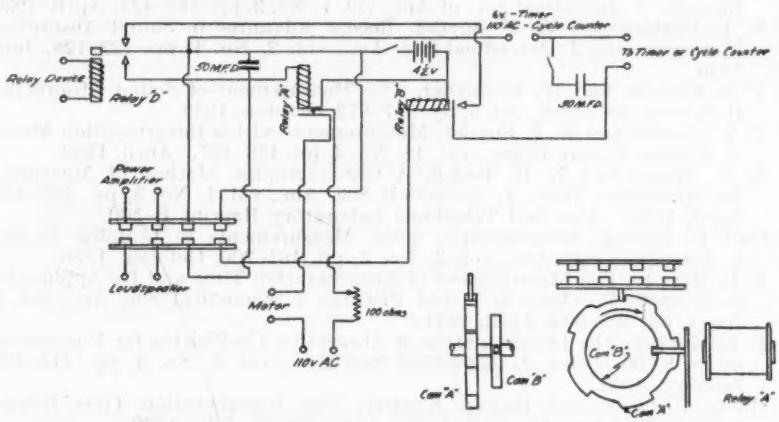

FIGURE 6.—*Relays and cams which provide automatic control for the reverberation meter*

normally opens at relay *D* as the sound comes on. It also closes the circuit of the winding of relay *B* which prevents the timer from operating. After a further rotation of the cam shaft the 4-pole switch suddenly springs open breaking the loud-speaker circuit, opening the motor circuit and allowing the contact of relay *B* to close, which starts the timer at the beginning of the decay. While the sound is on or as it is decaying the timer contact of relay *D* is closed. As the sound decays to the threshold of the instrument and the plate current suddenly increases in the pentode tube, relay *D* operates stopping the timer. At the same time the other contact on relay *D* closes and the motor is started. The whole process is repeated. This continues for five measurements. At the fifth measurement the pin on the armature of relay *A* drops back into the slot of cam *B* and stops the entire mechanism.

An average of 10 observations is usually taken at six different sound levels spaced at 10 decibel intervals making a range of 50 decibels. This is sufficient for most absorption measurements. The apparatus has a range, however, of about 70 decibels.

The apparatus described above offers a statistical method of dealing with a type of measurement that presents certain difficulties, since we are determining a rate of decay that is seldom uniform. The method averages a series of observations in a mechanical fashion and is almost entirely automatic. This being true, the human equation in reverberation and absorption measurements has been practically eliminated.

BIBLIOGRAPHY OF PUBLISHED ARTICLES REFERRING TO MECHANICAL AND ELECTRICAL METHODS OF MEASURING REVERBERATION TIME

1. E. Meyer and Paul Just, On the Measurement of Reverberation Time and Sound Absorption, Elek. Nach. Tech., vol. 5, pp. 293–300, 1928.
2. E. Meyer, Automatic Reverberation Measurement, Zeit. f. Tech. Physik., vol. 11, pp. 253–259, 1930.
3. M. J. O. Strutt, Automatic Reverberation Measuring Instrument, Elek. Nach. Tech., vol. 7, pp. 280–282, July, 1930.
4. V. L. Chrisler, The Measurement of Sound Absorption by Oscillograph Records, J. Acoustical Soc. of Am., vol. 1, No. 3, pp. 418–421, April, 1930.
5. V. L. Chrisler and W. F. Snyder, Recent Advances in Sound Absorption Measurements, J. Acoustical Soc. Am., vol. 2, No. 1, pp. 123–128, July, 1930.
6. V. L. Chrisler and W. F. Snyder, The Measurement of Sound Absorption, B. S. Jour. Research, vol. 5, pp. 957–972, October, 1930.
7. V. L. Chrisler and W. F. Snyder, Measurements with a Reverberation Meter, J. Motion Picture Engrs., vol. 18, No. 4, pp. 479–487. April, 1932.
8. E. C. Wente and E. H. Bedell, A Chronographic Method of Measuring Reverberation Time, J. Acoustical Soc. Am., vol. 1, No. 3, pp. 422–427, April, 1930. Also Bell Telephone Laboratory Reprint B–500.
9. Carl F. Eyring, Reverberation Time Measurements in Coupled Rooms, J. Acoustical Soc. Am., vol. 3, No. 2, pp. 181–206, October, 1930.
10. F. L. Hopper, The Measurement of Reverberation Time and Its Application to Acoustic Problems in Sound Pictures, J. Acoustical Soc. Am., vol. 2, No. 4, pp. 499–505, April, 1931.
11. F. L. Hopper, The Determination of Absorption Coefficients for Frequencies up to 8,000 cycles, J. Acoustical Soc. Am., vol. 3, No. 3, pp. 415–427, January, 1932.
12. Harry F. Olson and Barton Kreuzer, The Reverberation Time Bridge, J. Acoustical Soc. Am., vol. 2, No. 1, pp. 78–82, July, 1930.
13. R. F. Norris and C. A. Andree, An Instrumental Method of Reverberation Measurement, J. Acoustical Soc. Am., vol. 1, No. 3, pp. 366–372, April, 1930.
14. R. F. Norris, Application of Norris-Andree Method of Reverberation Measurement to Measurements of Sound Absorption, J. Acoustical Soc. Am., vol. 3, No. 3, pp. 361–370, January, 1932.

WASHINGTON, April 26, 1932.

NOTE ON THE PROBABLE PRESENCE OF 2, 2-DIMETHYLPENTANE IN A MIDCONTINENT PETROLEUM [1]

By Johannes H. Bruun [2] and Mildred M. Hicks-Bruun

ABSTRACT

This paper presents evidence which indicates that 2, 2-dimethylpentane is present in small amount (not more than a few hundredths of 1 per cent) in a midcontinent petroleum. The evidence consists in the approximate agreement of the measured properties of a petroleum fraction containing 46 mole per cent of cyclohexane with those computed on the assumption that the remaining 54 per cent is 2, 2-dimethylpentane.

The properties compared were initial freezing point, boiling point, refractive index, molecular weight and eutectic temperature. The evidence thus obtained was confirmed by comparing the infra-red absorption spectrum of the petroleum fraction with that of a synthetic mixture having the assumed composition.

CONTENT

		Page
I.	Introduction	53
II.	Experimental procedure and results	53
III.	Analysis of the final fraction	55
IV.	Correlation of the properties of the final fraction with its composition	57
V.	Acknowledgment	59
VI.	Bibliography	59

I. INTRODUCTION

From a Caucasian petroleum, Markownikoff (1) [3] obtained a fraction boiling between 78.5° and 79° C. From the boiling range and the specific gravity of this fraction, as well as from its unusual stability toward strong nitric acid, he concluded that 2,2-dimethylpentane was probably present in the Caucasian petroleum. With the exception of Markownikoff, it seems that no one has reported any indication of the presence of 2,2-dimethylpentane in any petroleum.

II. EXPERIMENTAL PROCEDURE AND RESULTS

The present investigation deals with the same fractions of an Oklahoma petroleum which were used for the isolation and determination of cyclohexane (2).

It was found that a large cut (5.5 kg) boiling between 80° and 80.5° C. consisted of about 94 mole per cent of cyclohexane and had a refractive index of 1.422 which is 0.003 unit lower than that of pure cyclohexane. It was therefore apparent that some compound

[1] Financial assistance has been received from the research fund of the American Petroleum Institute. This work is part of project No. 6, The Separation, Identification, and Determination of the Constituents of Petroleum.

[2] Research Associate, representing the American Petroleum Institute.

[3] Figures in parenthesis here and elsewhere in the text indicate references given in the bibliography at the end of this paper.

or compounds with lower refractive index than that of cyclohexane must also be present in this fraction. The object of the present investigation was to concentrate this unknown constituent for possible identification.

While working on the isolation of cyclohexane, it was noted that if the cut boiling between 80° and 80.5° C. was subjected to fractionation by equilibrium melting, fractions of rapidly decreasing refractive indices were obtained. Thus by a single fractionation the following changes in the physical constants were obtained:

	Stage I Stage II
$n\frac{20}{D}$ changed from	1.422 to 1.417
Freezing point changed from	−12° to −28° C.
Boiling point changed from	80.4° to 80.0° C.
Molecular weight changed from	85.1 to 86.1

In view of this apparently efficient separation it was decided to subject the material to systematic equilibrium melting. The progress of the fractionation is shown by the chart in Figure 1. The large circle at the upper left corner (R. I. 1.416) represents the original fraction (obtained by distillation) which had the boiling range 79° to 80° C. The other nine large circles at the top represent fractions which were obtained by subjecting the 80.0° to 80.5° C. cut to equilibrium melting. (This fractionation is described in the cyclohexane paper (2).) The numbers inside the large circles indicate the refractive indices and the initial freezing points of the fractions. As indicated by the solid lines, the large fractions were separated by equilibrium melting into a number of smaller fractions, indicated by the smaller circles. The refractive indices of these fractions are given by the numbers inside the circles. The fractions having similar refractive indices were then mixed for further fractionation. This is indicated by the broken lines in Figure 1. As shown in the chart, the molecular weight was determined for some of the fractions.

As a result of the fractionation shown in Figure 1, the material was separated into comparatively large fractions consisting mainly of cyclohexane (fractions with high refractive indices) and into small quantities of material with low refractive index and low freezing point. Fractionation of this material, which contained the unknown constituent, was continued until its refractive index had been brought down to 1.392 and its freezing point had reached −124.6° C. (Stage III.) At this point, however, the available quantities of this material were too small to attempt further purification.

The time-temperature cooling curve of the final fraction is shown in Figure 2. Table 1 shows some of the physical constants of synthetic 2, 2-dimethylpentane, of cyclohexane, and of the petroleum fractions during three stages of the fractionation. Stage I represents the large cut boiling between 80° and 80.5° C. The material in Stage II was obtained by a single fractionation of the mixture in Stage I by equilibrium melting. (See p. 54 and upper left of fig. 1.) Stage III represents the fraction which was obtained as a final result of the systematic equilibrium melting. (See bottom of fig. 1.)

TABLE 1.—*Some physical constants of 2, 2-dimethylpentane, of cyclohexane, and of the petroleum fractions during three stages of the fractionation*

	Cyclohexane (C_6H_{12}) synthetic [a]	The petroleum fractions			2, 2-dimethylpentane (C_7H_{16}) synthetic [b]
		Stage I	Stage II	Stage III	
n_D^{20}	1.426	1.422	1.417	1.392	1.382
Molecular weight	84.09	[c] 85.1	[c] 86.1	[c] 93.7	100.12
Normal boiling point in ° C	80.8	80.4	80.0	79.5	78.9
Freezing point in ° C	6.4	−12	−28	−124.6	−125.6

[a] J. Timmermans, J. chim. phys., vol. 23, p. 760, 1926.
[b] G. Edgar and G. Calingaert, J. Am. Chem. Soc., vol. 51, p. 1544, 1929.
[c] For method, see M. M. Hicks-Bruun, B. S. Jour. Research, vol. 5, pp. 575–583, 1930.

As the fractionation proceeded a definite increase was noted in the molecular weight. Thus, while the molecular weight for Stage I was 85.1, the material in Stages II and III was found to have molecular weights of 86.1 and 93.7, respectively. This is unmistakable evidence of the presence of a constituent having a higher molecular weight than that (84.09) of cyclohexane.

The material in Stage III had a distillation range of about 0.5° C. It did not react with bromine or iodine and it was insoluble in water. Furthermore this fraction exhibited an unusual stability when heated with fuming nitric or with chlorosulphonic acid.

By correlating the values of the molecular weight (93.7), the refractive index and the boiling point of this fraction with the corresponding constants of known hydrocarbons, it was concluded that a heptane was probably present in the cyclohexane fraction.

It should be further noted that the boiling point of the material in Stage I (which contained 94 mole per cent of cyclohexane) was 80.4° C. as compared with 80.8° C. for pure cyclohexane. As a result of further fractionation by equilibrium melting fractions of still lower boiling points (80.0° C. in Stage II and 79.5° C. in Stage III) were obtained. This fact indicates clearly that the presumed heptane is one with a boiling point below that of cyclohexane or that the mixture is azeotropic with a boiling point minimum. The only heptane with a boiling point below 80.8° is 2,2-dimethylpentane.

The above-mentioned great stability of the material in Stage III against chemical reagents is in accordance with the structure of 2,2-dimethylpentane, because of all the isomeric heptanes, only the following three do not possess a reactive tertiary carbon atom: 2,2-dimethylpentane (boiling point 78.9° C.); 3,3-dimethylpentane (boiling point 86° C.); and *n*-heptane (boiling point 98.4° C.).

III. ANALYSIS OF THE FINAL FRACTION

For the purpose of determining the approximate composition of the material (Stage III, Table 1) having the lowest refractive index (1.392), the following procedure was used. The freezing point of cyclohexane was determined with a Beckmann thermometer. A solution of known concentration of the material (Stage III) in the cyclohexane was then made up, after which the lowering of the freez-

ing point was determined. It is evident that the cyclohexane present in the material (Stage III) will have no effect upon the freezing point, and that the total lowering will be caused by the other con-

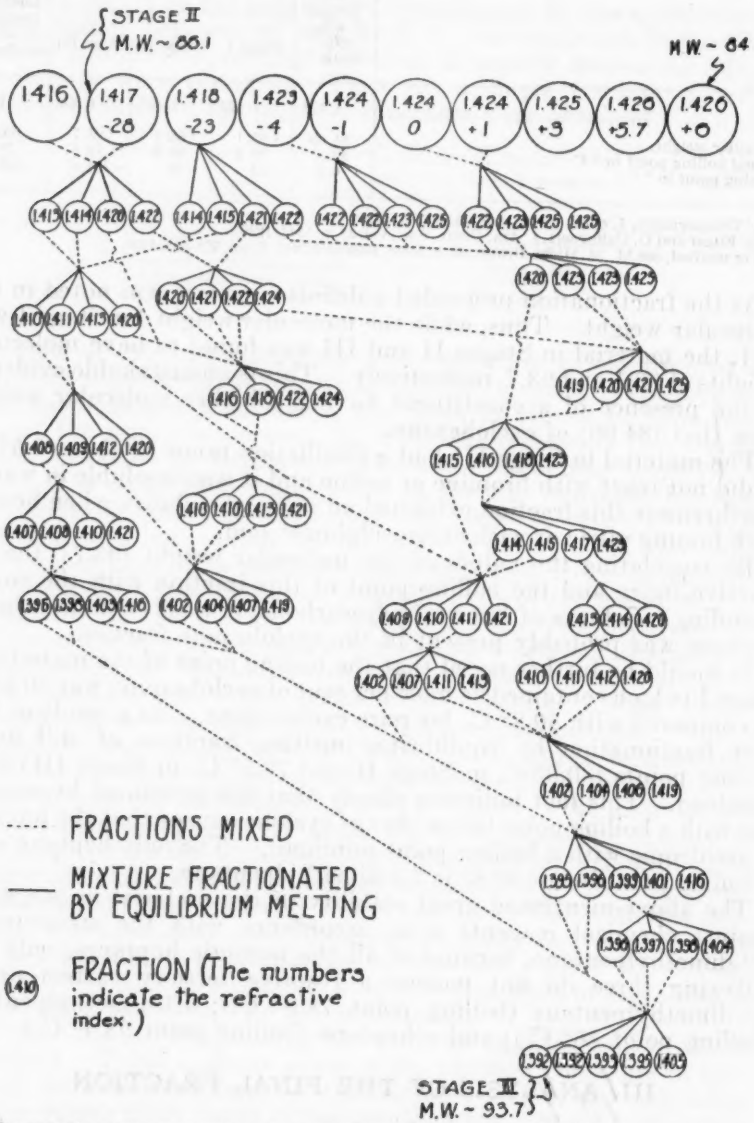

FIGURE 1.—*Chart showing the fractionation by means of equilibrium melting*

stituents in this material. From the lowering thus obtained the mole percentage of cyclohexane for the material in Stage III could be calculated. However, the two most recent values reported in the literature for the heat of fusion (L_{f_o}) of cyclohexane differ by more

than 20 per cent. Hence calculations were made using each value, with these results:

$L_{f_0} = 5.87$ cal./g (3).
45.9 mole per cent of cyclohexane and
54.1 mole per cent of other constituents.
$L_{f_0} = 7.4$ cal./g (4).
30.8 mole per cent of cyclohexane and
69.2 mole per cent of other constituents.

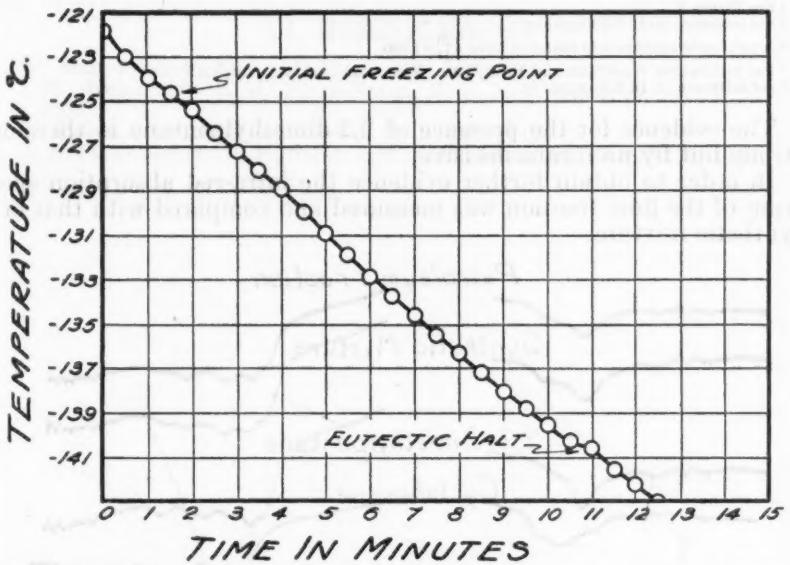

FIGURE 2.—*Time-temperature cooling curve of the final fraction. (Stage III)*

IV. CORRELATION OF THE PROPERTIES OF THE FINAL FRACTION WITH ITS COMPOSITION

The amount of the final fraction (Stage III) was so small that further fractionation for the purpose of isolating a pure sample of the presumed heptane was impossible. Under these circumstances the best that can be done is to compare the measured properties of the final fraction with those of a mixture consisting of 45.9 moles of cyclohexane and 54.1 moles of 2,2-dimethylpentane. This comparison is shown in Table 2. The calculated values are based on the assumption that the mixture is an ideal solution.

It will be observed that the agreement is good except in the case of the refractive index, where the observed value is low by 0.008 unit, which might be caused by the presence of a small amount of a third constituent, such as normal hexane, for example.

TABLE 2.—*Observed and calculated properties of the final fraction*

Property=	F. P.[a]	B. P.[a]	Molecular weight	n_D^{20}	Eutectic halt
	°C.	°C.			°C.
Observed values	−124.6	79.5	93.7	1.392	[b] −140.2
Values calculated from L_{fo}=5.87 cal./g[c]	−124.6	79.8	92.8	[d] 1.399	[e] −138.2
L_{fo}=7.4 cal./g[f]	−136.8		95.1	1.394	[e] −136.0

[a] Initial.
[b] See Figure 2.
[c] See reference (3) in bibliography.
[d] A synthetic mixture was found to have n_D^{20}=1.400.
[e] For method see Washburn and Read, Proc. Nat. Acad., vol. 1, p. 191, 1915.
[f] See reference (4) in bibliography.

The evidence for the presence of 2,2-dimethylpentane is therefore strong but by no means decisive.

In order to obtain further evidence the infra-red absorption spectrum of the final fraction was measured and compared with that of a synthetic mixture.

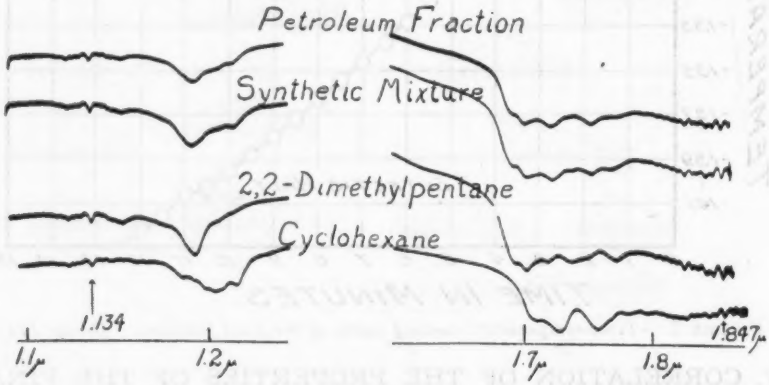

FIGURE 3.—*The infra-red absorption spectra of the final petroleum fraction (Stage III), the synthetic mixture, the 2,2-dimethylpentane, and the cyclohexane*

Measured by U. Liddel, of the Fixed Nitrogen Research Laboratory of the Department of Agriculture.

Through the courtesy of G. Edgar and G. Calingaert, of the Ethyl Gasoline Corporation, a small sample of synthetic 2,2-dimethylpentane was obtained. This sample was mixed with pure cyclohexane (and a small amount of *n*-hexane) so as to yield a mixture of approximately the same composition as that calculated for the material in Stage III. The spectra of the two mixtures as well as those of the pure samples of cyclohexane and of 2,2-dimethylpentane were then measured by U. Liddel, of the Fixed Nitrogen Research Laboratory of the United States Department of Agriculture, and are shown in Figure 3. The two upper curves reveal a striking resemblance between the synthetic mixture and the final fraction (Stage III), which was presumably of the same composition.

The characteristic minimum at about 1.19μ is clearly evident in the spectrum of the petroleum fraction. This evidence when taken together with that shown in Table 2 renders it highly probable that 2,2-dimethylpentane is a major constituent of the petroleum fraction

(Stage III). Based upon the crude oil the amount present can not, however, exceed a few hundredths of 1 per cent. With larger amounts of material to work with, there should be no difficulty in isolating the pure hydrocarbon.

V. ACKNOWLEDGMENT

The authors acknowledge the technical advice and suggestions of E. W. Washburn, director of American Petroleum Institute project No. 6.

VI. BIBLIOGRAPHY

1. W. Markownikoff, Ber., vol. 33, p. 1908, 1900.
2. J. H. Bruun and M. M. Hicks-Bruun, B. S. Jour. Research, vol. 7, p. 607, 1931.
3. M. Padoa, Atti Accad. Lincei, vol. 28, p. 240, 1919.
4. G. S. Parks and H. M. Huffman, Ind. Eng. Chem., vol. 23, p. 1139, 1931.

WASHINGTON, May 3, 1932.

NOTES ON THE ORIFICE METER; THE EXPANSION FACTOR FOR GASES

By Edgar Buckingham

ABSTRACT

The discharge coefficient of an orifice meter, determined with water, is applicable when the meter is used for measuring the flow of a gas, provided that the differential pressure is so small that the accompanying change of density is insignificant. But if the differential is a considerable fraction of the absolute static pressure, the water coefficient must be multiplied by an "expansion factor" which allows for the effects of change of density.

The paper contains a discussion of recent experimental data which show how the expansion factor depends on the form of the meter, the ratio of downstream to upstream pressure, and the specific heat ratio of the gas. The conclusions are summarized in an empirical equation which may be used for computing the value of the expansion factor in certain practically important cases.

A theoretical method of computing the expansion factor is developed and is shown to agree reasonably well with the facts observed under conditions that are approximately in accordance with those postulated by the theory.

CONTENTS

	Page
I. Introduction	61
II. The orifice meter equation	63
III. Restriction to high values of the Reynolds number	63
IV. The expansion factor	64
V. Coordination of the experimental values of ϵ	68
1. Throat taps	68
2. Flange and corner taps	69
VI. Theoretical computation of Y	71
VII. Comparison of the theoretical with experimental values of Y	73
1. Throat taps	74
2. Corner taps	75
VIII. Summary	77
1. Notation	77
2. Conclusions	77
IX. References	79

I. INTRODUCTION

The type of meter to which the following notes refer is illustrated diagrammatically by Figure 1, which shows some of the notation to be used, as well as certain limitations on the relative dimensions of the parts. It may be assumed that the readers to whom these notes are addressed would find a detailed description of the orifice meter superfluous.

Since the pressures p_1 and p_2, observed at the upstream and downstream side holes or pressure taps, depend on the locations of the holes, it is necessary to specify the distances, l_1 and l_2, from the

center of each hole to the nearer face of the orifice plate, and some one of the following four schemes is usually adopted:

(*a*) Pipe taps, $l_1 = 2.5D$, $l_2 = 8D$.
(*b*) Throat taps, $l_1 = D$, $l_2 = 0.5D$.
(*c*) Flange taps, $l_1 = l_2 = 1$ inch for all sizes of pipe.
(*d*) Corner taps, the side holes are at the faces of the plate, or the pressures are taken off through narrow circumferential slits between the plate and the flanges, as illustrated in the lower half of Figure 1.

Combinations (*a*), (*b*), and (*c*) are in common use in the United States, and (*d*) has been adopted as standard by the Society of German Engineers (1).[1]

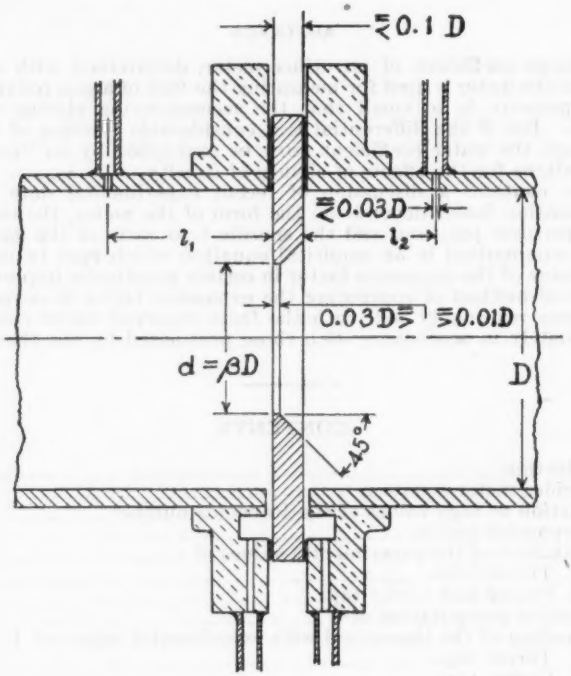

FIGURE 1.—*The orifice meter*

Side holes are shown above and ring slits below

There are advantages in adopting an arrangment such that meters of different sizes shall be geometrically similar as regards location of the side holes, a condition satisfied by (*a*), (*b*), and (*d*), but not by (*c*).

When the pipe diameter, D, is 8 inches or more and the orifice diameter, d, is not more than about $0.75D$, arrangements (*c*) and (*d*) give nearly the same pressure readings and may be regarded as equivalent, except in work of high precision. But with pipes as small as 4 inches in diameter, this assumption is no longer safe; and even with larger pipes, the two arrangements may give appreciably different results if the diameter ratio is as large as 0.8.

[1] Figures in parenthesis here and throughout the text indicate references given at the end of this paper.

II. THE ORIFICE METER EQUATION

The indications of an orifice meter are usually, and most conveniently, interpreted by means of some equation which is substantially equivalent to

$$M = N\,C\,A\sqrt{2\rho(p_1 - p_2)} \tag{1}$$

in which

M = the required rate of mass flow, or the mass discharged per unit time;
A = the area of the orifice;
ρ = the density of the fluid being metered;
p_1, p_2 = the pressures at the upstream and downstream taps;
N = a numerical constant dependent on the units; and
C = the discharge coefficient of the orifice, a number which does not depend on the units.

If the fluid is a gas, its density must be referred to some specified pressure and temperature, and these are most commonly taken to be the upstream pressure p_1 and the temperature t_1 of the gas approaching the orifice. We shall adopt this convention and denote the density under these conditions by ρ_1. For the sake of simplicity, it will also be supposed that all quantities are measured by a system of normal units, such as "British absolute" or cgs, because we then have $N = 1$; and with these two conventions, equation (1) takes the form

$$M = CA\sqrt{2\rho_1(p_1 - p_2)} \tag{2}$$

Before an orifice can be used as a flow meter, the value of C must be known, and this value depends on the rate of flow, the properties of the gas, the dimensions of the apparatus, the location of the pressure taps, etc. In the experimental investigations needed for the elucidation of this subject, observations of pressure and temperature at the orifice are combined with measurements of the rate of discharge by some independent method, and the equation is used in the form

$$C = \frac{M}{A\sqrt{2\rho_1(p_1 - p_2)}} \tag{3}$$

which may be regarded as a definition of C.

It may be remarked that ρ_1 denotes the true density at p_1, t_1; and if the gas in question is one that shows large departures from Boyle's law under the anticipated working conditions, the use of the familiar equation $pv = RT$, in computing the value of ρ_1 from the results of a density determination under laboratory conditions that are very different from the working conditions, may lead to large errors (2).

III. RESTRICTION TO HIGH VALUES OF THE REYNOLDS NUMBER

Let R_d be the Reynolds number defined by the equation

$$R_d = \frac{4M}{\pi d\eta} \tag{4}$$

in which η is the viscosity of the fluid.

If R_d is large, say $R_d > 200{,}000$, the value of C found by testing an orifice with water, or other liquid, is sensibly independent of the rate

of flow (3), and this shows that the effects of viscosity have become negligible. But if the same orifice is tested with a gas, such as air, the value obtained for C varies with the rate of flow, even though R_d be high enough to make the effects of viscous forces insignificant; for the decrease of density as the pressure falls from p_1 to p_2, in contradistinction to the constancy of density of a liquid, introduces a new element into the phenomena of flow (5, 6, 7).

The condition that R_d shall have the required high value is nearly always satisfied in the commercial metering of gases, and since the object of this paper is to discuss the changes of C which are due to compressibility alone, it will be assumed, from this point onward, that the requirement is fulfilled.

IV. THE EXPANSION FACTOR

In discussing the effects of compressibility, it will be convenient to employ the following notation:

$\beta = d/D$ = the diameter ratio of the orifice, or

$m = \beta^2$ = the area ratio;

K = the value found for C when the orifice is tested with a liquid at high values of R_d: so long as the installation remains unchanged, K is a constant of the orifice;

$y = p_2/p_1$ = the pressure ratio at which the discharge coefficient determined by experiments on the gas has the value C;

$\gamma = C_p/C_v$ = the specific heat ratio of the gas; and

$Y = C/K$ = the expansion factor.

If the fall of pressure at the orifice is made so small that the accompanying decrease of density is insignificant, the gas must behave very nearly like a liquid; and experiment confirms the conclusion that $C \doteq K$ when $y \doteq 1$.

We therefore write

$$C = KY \tag{5}$$

in which the expansion factor, Y, describes, or allows for, the varying effect of compressibility on the discharge coefficient; and $Y \doteq 1$ when $y \doteq 1$.

In many important cases, the relation $Y = f(y)$ is very nearly linear, as is illustrated by the simultaneous values of y and C given in Table 1 and plotted in Figure 2.

TABLE 1.—*Relation of C to y*

Diameter ratio 0.6209. Specific heat ratio 1.283. Throat taps

$\frac{p_2}{p_1}=y$	C observed	$\frac{0.6669-0.23}{(1-y)}$	Difference	$\frac{p_2}{p_1}=y$	C observed	$\frac{0.6669-0.23}{(1-y)}$	Difference
0.549	0.5618	0.5632	−0.0014	0.797	0.6211	0.6202	+0.0009
.558	.5660	.5652	+.0008	.904	.6444	.6448	−.0004
.560	.5654	.5657	−.0003	.911	.6469	.6464	+.0005
.647	.5866	.5857	+.0009	.913	.6486	.6469	+.0017
.651	.5872	.5866	+.0006	.947	.6543	.6547	−.0004
.650	.5879	.5864	+.0015	.948	.6527	.6549	−.0022
.700	.5973	.5979	−.0006	.953	.6557	.6561	−.0004
.703	.5979	.5986	−.0007	.975	.6589	.6612	−.0023
.711	.5999	.6004	−.0005	.977	.6620	.6616	+.0004
.808	.6250	.6227	+.0023	.977	.6605	.6616	−.0011
.799	.6213	.6207	+.0006				

This is one of a large number of results of experiments carried out under the direction of H. S. Bean, of the Bureau of Standards, for the Committee on Gas Measurement of the Natural Gas Department of the American Gas Association. In this instance, the experimental work was done at Los Angeles in 1929, with a natural gas of specific heat ratio $\gamma = 1.283$, and the pressures were taken at throat taps.

The Los Angeles experiments included tests of 23 orifices in pipes of 4, 8, and 16 inches nominal diameter, and Table 2 gives a list of the orifices, together with the number of tests on each and the lowest value of y, for throat taps, to which the tests extended.

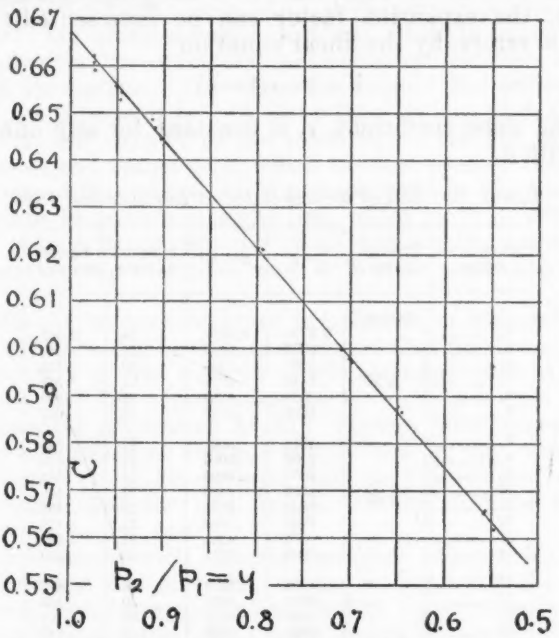

FIGURE 2.—*Relation of discharge coefficient to pressure ratio*

From Table 1

The orifice plates were one-eighth inch thick, with the edges of the orifice square and sharp at both faces. They were installed in commercial steel pipes which had been selected for smoothness, and a short nest of smaller pipes was placed in each of the three pipes at a distance of $10D$ to $15D$ ahead of the orifice, to insure straightness of flow. Pipe, throat, and flange taps were provided, and pressures were read at all three pairs. The absolute pressure was never more than 2.6 atmospheres so that departures from Boyle's law could be ignored. Since it was not practicable to measure the rates of flow by means of a gasometer, they were determined by passing the discharge from the orifice under test through standard reference orifices, of which any number up to 6 could be used in parallel. Details of the experiments and their results will be described in a later publication.

The linear relationship shown by Table 1 and Figure 2 is characteristic of the orifices for which $0.2 \leqq \beta \leqq 0.75$. In general, the depar-

tures of the plotted points from the best straight line that could be drawn among them by simple inspection were somewhat greater than in this series, but they were not systematic.

For diameter ratios of 0.8 or more, when the range of y was long enough to give a well defined band of points, the axis of the band was concave upward, the curvature increasing with β; and the tests of the orifice for which $\beta=0.1241$ indicated that a curve, slightly convex upward, would be a little better than a straight line, a result in accordance with other observations on orifices of diameter ratios below about 0.2. But the general conclusion may be drawn from the Los Angeles observations with throat taps, that, over the ranges $0.2\leqq\beta\leqq0.75$ and $1.0>y>0.5$, the expansion factor can be represented,[¶] within the experimental errors, by the linear equation

$$Y=1-\epsilon(1-y) \tag{6}$$

in which the slope coefficient, ϵ, is constant for any one orifice but increases with β.

TABLE 2.—*List of orifices tested at Los Angeles, 1929*

Number of orifice	Pipe diameter D	$\frac{d}{D}=\beta$	$\beta^4=m^2$	Number of tests	Lowest value of y
	Inches				
1	4.03	0.3724	0.0192	24	0.533
2		.4967	.0609	21	.541
3		.6207	.1484	20	.516
4		.7449	.3079	31	.544
5		.8069	.4239	25	.503
6		.8691	.5705	24	.607
7	8.05	.1241	.0002	21	.543
8		.3105	.0093	21	.529
9		.4967	.0609	21	.515
10		.6209	.1486	21	.549
11		.6829	.2175	28	.495
12		.7450	.3080	31	.479
13		.8070	.4241	31	.486
14		.8693	.5711	29	.550
15	15.38	.1951	.0014	26	.472
16		.3901	.0231	30	.523
17		.5527	.0933	25	.597
18		.6501	.1786	22	.741
19		.6989	.2386	21	.798
20		.7477	.3125	14	.875
21		.7963	.4021	12	.887
22		.8289	.4721	18	.933
23		.8615	.5508	12	.952

When the measurements of pressure were made with flange taps ($l_1=l_2=1$ inch instead of $l_1=D$, $l_2=0.5D$), the results were similar to those for throat taps, the only difference being that the values of ϵ were a trifle larger and that the linear relationship persisted up to higher values of β.

Experiments by R. Witte (3, 4), with corner taps, have also given a linear relation of Y to y for air and nitrogen; and the same was true of his more extensive experiments on superheated steam, except for an as yet unexplained anomaly at the highest values of y, which may be connected with the phenomena of delayed condensation. The remaining points lay along straight lines. (See reference 4, figs. 14 and 15, p. 295.)

The experimental data cited above seem to be the most extensive and trustworthy available, though not the only ones. For example,

J. L. Hodgson (5) has published curves representing the results of experiments with corner taps on air for diameter ratios $\beta = 0.421$, 0.632, and 0.843, and they are all convex upward; but for the two lower diameter ratios one can not be certain, from the small figure published, that straight lines would not do as well as the curves. For $\beta = 0.843$ there is no doubt about the curvature, but, unfortunately, there are no other published data with which this curve can be compared, so that it stands alone.

In the Los Angeles experiments with flange taps, the orifices numbered 5, 13, and 14, in Table 2 ($\beta = 0.8069$, 0.8070, and 0.8693) gave well-defined straight lines, while the observed points for number 6 ($\beta = 0.8691$) lay along a curve that was strongly concave upward. There is, however, no necessary inconsistency between these observations and Hodgson's. For when the edge of the orifice is as near the wall of the pipe as it is with these large values of β, the pressure at the wall in the vicinity of the plate varies rapidly with distance from the plate; and flange taps, which are merely near the plate, may well give quite different results from taps right in the corners. The fact that plate 14 gave a straight line, while plate 6, with the same value of β, gave a curve, was doubtless due partly, if not wholly, to the fact that the tap distances were $D/8$ in the one case and $D/4$ in the other.

The results of the early work of the Bureau of Standards on compressed air (6) were also presented as curves that were convex upward; but the observed points were so much scattered that straight lines might equally well have been used, for all but the lowest values of β. The experimental conditions at Los Angeles were more favorable, both in the steadiness of the gas supply and in the longer range of values of y that could be covered, and they permitted of so much higher precision that the Los Angeles results may be regarded as superseding the earlier ones.

Many experiments with natural gas from other fields have been carried out under the direction of H. S. Bean for the committee named above, and have given results like those already described; but the experimental conditions were generally less satisfactory and a detailed discussion of the results would not change or invalidate the conclusions drawn from the more precise data gathered at Los Angeles. These additional experiments will not be further considered here, nor will an exhaustive review of the literature be attempted; but one excellent set of observations remains to be mentioned, although the arrangement of the apparatus did not correspond exactly to any of the four usual pressure tap combinations.

H. Bachmann (7), working with air, determined the discharge coefficient of an orifice on the end of a pipe, with the jet issuing into the atmosphere. The dimensions were $D = 82.5$ mm (3.25 inches), $d = 20.032$ mm, $\beta = 0.2428$, and $l_1 = 1.82D$; and p_2 was taken to be the barometric pressure.

In view of the low value of β, this arrangement must have given very nearly the same results as if the pipe had been continued downstream and the pressures had been measured at throat taps.

The values of C from 17 experiments covering the range $0.996 \geqq y \geqq 0.535$ are reproduced without systematic error by the equation

$$C = 0.600\,[1 - 0.302\,(1 - y)] \qquad (7)$$

the greatest departure being −0.6 per cent, and the mean ±0.2 per cent.

One experiment, at $y=0.997$, gave $C=0.5907$ as compared with 0.5995 from equation (7); but having regard to the admirable consistency of the other values, it seems fair to assume that this one experiment was affected by an unusually large error of some sort.

From the foregoing brief review of experimental data, it appears that, over the range $1.0 > y > 0.5$, the expansion factor may be represented, within the present accuracy of orifice meter testing, by linear equations of the form of equation (6), provided that: (*a*) The tap distances are not greater than $l_1=D$ and $l_2=0.5D$; and (*b*) the diameter ratio is within the limits $0.2 \leqq \beta \leqq 0.75$.

V. COORDINATION OF THE EXPERIMENTAL VALUES OF ϵ

Admitting the substantial correctness of the general form of equation (6), we have next to intercompare the values of the slope coefficient ϵ that fit the various sets of observations.

1. THROAT TAPS

For each of the orifices tested at Los Angeles the values of $C\sqrt{1-m^2}$ were plotted as ordinates[2] against y as abscissa; and for each orifice for which $\beta<0.75$, the result was a more or less definite and straight band of points. By stretching a fine thread along the band and making readings at $y=0.5$ and $y=1.0$, two straight lines, of greatest and least slope, were determined, between which any line that could reasonably be drawn to represent the band must lie. The values of ϵ for these lines were computed, and their mean is recorded as ϵ_{obs} in column 5 of Table 3.

TABLE 3.—*Slope coefficient of Y for throat taps or free discharge*

Observer	D	$\frac{d}{D}=\beta$	$\beta^4=m^2$	$\epsilon_{obs.}$	$\delta\epsilon_{obs.}$	$\frac{0.41+0.33m^2}{\gamma}=\epsilon_{calc.}$	$\epsilon_{obs.}-\epsilon_{calc.}$	Column 8 − column 6	K_{obs}
1	2	3	4	5	6	7	8	9	10
	Inches								
	4.03	0.3724	0.0192	0.336	±0.006	0.324	+0.012	+0.006	0.614
		.4967	.0609	*.342	.002	.335	+.007	+.005	.630
		.6207	.1484	*.363	.003	.358	+.005	+.002	.668
		.7449	.3079	.386	.006	.399	−.013	−.007	.748
	8.05	.1241	.0002	*.313	.003	.320	−.007	−.004	.595
		.3105	.0093	*.329	.003	.322	+.007	+.004	.606
H. S. Bean, throat taps, $\gamma=1.283$		.4967	.0609	.331	.004	.335	−.004	-------	.634
		.6209	.1486	.344	.003	.358	−.014	−.011	.667
		.6829	.2175	*.383	.006	.376	+.007	+.001	.696
		.7450	.3080	*.403	.005	.369	+.004	-------	.737
	15.38	.1951	.0014	.304	.007	.320	−.016	−.009	.599
		.3901	.0231	.300	.022	.326	−.026	−.004	.613
		.5527	.0933	.307	.032	.344	−.037	−.005	.643
		.6501	.1786	.337	.017	.365	−.028	−.011	.679
		.6989	.2386	.379	.023	.381	−.002	-------	.705
		.7477	.3125	.386	.022	.400	−.014	-------	.733
H. Bachmann, free discharge, $\gamma=1.40$	3.25	.2428	.0035	.302	.010	.294	+.008	-------	.600

[2] Values of C might equally well have been used.

The number in column 6 is, in each case, one-half the difference between the two extreme values and gives a rough estimate of the uncertainty of the value of $\epsilon_{obs.}$

The foregoing procedure evidently involves a considerable exercise of personal judgment which might have been avoided by utilizing the method of least squares. But there was no satisfactory method for weighting the separate points—which were certainly not all of equal weight—and the result of any arbitrary assignment of weights would have been no more authoritative or probable than that obtained, as described, by simple inspection.

If tests were carried out on a series of orifices which differed only in diameter ratio, the values found for ϵ should evidently lie along some smooth curve, $\epsilon = f(\beta)$, within the errors of experiment; and it appears that the relation would be approximately linear in β^4 or m^2. Column 7 of Table 3 contains values computed from the empirical equation

$$\epsilon_{calc.} = \frac{0.41 + 0.33m^2}{\gamma} \tag{8}$$

and column 8 contains the values of $(\epsilon_{obs.} - \epsilon_{calc.})$. Column 9 shows the positive or negative excess of $(\epsilon_{obs.} - \epsilon_{calc.})$ over the estimated uncertainty of $\epsilon_{obs.}$, given in column 6. For 5 of the 17 orifices, including Bachmann's, $(\epsilon_{obs.} - \epsilon_{calc.})$ is within the estimated uncertainty, while for the other 12 it is outside, by amounts up to 0.011.

It is quite possible that the errors in determining ϵ were larger than the admittedly rough estimates shown in column 6; and there may also have been differences of finish between the different plates, so that even if there had been no experimental errors, the points would not have lain on a smooth curve or a straight line. But in any event, the departures are not so important as might appear at first sight. An error of 0.010 in ϵ changes C by 0.4 per cent at $y = 0.6$, or by 0.2 per cent at $y = 0.8$, which is a lower value of y than is often encountered in practice; and it seems probable that when an orifice meter for gas is used with throat taps, the equation

$$Y_{calc.} = 1 - \frac{0.41 + 0.33m^2}{\gamma}(1 - y) \tag{9}$$

will always give values of Y that are accurate enough for ordinary commercial purposes.

2. FLANGE AND CORNER TAPS

In Table 4, with the same notation as Table 3, the data in the upper part refer to Bean's observations with flange taps on the Los Angeles natural gas, the values of $\epsilon_{obs.}$ and $\delta\epsilon_{obs.}$ having been found from the observations in the manner described above for throat taps. The lower part of the table refers to Witte's (4) observations with corner taps on superheated steam, air, and nitrogen: and the values of $\epsilon_{obs.}$ were obtained by readings from the published plots of Y against y. (See reference 4, figs. 14 and 15, p. 295.)

TABLE 4.—*Slope coefficient of Y for flange and corner taps*

Observer	D	$\frac{d}{D}=\beta$	$\beta^4=m^2$	$\epsilon_{obs.}$	$\delta\epsilon_{obs.}$	$\frac{0.41+0.37m^2}{\gamma}=\epsilon_{calc.}$	$\epsilon_{obs.}-\epsilon_{calc.}$	Column 8—column 6
1	2	3	4	5	6	7	8	9
	Inches							
	4.03	0.3724	0.0192	0.333	±0.009	0.325	+0.008	.....
		.4967	.0609	.341	.003	.337	+.004	+0.001
		.6207	.1484	.367	.003	.362	+.005	+.002
		.7449	.3079	.387	.015	.408	−.021	−.006
		.8069	.4239	.441	.005	.442	−.001	.....
Bean, flange taps, $\gamma=1.283$	8.05	.1241	.0002	.310	.006	.320	−.010	−.004
		.3105	.0093	.335	.004	.322	+.013	+.009
		.4967	.0609	.329	.005	.337	−.008	−.003
		.6209	.1486	.350	.004	.362	−.012	−.008
		.6829	.2175	.393	.003	.382	+.011	+.008
		.7450	.3080	.412	.005	.408	+.004	.....
		.8070	.4241	.448	.002	.442	+.006	+.004
		.8693	.5711	.491	.003	.483	+.008	+.005
	15.38	.1951	.0014	.309	.006	.320	−.011	−.005
		.3901	.0231	.304	.012	.326	−.022	−.010
		.6501	.1786	.349	.015	.371	−.022	−.007
		.6989	.2386	.409	.018	.388	+.021	+.003
		.7477	.3125	.433	.030	.410	+.023	.....
Witte, corner taps, $\gamma=1.31$	3.94	.20	.0016	.328	.....	.313	+.015	.....
		.4935	.0595	.356	.....	.330	+.026	.....
		.58	.1136	.352	.....	.345	+.007	.....
		.70	.2401	.382	.....	.381	+.001	.....
		.76	.3329	.414	.....	.407	+.007	.....
Witte, corner taps, $\gamma=1.40$	.79	.152	.0005	.275	.....	.293	−.018	.....
		.326	.0112	.332	.....	.296	+.036	.....
	.197	.606	.1347	.312	.....	.328	−.016	.....

In Witte's experiments on steam, the rate of flow was determined by condensation and weighing, and the experimental accuracy was probably higher than could be attained with natural gas. On the other hand, in his experiments on air and nitrogen, the flow was measured by a small wet-drum meter; and while these measurements may have been accurate, the orifices were too small for exact reproduction, and comparison with larger orifices of ostensibly the same geometrical shape is of little significance. The most important result of these small-scale experiments is their satisfactory confirmation of the linear relationship between Y and y.

Since Witte's values of Y are published in the form of small plots, from which it is difficult to make accurate readings, the values of $\epsilon_{obs.}$ given in Table 4 may not do justice to the accuracy of the original data. No attempt has been made to estimate the uncertainty denoted by $\delta\epsilon_{obs.}$ It is impossible to assign definite weights to the 26 values of $\epsilon_{obs.}$; but the 5 values for the largest pipe at Los Angeles and Witte's 3 values for air and nitrogen seem to be considerably less trustworthy than the others.

The values in column 7 of Table 4 were computed from the equation

$$\epsilon_{calc.}=\frac{0.41+0.37m^2}{\gamma} \tag{10}$$

and columns 8 and 9 have the same meanings as in Table 3.

As with equation (9) for throat taps, so here it appears that the slightly modified equation

$$Y_{calc.} = 1 - \frac{0.41 + 0.37m^2}{\gamma}(1-y) \tag{11}$$

represents the facts to an approximation sufficient for ordinary commercial metering, under the following conditions: (*a*) for flange taps, up to $\beta = 0.8$ when $l_1 = l_2 \leqq D/4$, or up to $\beta = 0.87$ when $l_1 = l_2 \leqq D/8$; and (*b*) for corner taps up to $\beta = 0.76$, the highest value for which Witte gives data.

When an orifice for which $\beta = 0.869$ was tested at Los Angeles in the 4-inch pipe, with flange taps, the resulting band of points was strongly concave upward, whereas an orifice of the same diameter ratio in the 8-inch pipe gave a well-defined straight line. The simple linear relation persisted to a higher value of β when the pressure taps were relatively closer to the orifice plate; and in Witte's measurements with corner taps, values of β above 0.76 would probably still have given the linear relation described by the general equation (6) or, in particular cases, by equations (7), (9), and (11).

VI. THEORETICAL COMPUTATION OF *Y*

Some orifice-metering devices work with more than the critical pressure drop, but in the normal meter the range of pressure is less than 2 to 1, and usually very much less. Even with gases that show considerable departures from Boyle's law over the range from 1 atmosphere up to the high pressures at which they may be metered, the departures are nearly always neglible over the range of pressure in an orifice meter; and although the use of the ideal gas equation, $pv = RT$, for computing the density at p_1 from the density at atmospheric pressure, might lead to serious errors, it is permissible to treat the expansion through the orifice as subject to this equation. It may also be stated, without discussing the details of the experimental evidence, that when R_d is large, the flow is very nearly isentropic, at least as far as the vena contracta. The changes of density in the jet may therefore, without appreciable error, be treated as conforming to the thermodynamic equations for isentropic expansion of an ideal gas.

Let us now suppose that the pressure taps are so situated that p_1 is the static pressure in the approaching stream of gas just before it has begun to converge toward the orifice, and p_2 is the static pressure in the jet at the vena contracta, where the flow has become straight and the pressure in the jet sensibly uniform and equal to the static pressure of the gas in the surrounding space.

The area of the orifice being A, let μ_a be the contraction coefficient, so that the cross section of the jet at the vena contracta is $A\mu_a$. Then by the usual, familiar train of reasoning we arrive at the equation

$$M = A\mu_a \sqrt{\frac{2\gamma}{\gamma - 1} p_1 \rho_1 \frac{y^{\frac{2}{\gamma}} - y^{\frac{\gamma+1}{\gamma}}}{1 - \mu_a^2 m^2 y^{\frac{2}{\gamma}}}} \tag{12}$$

And upon comparing this with equation (2) in the form

$$M = KYA\sqrt{2\rho_1(p_1 - p_2)} \tag{13}$$

and introducing the abbreviation

$$\frac{\gamma}{\gamma - 1}\frac{y^{\frac{2}{\gamma}} - y^{\frac{\gamma+1}{\gamma}}}{1-y} \equiv Z \tag{14}$$

we get the equation

$$Y = \frac{1}{K}\sqrt{\frac{Z}{\frac{1}{\mu^2{}_a} - m^2 y^{\frac{2}{\gamma}}}} \tag{15}$$

from which Y may be computed, for any given values of m, K, γ, and y, if the value of μ_a can be determined.

In default of a solution of the equations of motion, μ_a can be found only by recourse to some plausible, simplifying assumption. In an earlier paper (8) it was assumed that, at any given mass flow, the force exerted by the gas on the upstream face of the orifice plate was the same, whether the subsequent flow through the orifice was isentropic or went on without change of density, as for liquids. If the jet issues into a space in which the static pressure is uniform, and is therefore the same all over the boundary of the jet and the downstream face of the plate as in the vena contracta, the assumption makes it possible to apply the momentum principle and obtain a relation between the contraction coefficient μ_a, and the contraction coefficient, μ, for a jet of liquid from the same orifice. The latter may readily be shown to satisfy the equation

$$\mu = \frac{K}{\sqrt{1 + m^2 K^2}} \tag{16}$$

so that μ may be computed from the diameter ratio of the orifice and the value of K, which is accessible to measurement, either by experiments with a liquid or as the limiting value of C in experiments with a gas.

The relation in question (equation (20) of reference 8) may be put into the form

$$\mu_a = \frac{Z}{y^{\frac{1}{\gamma}} B}\left(1 - \sqrt{1 - \frac{y^{\frac{2}{\gamma}} B}{Z^2}}\right) \tag{17}$$

where

$$B = \left(m^2 + \frac{2}{\mu} - \frac{1}{\mu^2}\right) Z - m^2 y^{\frac{2}{\gamma}} \tag{18}$$

and Z is defined by equation (14).

The value, or lack of value, of the assumption on which equation (17) is based is to be determined by comparing the resulting "theoretical" values of Y with values found by experiments with a gas on an orifice which is so installed that the conditions regarding p_1 and p_2 are satisfied.

The value of K, found either by testing with a liquid or by extrapolation to $y=1$ from the experiments with the gas, is substituted in equation (16), together with the measured value of $\beta^2=m$, to give the value of μ; a value of y is selected, and with the given value of γ the value of Z is computed from equation (14); and after these preliminaries, B, μ_a, and Y are computed, successively, from equations (18), (17), and (15). The value of Y may then be compared with the value found by experiment at the selected value of y.

VII. COMPARISON OF THEORETICAL AND EXPERIMENTAL VALUES OF Y

In the deduction of equation (12), p_1 and p_2 represent the static pressure in the stream just before it begins to converge toward the orifice, and the static pressure in the jet at the vena contracta; and if the theory is to be tested by comparing values of Y from equation (15) with values obtained by experiment, the pressure taps in the experimental apparatus must be so placed as to conform to the requirements of the theory. For diameter ratios up to 0.75, the former condition may be satisfied, within the precision of all but the most refined measurements, by placing the upstream side hole anywhere within the limits $0.5D \lessapprox l_1 \lessapprox 2D$; but the location of the downstream side hole requires more care.

Visual observations with orifices installed in glass pipes have shown that the vena contracta occurs at about the same cross section of the pipe as the minimum static pressure at the wall, and it is commonly assumed that this minimum pressure is identical with the pressure in the jet at the vena contracta. No direct experimental proof of this is known to the present writer, but there is no obvious reason for doubting that the assumption is substantially correct, and it will be accepted here.

For low values of β, the downstream minimum of pressure is about one pipe diameter from the orifice, but is too flat to be located accurately. As β is increased, the minimum becomes more pronounced and moves closer to the orifice, but its position also depends to some extent on the rate of flow, being blown farther downstream if the speed of the jet is raised (9). Nevertheless, the pressure in a fixed side hole at the distance $l_2=0.5D$ from the orifice plate is only very slightly higher than the minimum pressure, unless β is large; and up to $\beta=0.75$ the difference is not more than 0.005 (p_1-p_2), which corresponds to a change in C of only 0.25 per cent. It is therefore evident that measurements of p_1 and p_2 with throat taps will come very close to satisfying the conditions presupposed in the deduction of equation (15).

The deduction of equation (17) is subject to the further condition that the static pressure on the downstream face of the orifice plate, and over the bounding surface of the jet as far as the vena contracta, shall be uniform and equal to the pressure inside the jet at the vena contracta. This requirement is satisfied when the jet discharges into the open air, as in Bachmann's experiments (7), or in the ordinary installation when β is small. As β is increased, the static pressure in the region about the jet becomes less uniform, if we may judge by observations at a series of small side holes distributed along the wall of the pipe, and the conditions for the validity of equation (17) are less nearly satisfied.

1. THROAT TAPS

It is impossible to form a quantitative estimate of the effects of the departures from the theoretical conditions just considered, and the comparison of theory with experiment will therefore be carried up to $\beta=0.75$, which is as far as the Los Angeles experiments with throat taps gave well-determined values of Y.

To cover this range of diameter ratios six of the Los Angeles orifices were selected as having particularly well determined values of ϵ_{obs}; they are marked with asterisks (*) in column 5 of Table 3. Values of Y were computed from equation (15) at $y=0.5---0.9$, with $\gamma=1.283$ and the values of K shown in column 10 of Table 3, which were found graphically at the same time as the values of ϵ_{obs}.

The first result to be noted is that the theoretical curves, $Y=f(y)$, are slightly convex upward, the curvature being greatest for low values of β. For $y\gtrless 0.6$, the computed points are not far from the straight line drawn from the point ($y=1$, $Y=1$) through the point computed for $y=0.7$. The slope of this line will be denoted by $\epsilon_{0.7}$, and the ordinates by

$$Y_{0.7}=1-\epsilon_{0.7}\,(1-y) \tag{19}$$

The value of $(Y-Y_{0.7})$ at any value of y, is the amount by which the computed theoretical curve is above the straight line at that value of y, and these amounts are shown in Table 5.

TABLE 5.—*Curvature of the computed curve* $Y=f(y)$

γ	D	β	$K_{obs.}$	Values of $(Y-Y_{0.7})$				
				$y=0.5$	0.6	0.7	0.8	0.9
	Inches							
	8.05	0.1241	0.595	−0.0083	−0.0030	±0.0000	+0.0012	+0.0011
	8.05	.3105	.606	−.0080	−.0028	±.0000	+.0011	+.0011
	4.03	.4967	.630	−.0071	−.0026	±.0000	+.0010	+.0008
1.283	4.03	.6207	.668	−.0059	−.0020	±.0000	+.0008	+.0006
	8.05	.6829	.696	−.0049	−.0016	±.0000	+.0006	+.0004
	8.05	.7450	.737	−.0036	−.0011	±.0000	+.0003	+.0001
1.40	3.25	.2428	.600	−.0076	−.0028	±.0000	+.0012	+.0011

The fourth figure in Y is not certain, but the table suffices to give an idea of the degree of curvature and its regular increase as β decreases. As already noted, experiments indicate that when β is small the true curve is slightly convex upward, although for larger values of β it is sensibly a straight line.

The computations were also carried out for Bachmann's (7) orifice with $\beta=0.2428$, $K=0.600$, and $\gamma=1.40$; and Table 6 contains values of the following quantities for each of the seven orifices:

Y computed from equation (15);

$Y_{0.7}$ computed from equation (19); and

$Y_{obs.}$ computed from equation (6), with $\epsilon_{obs.}$ taken from column 5 of Table 3.

TABLE 6.—*Computed and observed values of Y for throat taps (Bean, $\gamma=1.283$) and free discharge (Bachmann, $\gamma=1.40$)*

$\epsilon_{0.7}$ ϵ_{obs} $\epsilon_{calc.}$	β	K		$y=0.5$	0.6	0.7	0.8	0.9
0.303	0.1241	0.595	Y	0.841	0.876	0.9094	0.941	0.971
.313			$Y_{0.7}$	.849	.879	.909	.940	.970
.320			Y_{obs}	.844	.875	.906	.937	.969
.313	.3105	.606	Y	.836	.872	.9062	.939	.970
.329			$Y_{0.7}$	.844	.875	.906	.937	.969
.322			Y_{obs}	.836	.868	.901	.934	.967
.333	.4967	.630	Y	.826	.864	.9000	.934	.968
.342			$Y_{0.7}$	.834	.867	.900	.933	.967
.335			Y_{obs}	.829	.863	.897	.932	.966
.365	.6207	.668	Y	.812	.852	.8904	.928	.964
.363			$Y_{0.7}$	.818	.854	.890	.927	.963
.358			Y_{obs}	.819	.855	.891	.927	.964
.387	.6829	.696	Y	.801	.843	.8838	.923	.962
.383			$Y_{0.7}$	.807	.845	.884	.923	.961
.376			Y_{obs}	.809	.847	.885	.923	.962
.419	.7450	.737	Y	.787	.831	.8742	.916	.958
.403			$Y_{0.7}$	.791	.832	.874	.916	.958
.399			Y_{obs}	.799	.839	.879	.919	.960
.283	.2428	.600	Y	.851	.884	.9151	.945	.973
.302			$Y_{0.7}$	.859	.887	.915	.943	.972
.294			Y_{obs}	.849	.879	.909	.940	.970

In the first column, values of $\epsilon_{0.7}$ are given for comparison with those of $\epsilon_{obs.}$ and $\epsilon_{calc.}$, repeated from columns 5 and 7 of Table 3.

Small discrepancies between Tables 6 and 5 are due to the dropping of subsequent figures.

2. CORNER TAPS

Observations of pressure at corner taps do not quite satisfy the conditions for which equation (15) was deduced, and if the results of such observations are to be used for testing the value of that equation, the experimental values of K must first be reduced to what they would have been if the pressures had been observed at throat taps, which conform more nearly to the requirements of the theory. This can not, at present, be done with any great accuracy, but in order not to neglect the opportunity offered by the publication of Witte's (4) observations on steam, the reduction will be attempted. It might be effected by means of Witte's observations on the longtitudinal distribution of pressure at the wall of the pipe near the orifice plate; but the uncertainty of readings from the rather small-scale curves by which the results are represented (see reference 4, Pt. II) has led me to prefer using the somewhat similar data obtained at Chicago in 1924 (9).

Letting K_c denote the value of K for corner taps and writing

$$K=b\,K_c \tag{20}$$

values of the reduction factor b were found, by interpolation in Table 19 of reference 9, from the equation

$$b=\frac{C(24,12)}{C(1,1)} \tag{21}$$

in which $C(24,12)$ and $C(1,1)$ represent the values of C for an orifice installed in a smooth pipe of 23.3 inches inside diameter, when the distances from the orifice plate to the side holes were, respectively, 24 and 12 inches, and 1 and 1 inch, the ratio being deduced from the observed longitudinal distribution of pressure.

The identification of $C(1,1)$ with the value $C(0,0)$ that would be obtained with the side holes right at the faces of the plate instead of $D/23.3$ away, is of course not exact; the difference is small but not yet accurately known, and it varies with the diameter of the side holes (4). Furthermore, the pressure distribution is not entirely independent of the pressure ratio. The values of b found as described above are therefore slightly uncertain, but in default of a detailed tabulation of Witte's measurements it appears that we can do no better at present.

Table 7 refers to the five orifices for which Witte gives values of $Y=f(y)$ determined with superheated steam (see reference 4, fig. 15): the notation and arrangement are the same as in Table 6, with the addition of two columns containing K_c, as given by Witte, and b, obtained as already described. The values of Y were computed from equation (15) with $\gamma=1.31$ and $K=bK_c$; and those of $\epsilon_{obs.}$ and $\epsilon_{calc.}$ in the first column are repeated from Table 4.

TABLE 7.—*Computed and observed values of Y for corner taps (Witte, $\gamma=1.21$)*

$\epsilon_{0.7}$ ϵ_{obs} $\epsilon_{calc.}$	β	K_c	b	$bK_c=K$		$y=0.5$	0.6	0.7	0.8	0.9
1	2	3	4	5	6	7	8	9	10	11
0.304	0.20	0.604	0.9984	0.6030	Y	0.840	0.875	0.9087	0.940	0.971
.328					$Y_{0.7}$	.848	.878	.909	.939	.970
.313					$Y_{obs.}$	.836	.869	.902	.934	.967
.318	.4935	.622	.9991	.6215	Y	.833	.870	.9046	.937	.969
.356					$Y_{0.7}$	.841	.873	.905	.936	.968
.330					$Y_{obs.}$	.822	.858	.893	.929	.964
.336	.58	.644	.9998	.6439	Y	.825	.863	.8992	.934	.967
.352					$Y_{0.7}$	.832	.866	.899	.933	.966
.345					$Y_{obs.}$	.824	.859	.894	.929	.965
.378	.70	.692	1.0081	.6976	Y	.805	.847	.8866	.925	.963
.382					$Y_{0.7}$	.811	.849	.887	.924	.962
.381					$Y_{obs.}$	.809	.847	.885	.924	.962
.416	.76	.730	1.0202	.7447	Y	.788	.832	.8753	.917	.959
.414					$Y_{0.7}$	.792	.834	.875	.917	.958
.407					$Y_{obs.}$	.793	.834	.876	.917	.959

A question might arise here concerning the values of $\epsilon_{obs.}$. Let p_1' and p_2' be the pressures measured at corner taps, while p_1 and p_2 are the upstream and downstream minimum pressures dealt with by the theory. To be comparable with values of Y computed from the reduced values of K, the observed values of Y should be plotted against the simultaneous values of p_2/p_1; and if, by an oversight, the abscissa in the plot were p_2'/p_1', the values of $\epsilon_{obs.}$ read from the plot would need slight corrections, which would, however, be negligible except for the two largest orifices. In reality, the abscissa in the figure is stated to be p_2/p_1, and since it must be assumed that the statement is correct, no further reduction has been undertaken.

In view of the uncertainties involved in the foregoing reduction of Witte's experimental data, to say nothing of the difficulty of making accurate readings from his published figure, the surprisingly close agreement of Y and Y_{obs} for the two largest orifices is not to be taken too seriously. Nevertheless, it appears that, over the range $0.6 < y < 1.0$ and $0.2 \leqq \beta \leqq 0.76$, equation (15), developed by theoretical reasoning from an initial approximating assumption, does give a fairly good representation of the best established experimental facts for steam ($\gamma = 1.31$), as well as for natural gas ($\gamma = 1.283$) and for air ($\gamma = 1.40$).

VIII. SUMMARY

1. NOTATION

With all quantities expressed in terms of normal units, such as "British absolute" or cgs, let C be the discharge coefficient of an orifice meter of the type illustrated by Figure 1, as defined by the equation

$$M = CA\sqrt{2\rho_1(p_1 - p_2)} \tag{A}$$

in which:

M = the mass discharged per unit time;
A = the area of the orifice;
p_1, p_2 = the static pressures observed at the upstream and down-stream side holes or pressure taps; and
ρ_1 = the density of the gas at p_1 and the upstream temperature.

In addition to the foregoing notation, let

d = the diameter of the orifice;
D = the diameter of the pipe in which it is installed;
$\beta = d/D$ = the diameter ratio, or
$m = \beta^2$ = the area ratio;
l_1, l_2 = the distances from the orifice plate to the centers of the upstream and downstream side holes;
$y = p_2/p_1$ = the pressure ratio;
$\gamma = C_p/C_v$ = the specific heat ratio of the gas;
η = the viscosity of the gas;
$R_d = 4M/\pi d\eta$ = the Reynolds number;
K = the value obtained for C when the meter is tested with water or other liquid under conditions that make $R_d > 200{,}000\text{–}M$, ρ_1, and η now referring to the liquid;
$Y = C/K$ = the expansion factor for the gas; and
$\epsilon = (1 - Y)/(1 - y)$, so that

$$C = KY \tag{B}$$

and

$$Y = 1 - \epsilon\,(1 - y) \tag{C}$$

2. CONCLUSIONS

The following statements and conclusions are subject to the restriction that $R_d > 200{,}000$, a condition which is nearly always satisfied in the commercial measurement of gas by orifice meters except when the orifices are very small.

1. The water coefficient, K, is sensibly constant for any one orifice when installed and operated in a prescribed manner.

2. When the meter is used for gas, $C \doteq K$ or $Y \doteq 1$, when $y \doteq 1$.

These two facts are already familiar from the published work of Witte and others. The condition $R_d > 200{,}000$ results from Witte's experiments (3). The following statements are conclusions from the discussion in the present paper of experimental data obtained with pressure taps located within the limits $l_1 \leqq 2D$ and $l_2 \leqq 0.5D$: they may or may not be true outside those limits.

3. When $\beta < 0.2$, the curve $Y = f(y)$ is slightly concave toward the y axis, but the data for low values of β are scanty and no more specific statement is possible.

4. When $0.2 \leqq \beta \leqq 0.75$, $Y = f(y)$ is linear within the present accuracy of orifice meter measurements, at least as far down as the critical value of y; in other words, ϵ is a constant for any one orifice meter.

5. When $\beta > 0.75$, the linearity of $Y = f(y)$ may or may not persist, according to the location of the pressure taps.

(*a*) For $l_1 = D$ and $l_2 = 0.5D$ (throat taps), the curve is convex toward the y axis at $\beta = 0.8$ and still more so when $\beta = 0.87$. Presumably, the linear relationship ceases to hold soon after β exceeds 0.75.

(*b*) For $l_1 = l_2 = D/4$ (flange taps in a 4-inch pipe), $Y = f(y)$ is still represented by a straight line at $\beta = 0.8$; but at $\beta = 0.87$ the curve is strongly convex toward the y axis.

(*c*) For $l_1 = l_2 = D/8$ (flange taps in an 8-inch pipe) the linear relationship still persists at $\beta = 0.87$.

(*d*) For corner taps there are no satisfactory data above $\beta = 0.76$; but (*b*) and (*c*), above, indicate that $Y = f(y)$ would still be linear at considerably higher values of β.

6. Within the limits $0.2 \leqq \beta \leqq 0.75$, where each of the foregoing arrangements of the pressure taps gives a linear change of Y with y, or a constant ϵ for each orifice, the values of ϵ vary systematically with β and γ, and the values of Y are given approximately by the equation

$$Y = 1 - \frac{0.41 + 0.35m^2}{\gamma}(1 - y) \qquad \text{(D)}$$

The available observations may be slightly better represented by using separate equations for throat, and for corner and flange taps; but the difference is little, if at all, greater than the experimental uncertainties. And it seems probable that when the pressure ratio is greater than 0.8, as it is in the vast majority of practical metering operations, the mean equation (D) will always give the value of Y correctly within 0.5 per cent, and usually much closer than that, provided that the pressure taps are located within the limits $l_1 \leqq 2D$ and $l_2 \leqq 0.5D$.

Further accumulation of experimental data may require some modification of the numerical coefficients of equation (D), but it seems improbable that the changes will be of serious importance to gas engineers.

Although the variations of the limiting or liquid coefficient, K, have not been discussed in this paper, it may be stated here that the values of Y, or of the slope coefficient ϵ, are much less sensitive to changes of tap location or roughness of the pipe than the values of K.

7. In continuation of an earlier paper (8), a theoretical method for computing Y has been developed, and has been shown to be in fair agreement with the experimental facts in a number of typical cases.

IX. REFERENCES

1. Regeln für die Durchflussmessung mit genormten Düsen und Blenden, V. D. I. Verlag, Berlin, 1930.
2. H. S. Bean, An Apparatus and Method for Determining the Compressibility of a Gas and the Correction for "Supercompressibility," B. S. Jour. Research, vol. 4 (RP170), p. 645, May, 1930.
3. R. Witte, Durchflusszahlen von Düsen und Staurändern; Techn. Mech. u. Thermodynamik, vol. 1, Nos. 1, 2, 3, 1930. (Forschung, vol. 1.)
4. R. Witte, Die Strömung durch Düsen und Blenden; Forschung, vol. 2, pp. 245 and 291, July and August, 1931.
5. John L. Hodgson, The Orifice as a Basis of Flow Measurement; Inst. Civ. Eng., 1925, Selected Engineering Papers, No. 31.
6. B. S. Jour. Research, vol. 2 (RP49), p. 561, March, 1929.
7. H. Bachmann, Beitrag zur Messung von Luftmengen; Dissertation, Darmstadt, 1911.
8. Edgar Buckingham, Note on Contraction Coefficients of Jets of Gas, B. S. Jour. Research, vol. 6 (RP303), p. 765, May, 1931; or Beitrag zur Berechnung der Kontraktionszahl, Forschung, vol. 2, p. 185, May, 1931.
9. Howard S. Bean, M. E. Benesh, and Edgar Buckingham, Experiments on the Metering of Large Volumes of Air; B. S. Jour. Research, vol. 7 (RP335), p. 93, July, 1931.

WASHINGTON, May 23, 1932.

122486—32——6

THEORY OF VOLTAGE DIVIDERS AND THEIR USE WITH CATHODE RAY OSCILLOGRAPHS

By Melville F. Peters, George F. Blackburn, and Paul T. Hannen

ABSTRACT

Four requirements are given for voltage dividers, and equations have been developed for the most general type of capacitance voltage divider. Special cases of the most general type are discussed. These equations show that if the capacitance of the voltage divider is small, the capacitance to ground can not be neglected if the deflection of the cathode beam is to be proportional to the applied voltage. A number of oscillograms of spark discharge using five types of circuits confirm the equations. It was found that resistors had to be placed in the voltage divider to damp out oscillations set up in the divider. Equations are given for resistance voltage dividers expressing the relation between the divided voltage and the applied voltage in terms of the resistance and self-capacitance of the resistors. The equations show that only under special conditions will the deflection of the cathode beam be proportional to the applied voltage. Oscillograms taken at frequencies of 20 to 1,000 kc confirm the equations as closely as can be expected with the simple assumptions used in deriving them. Methods are given for the determination of the sensitivity of the cathode beam at the photographic plate, as well as the determination of the reduction ratio of the voltage divider.

CONTENTS

		Page
I.	Introduction	81
II.	General requirements for a voltage divider	82
III.	Analysis of voltage divider characteristics	82
	1. Capacitance voltage divider	82
	2. Resistance voltage divider	92
IV.	Description of apparatus	94
V.	Experimental results with circuits 1 to 5	97
	1. Method of balancing voltage divider to satisfy equation (5)	97
	2. Experimental verification of requirement 2 and equation (6)	98
	3. Oscillograms showing the variation of voltage in magneto spark discharges	99
VI.	Experimental results with resistance voltage dividers	104
VII.	Oscillograph technique	104
	1. Alignment of the cathode tube	105
	2. Sensitivity of the cathode beam	106
VIII.	Calibration of the capacitance voltage divider	110
	1. Calibration by application of known voltages	111
	2. Calibration by use of the oscillator	112
IX.	Conclusion	114
X.	Acknowledgements	114

I. INTRODUCTION

A fundamental requirement for an instrument designed to measure potential difference in an electric circuit is that the measuring instrument shall not introduce more than a negligible change in the character of the circuit under consideration. This sometimes imposes limiting conditions upon the instrument, especially in the case of measuring the voltage across a spark gap with a cathode ray oscillograph under conditions found in practice.

In automotive ignition systems the capacitance and inductance are low. Measurements made on aircraft engines showed the capacitance of the leads to vary from 40 to 180 $\mu\mu$f. On radio-shielded engines the capacitance is usually greater than this and has been found to be as high as 400 $\mu\mu$f. The proximity of the leads to the engine causes the inductance to change with frequency. At high frequencies the iron has very little importance and computations made for the shorter leads, disregarding the effect of iron, showed the inductance to be approximately 1 μh.

If the voltages are sufficiently low so that they may be applied directly to the deflection plates of the oscillograph, the latter increases the capacitance of the circuit by approximately 20 $\mu\mu$f. If a short lead is used from the magneto to the spark gap the combined capacitance of the circuit need not exceed 40 $\mu\mu$f, which enables the experimenter to set up a test circuit which is a sufficiently close approximation to the actual circuit as regards capacitance.

If the voltage is too high to be applied directly to the deflection plates a voltage divider must be used. In a study of magneto discharges it was found that a voltage divider was required, and one was designed which introduced a capacitance of 20 $\mu\mu$f. This voltage divider proved unsatisfactory and the present investigation was undertaken to study various possible arrangements and to determine which would be the most suitable for measuring the voltage characteristics of magneto spark discharges.

II. GENERAL REQUIREMENTS FOR A VOLTAGE DIVIDER

The oscillograph records the difference of potential between the two deflection plates at any instant. In order that the voltage recorded by the oscillograph shall be a true representation of the voltage to be measured it is necessary that the following conditions be satisfied.

1. Introduction of the voltage divider must not affect materially the character of the circuit.
2. The potential difference across the deflection plates must at every instant be proportional to that across the divider, and the ratio must remain constant at all frequencies. This insures that the two potential differences will be in phase.
3. The voltage between the deflection plates and ground must not be sufficient to cause a breakdown in the deflection tube or introduce spurious effects on the cathode beam.
4. There must be no natural oscillation in any part of the voltage divider which will produce spurious effects.

In the following discussion these requirements will be referred to by number.

III. ANALYSIS OF VOLTAGE DIVIDER CHARACTERISTICS

1. CAPACITANCE VOLTAGE DIVIDER

The most general type of capacitance voltage divider is shown diagrammatically in Figure 1. Referring to the figure let A and A' be two points, which may be the electrodes of a sphere gap or spark plug, having potentials V_A and V_A' with respect to ground. Let V_B and V_B' be the potentials with respect to ground of the two deflection

plates as indicated. Let C_1 and C_1' be the capacitances of the two series capacitors, and C_3' the capacitance of the capacitor shunted across the deflection plates of the oscillograph. The capacitance of these plates is C_3. Let C_2 and C_2' be capacitances to ground, which are the effective capacitances to ground of the portion of the circuit metallically connected to C_2 and C_2', respectively. By an inspection of Figure 1 equations (1) and (2) may be written

$$(V_A - V_B)C_1 = V_B C_2 + (V_B - V_B')(C_3 + C_3') \tag{1}$$

$$(V_A' - V_B')C_1 = V_B' C_2' + (V_B' - V_B)(C_3 + C_3') \tag{2}$$

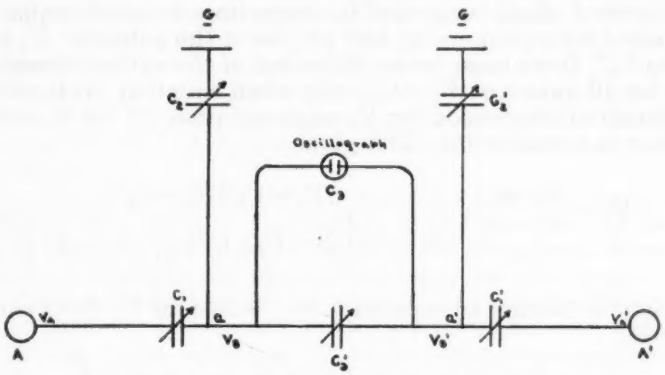

FIGURE 1.—*Capacitance voltage divider circuit*

Subtracting (2) from (1) an expression is obtained for

$$V_A - V_A' = V_B\left[1 + (C_3 + C_3')\left(\frac{1}{C_1} + \frac{1}{C_1'}\right) + \frac{C_2}{C_1}\right] - V_B'\left[1 + (C_3 + C_3)\left(\frac{1}{C_1'} + \frac{1}{C_1'}\right) + \frac{C_2'}{C_1'}\right] \tag{3}$$

In a similar manner an expression may be obtained for $V_B - V_B'$ which reduces to

$$V_B - V_B' = \frac{(V_A - V_A')\left[C_1C_1' + \frac{C_1C_2' + C_1'C_2}{2}\right] + \frac{(V_A + V_A')}{2}\left[C_1C_2' - C_1'C_2\right]}{(C_1 + C_2)(C_1' + C_2' + C_3 + C_3') + (C_1' + C_2')(C_3 + C_3')} \tag{4}$$

Equation (4) shows that the deflection which corresponds to $V_B - V_B'$ will, in general, depend not only on the potential difference $V_A - V_A'$ which is to be measured, but also on the average potential $\frac{V_A + V_A'}{2}$ of the points A and A' above ground. This latter effect can be eliminated by adjusting the circuit to make

$$\frac{C_2}{C_1} = \frac{C_2'}{C_1'} \tag{5}$$

When this adjustment is made equations (3) and (4) may be written

$$\frac{V_B - V_B'}{V_A - V_A'} = \frac{1}{K} \tag{6}$$

where

$$K = \left[1 + (C_3 + C_3')\left(\frac{1}{C_1} + \frac{1}{C_1'}\right) + \frac{C_2}{C_1}\right]$$

and will be referred to as the reduction factor. Equation (6) shows that if the capacitances of the capacitors are independent of frequency the voltage divider will satisfy the second general requirement.

The method of adjustment of the capacitors to satisfy equation (5) is suggested by equations (3) and (4), for if the potential V_A is made equal to V_A', there must be no deflection of the cathode beam. This is true for all values of $V_A = V_A'$ only when equation (5) is satisfied.

To obtain an expression for V_B solve equation (1) for $V_B - V_B'$ and substitute in equation (5). This gives

$$V_B = \frac{V_A C_1}{C_1 + C_2} - \frac{(V_A - V_A')(C_3 + C_3')}{(C_1 + C_2)\left[1 + (C_3 + C_3')\left(\frac{1}{C_1} + \frac{1}{C_1'}\right) + \frac{C_2}{C_1}\right]} \tag{7}$$

In a similar manner an expression is obtained for V_B' from equations (2) and (5)

$$V_B' = \frac{V_A' C_1'}{C_1' + C_2'} + \frac{(V_A - V_A')(C_3 + C_3')}{(C_1' + C_2')\left[1 + (C_3 + C_3')\left(\frac{1}{C_1} + \frac{1}{C_1'}\right) + \frac{C_2'}{C_1'}\right]} \tag{8}$$

Equations (7) and (8) give the potentials of the two deflection plates to ground in terms of the applied potential to ground and the electrical constants of the voltage divider. The maximum value which V_B and V_B' may have to satisfy the third requirement depends upon the limitations imposed by the oscillograph. For this reason they must be estimated or determined experimentally, in which case, it may be more desirable to solve equations (7) and (8) for $\frac{C_2}{C_1}$ and $\frac{C_2'}{C_1'}$ respectively, in terms of $\frac{(C_3 + C_3')}{C_1}$, $\frac{(C_3 + C_3')}{C_1'}$. This solution leads to the following relations:

$$\frac{C_2}{C_1} = \frac{1}{2}\left[\frac{V_A}{V_B} - (C_3 + C_3')\left(\frac{1}{C_1} + \frac{1}{C_1'}\right) - 2\right] \pm \frac{1}{2}\sqrt{(C_3 + C_3')^2\left(\frac{1}{C_1} + \frac{1}{C_1'}\right)^2 + 2(C_3 + C_3')\left(\frac{1}{C_1} + \frac{1}{C_1'}\right)\frac{V_A}{V_B} - 4\frac{(C_3 + C_3')}{C_1}\frac{(V_A - V_A')}{V_B} + \frac{V_A^2}{V_B^2}} \tag{9}$$

$$\frac{C_2'}{C_1'}=\frac{1}{2}\left[\frac{V_A'}{V_B'}-(C_3+C_3')\left(\frac{1}{C_1}+\frac{1}{C_1'}\right)-2\right]$$

$$\pm\frac{1}{2}\sqrt{(C_3+C_3')^2\left(\frac{1}{C_1}+\frac{1}{C_1'}\right)^2+2(C_3+C_3')\left(\frac{1}{C_1}+\frac{1}{C_1'}\right)\frac{V_A'}{V_B'}+4\frac{(C_3+C_3')}{C_1'}\frac{(V_A-V_A')}{V_B}+\frac{V_A'^2}{V_B'^2}} \tag{10}$$

If the maximum potentials V_A, V_A', V_B and V_B' are known approximately, the problem is to determine the five variable capacitors so as to obtain the desired deflection of the cathode beam and at the same time satisfy the four requirements. Methods of making calculations will now be given, and to simplify the presentation four cases will be considered governed by the maximum potentials of V_A and V_A', and a fifth case pertaining to the elimination of oscillations in the voltage divider. The five corresponding circuits will be designated hereafter as circuits 1, 2, 3, 4, and 5. They are shown diagrammatically in Figure 2.

An experimental study of these five circuits has been made at frequencies from 20 to 1,000 kc per second. It was found that at frequencies above 1,000 kc care must be taken in the design and selection of the capacitors and that the drop in the leads from the source to the voltage divider, as well as in the leads in the voltage divider itself become important. It was also found that resonance occurred in the voltage divider when voltage at 10^4 kc frequency was applied across A and A'. This was first observed when sparking occurred across the plates of the capacitors C_1 and C_1', and later verified by connecting a milliammeter between A and C_1. At resonance the milliammeter indicated a large current.

To eliminate repetition, certain characteristics of the circuits in the five cases are given.

1. To satisfy requirement 1 the maximum capacitance of C_1 was taken as 10 μf.

2. The cathode beam was deflected 1 cm at the photographic plate for each 250 volts applied to the horizontal deflection plates. The maximum deflection which can be measured is approximately 5.6 cm, so that V_B-V_B' must not be greater than 1,400 volts.

3. With a potential difference of 60,000 volts applied to the cathode tube the average potential gradient between cathode and anode is $\frac{60{,}000}{17.5}=3{,}500$ volts per centimeter. The distance between the two pairs of deflection plates is 11 mm, and to insure against appreciable leakage from one pair to the other the average potential gradient between them was arbitrarily limited to half of that between cathode and anode. The potential difference between the pairs of deflection plates was accordingly limited to $\frac{3{,}500}{2}\times 1.1=1{,}925$ volts. Since the maximum potential of the oscillator plate to ground may be ± 700 volts but was usually 500 volts, the greatest potential V_B or V_B' should have is $1{,}925-500=1{,}425$ volts. This is also the potential of V_B when $V_B'=0$ and the deflection of the cathode beam at the photographic plate is 5.6 cm.

4. The capacitance C_3 in this treatment signifies the capacitance of the circuit metallically connected to one plate of the capacitor C_3 with respect to the circuit metallically connected to the other plate of C_3 with C_3' omitted. The capacitance C_3 was estimated to be 25 $\mu\mu$f.

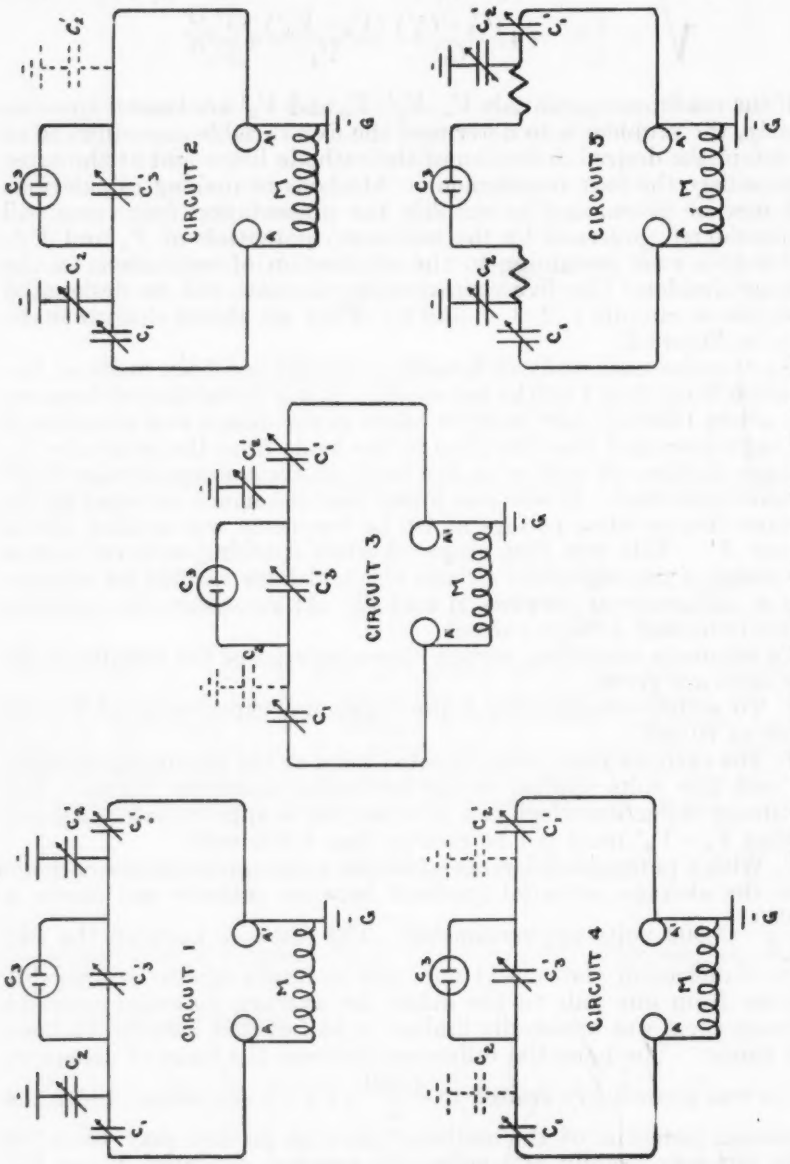

FIG. 2.—*Five types of capacitance voltage divider circuits*

5. The capacitance C_2 signifies the capacitance to ground of the circuit consisting of the ungrounded plate of C_2 and the parts metallically connected to it, and C_2' has the corresponding meaning. It was estimated that when C_1 and C_1' had their maximum values of 10

$\mu\mu$f each, the capacitances designated as C_2 and C_2' would not be less than 25 $\mu\mu$f each, even though the capacitors C_2 and C_2' were removed.

Circuit 1. V_A and V_A' large.—Let the maximum potential of A be 10,000 volts and suppose that at the same instant A' has a maximum potential of 6,000 volts. To simplify the problem make the circuit symmetrical; that is, $C_1=C_1'$, $C_2=C_2'$.

If the value $V_A-V_A'=4{,}000$ volts be substituted in equation (6) it is found that in order to obtain a deflection of the cathode beam corresponding to 1,400 volts, K must be equal to 2.86.

It does not follow that it is permissible to adjust the circuit so that K shall have this value, and it is found that with this value of K, it is not possible to satisfy the third requirement, concerning the maximum potentials of V_B and V_B'. It is therefore necessary to use a larger value of K; that is, to work with less than the full deflection of the cathode beam.

To find the smallest value of K which makes it possible to satisfy the first three requirements it is necessary to use equation (9). Substituting in equation (9) the values

$$\frac{V_A}{V_B}=\frac{10{,}000}{1{,}400}=7.14,\quad \frac{V_A-V_A'}{V_B}=\frac{10{,}000-6{,}000}{1{,}400}=2.86,\quad C_1=C_1'$$

and plotting $\frac{C_2}{C_1}$ versus $\frac{C_3+C_3'}{C_1}$ the curve shown at (a) in Figure 3 was obtained. From this curve may be obtained the value which $\frac{C_2}{C_1}$ must have when $\frac{C_3+C_3'}{C_1}$ is selected, or vice versa, in order that V_B shall be equal to 1,400 volts when V_A and V_A' have their maximum values. If K is computed from curve (a) and the value plotted versus $\frac{C_3+C_3'}{C_1}$ the curve shown at (b) is obtained. This curve shows that the smallest value of K is obtained when $\frac{C_3+C_3'}{C_1}=0$, and the value of K increases as $\frac{C_3+C_3'}{C_1}$ increases. To make $\frac{C_3+C_3'}{C_1}$ as small as possible C_3' is made zero, and C_1 is given its largest value of 10 $\mu\mu$f. C_3 is constant and equal to 25 $\mu\mu$f so that the smallest value of $\frac{C_3+C_3'}{C_1}$ is $\frac{0+25}{10}=2.5$. The corresponding value of $\frac{C_2}{C_1}$, curve (a), is 5.52, hence $C_2=55.2$ $\mu\mu$f and $K=11.52$. Substituting this value of K in equation (6), $V_B-V_B'=347$ volts, which is the maximum possible potential difference across the deflection plates when all the requirements are complied with.

Since this corresponds to a deflection of less than 2 cm at the photographic plate it is worth while to consider whether this deflection could be appreciably increased by removing the restrictions on the values of V_B and V_B'. Plotting V_B and V_B' as given by equations (7) and (8) with C_2 as the independent variable the two curves shown at (a) and (b) in Figure 4 were obtained. Determining V_B-V_B' from curves (a) and (b) for a number of values of C_2, the curve shown at (c) was plotted. This curve shows that with the value $C_1=C_1'=$ 10 $\mu\mu$f, $C_3+C_3'=25$ $\mu\mu$f, and the smallest value of $C_2=C_2'=25$ $\mu\mu$f,

FIG. 2.—*Five types of capacitance voltage divider circuits*

the greatest deflection which can be obtained at the photographic plate corresponds to 450 volts at the deflection plates. Curve (*a*) shows however that V_s would be 2,500 volts, and since, as has been mentioned previously, the other pair of deflection plates may have a potential to ground of opposite sign and amounting to 500 volts, the

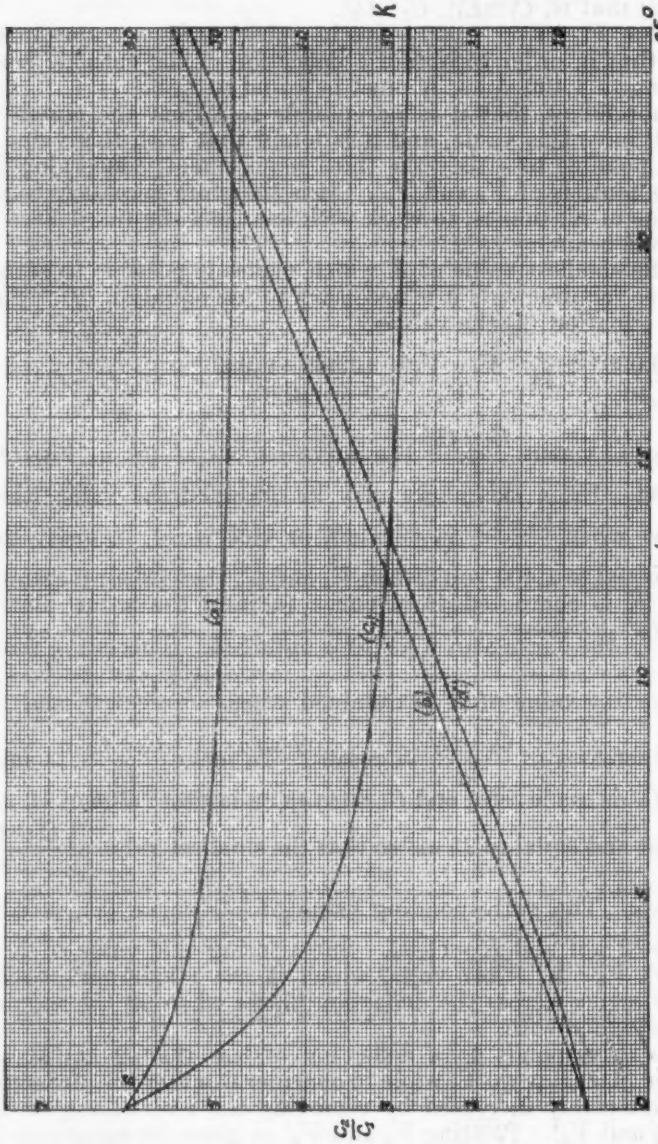

FIGURE 3

Curves *a* and *c* show the change in $\frac{C_2}{C_1}$ with $\frac{C_3+C_3'}{C'}$. Curves *b* and *d* show the change in *K* with values taken from curves *a* and *c*.

potential difference between the pairs of plates might be sufficient to cause a discharge to take place between them.

The manner in which the capacitors C_1, C_1', and C_3', may be varied to increase the deflection are obvious and need not be further considered.

If V_A' becomes negative to V_A the greatest voltage which may be measured is $K(V_B - V_B') = 11.5 \times 1{,}400 = 16{,}100$. Thus, if the absolute value of V_A is not greater than 10,000 volts, V_A' may have any absolute value not exceeding 6,100 volts. Since the arrangement is symmetrical the absolute potential V_A' may be 10,000 volts if the absolute potential of V_A does not exceed 6,100 volts.

Circuit 2. V_A large, $V_A' = 0$.—If computations for circuit 1 are made for $V_A = 10{,}000$ volts and $V_A' = 0$, instead of 6,000 volts, the maximum

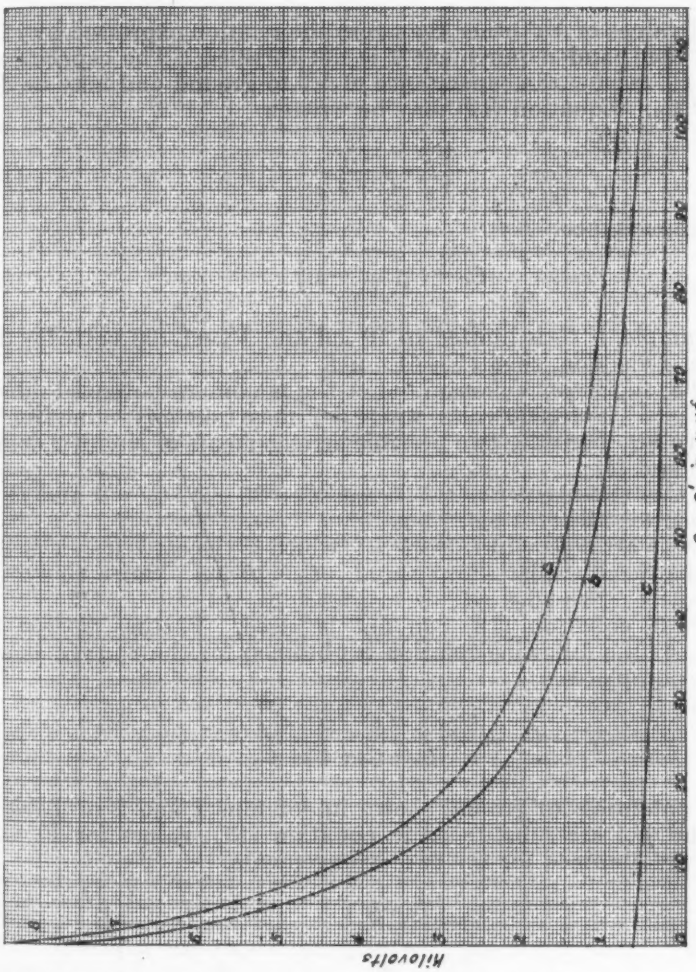

FIGURE 4

potential difference across the deflection plates is 870. With the data given C_2 may be determined from equation (9). Curves (*c*) and (*d*) are shown in Figure 3 with $V_A' = 0$, so that a comparison may be made with curves (*a*) and (*b*) which were calculated with $V_A = 6{,}000$ volts. If C_2, C_2' and $C_3 + C_3'$ are given their smallest capacitance, 25 $\mu\mu$f each, and C_1, C_1', their largest capacitance, 10 $\mu\mu$f each, the greatest potential difference $V_B - V_B'$ is $\frac{10{,}000}{10.25} = 975$ volts. In order to

get a greater deflection it is customary to make $C_1' = \infty$. Equation (3) becomes

$$V_A - V_A' = V_B\left[1 + (C_3 + C_3')\left(\frac{1}{C_1}\right) + \frac{C_2}{C_1}\right] - V_B'\left[1 + (C_3 + C_3')\left(\frac{1}{C_1}\right)\right] \quad (11)$$

and since $V_B' = V_A' = 0$

$$\frac{V_B}{V_A} = \frac{C_1}{C_1 + C_2 + C_3 + C_3'} \quad (12)$$

For all values of V_B' other than zero the relation expressed by (12) does not hold, and requirement 2 is not satisfied. The capacitance $C_2 + C_3 + C_3'$ is now the capacitance of V_B to ground and may be denoted by C_G. Equation (12) may be written

$$\frac{V_B}{V_A} = \frac{C_1}{C_1 + C_G} \quad (13)$$

and the capacitance

$$C_G = C_1\left(\frac{V_A}{V_B} - 1\right) \quad (14)$$

For example, if C_1 is limited to 10 $\mu\mu$f and $V_B = 1{,}400$ volts for the maximum deflection, then $C_G = 61.4$ $\mu\mu$f.

Circuit 3. V_A large, V_A' small.—Let the maximum potential difference of $V_A - V_A' = 10{,}000$ volts, where V_A' may take any value from 0 to 1,000 volts. Consider two possible arrangements of circuit 2 designated (*a*) and (*b*):

(*a*) In this arrangement $C_1 = 10$ $\mu\mu$f, $C_3 = 25$ $\mu\mu$f, $C_3' = 0$ and $C_2 = C_G - C_3 = 61.4 - 25 = 36.4$ $\mu\mu$f.

(*b*) In this arrangement $C_2 = 25$ $\mu\mu$f, which is the capacitance of the leads and capacitor plates to ground. $C_1 = 10$ $\mu\mu$f. Since $C_G = 61.4$, $C_3 + C_3' = 61.4 - 25 = 36.4$ $\mu\mu$f.

If $V_A' \pm 0$, equation (12) can not be used. Putting $C_1' = \infty$ in equation (4) the following relation is obtained for the voltage across the deflection plates.

$$V_B - V_B' = \frac{V_A C_1 - V_A'(C_1 + C_2)}{C_1 + C_2 + C_3 + C_3'} \quad (15)$$

If the potentials to ground shown in columns 1 and 2 of Table 1 for V_A and V_A' are substituted in equation (15), values for V_B and $V_B - V_B'$ are obtained for the two arrangements.

TABLE 1

V_A	$V_A' = V_B'$	(*a*)		(*b*)	
		V_B	$V_B - V_B'$	V_B	$V_B - V_B'$
10,000	0	1,400	1,400	1,400	1,400
10,200	200	1,490	1,290	1,530	1,330
10,400	400	1,590	1,190	1,660	1,260
10,600	600	1,690	1,090	1,790	1,190
10,800	800	1,790	990	1,920	1,120
11,000	1,000	1,890	890	2,050	1,050

These computations show that unless V_A' remains at ground potential the deflection is not proportional to the applied potential difference.

When the magneto is used as a source of voltage V_A' is usually small compared to V_A until the spark gap breaks down. If peak-voltage measurements are to be made the capacitance C_1' may be made large in which case C_2' is also increased so that $\frac{C_2}{C_1}=\frac{C_2'}{C_1'}$. Table 2 gives the values for V_B and V_B-V_B' using circuit 1 with the following capacitances.

(*c*) $C_1=C_1'=10$ $\mu\mu$f, $C_2=C_2'=44.3$ $\mu\mu$f, $C_3=25$ $\mu\mu$f and $C_3'=0$, which are the same values given in circuit 2.

(*d*) $C_1=10$ $\mu\mu$f, $C_1'=60$ $\mu\mu$f, $C_2=38.5$ $\mu\mu$f, $C_2'=231$ $\mu\mu$f, $C_3=25$ $\mu\mu$f, and $C_3'=0$.

TABLE 2

V_A	V_A'	(*c*)		(*d*)	
		V_B	V_B-V_B'	V_B	V_B-V_B'
10,000	0	1,400	960	1,400	1,290
11,000	1,000	1,580	960	1,600	1,290

In both (*c*) and (*d*) the deflection is proportional to the applied potential difference. At low frequencies, arrangement (*d*) is superior to arrangement (*c*). At high frequencies the large capacitance of C_1', C_2' to ground which is $\frac{C_1'\times C_2'}{C_1+C_2}$ will allow large currents to flow and the drop in the leads from A' to C_1' and C_1' to C_2' will affect the voltage across the deflection plates. At frequencies not greater than 10^3 kc this should not be serious when V_A' is small. This circuit can be used to advantage when it is uncertain as to whether or not V_A' remains at zero potential.

Circuit 4. V_A and V_A' both small.—When V_A and V_A' are both small, but V_A-V_A' exceeds 1,400 volts, the capacitances C_2 and C_2' are made as small as practicable by omitting the two capacitors C_2 and C_2'.

Substituting in equation (8) the limiting values previously mentioned $C_1=C_1'=10$ $\mu\mu$f, $C_2=C_2'=25$ $\mu\mu$f, and $C_3+C_3'=25$ $\mu\mu$f, $\frac{V_B-V_B'}{V_A-V_A'}=1/8$, which is the largest value $1/K$ may have with this arrangement under the conditions specified. If C_1 and C_1' are increased, $\frac{C_2}{C_1}$, $\frac{C_2'}{C_1'}$ and $(C_3+C_3')\left(\frac{1}{C_1}+\frac{1}{C_1'}\right)$ become less, and $1/K$ increases. Rogowski, Wolff, and Klemperer[1] have described this circuit for which the capacitances of C_1, (C_3+C_3'), and C_1' are much greater.

Circuit 5. Aperiodic voltage divider circuit.—If the voltage divider is used to measure spark discharges, oscillations may be expected in any circuit where $\frac{R^2}{4L^2}<\frac{1}{LC}$. Such oscillations were present and the cir-

[1] Rogowski, Wolff, and Klemperer: "Die Spannungsteilen Kathodenoszillographen," Archiv für Elektrotechnik, vol. 23, p. 579, 1929–30.

cuit was made aperiodic by inserting resistors at (a) and (a'), (fig. 1 or 2) so as to make $\frac{R^2}{4L^2} > \frac{1}{LC}$, where L is the inductance of the lead C_1C_3, and C the smaller of the two capacitances C_1 and C_3. In this manner requirement 4 is satisfied.

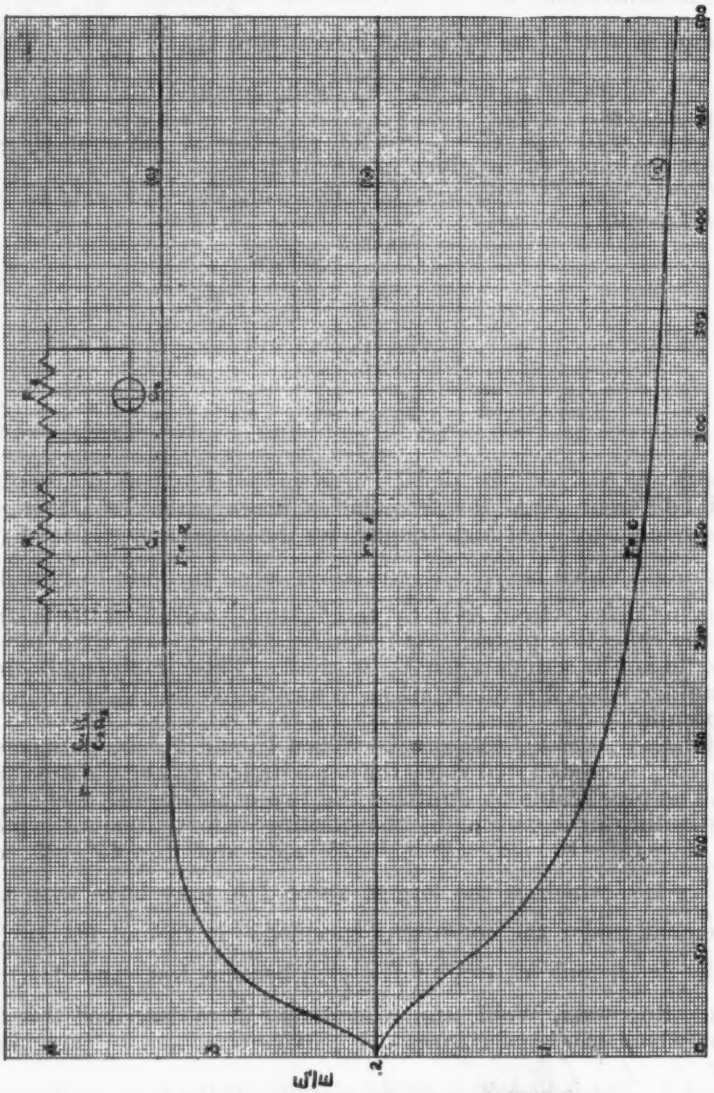

FIGURE 5.—*Relation of reduction ratio of resistance voltage divider to frequency of applied voltage*

2. RESISTANCE VOLTAGE DIVIDERS

The resistance voltage divider arrangement is shown in Figure 5. At low frequencies the impedance of the deflection plates is so high compared with that of the portion R_2 of the voltage divider that only a small part of the current is shunted to the plates, so that the ratio of the voltage to be measured to that across the deflection plates is

independent of frequency. The difference in phase between the two is also small. Computations which follow show that in order to keep the reduction ratio constant as the frequency is increased, resistance of the divider must be decreased, and at frequencies found in spark discharges a suitable resistance would be so low as to prevent a spark passing across the gap. If the resistance has a small capacitance and inductance the relation becomes more complicated. When grid leaks are used for resistance the inductance is small, whereas the capacitance across the grid leaks when supported in holders becomes important at high frequencies. Neglecting the inductance of the resistors and their capacitance to ground, an equation showing the relation between the voltage applied to the divider and the voltage across the deflection plates may be determined in terms of the resistance and capacitance of each portion of the voltage divider.

Let R_1 and R_2 designate the resistances of the resistors shown in the diagram of Figure 5, and let C_1 represent the capacitance of the resistor R_1, and C_2 the combined capacitance of the resistor R_2 and the oscillograph deflection plates. The impedance of each branch may be written

$$Z_1=\frac{R_1}{1+j\omega C_1R_1} \text{ and } Z_2=\frac{R_2}{1+j\omega C_2R_2}$$

where ω is 2π times the frequency η and $j=\sqrt{-1}$. The total impedance for the circuit is

$$Z=\frac{R_1}{1+j\omega C_1R_1}+\frac{R_2}{1+j\omega C_2R_2}$$

and since $E=IZ$, where E is the voltage across the divider and I the current, the relation becomes

$$\frac{E}{E_2}=\frac{\dfrac{R_1}{1+j\omega C_1R_1}+\dfrac{R_2}{1+j\omega C_2R_2}}{\dfrac{R_2}{1+j\omega C_2R_2}}$$

which reduces to

$$\frac{E_2}{E}=\frac{1}{\sqrt{\left[\dfrac{R_1\,(1+\omega^2C_1C_2R_1R_2)}{R_2\,(1+\omega C_1R_1{}^2)}+1\right]^2+\left[\dfrac{\omega R_1\,(C_2R_2-C_1R_1)}{R_2\,(1+\omega C_1R_1{}^2)}\right]^2}} \tag{16}$$

which expresses the relation between the voltage across the deflection plates and that applied to the voltage divider.

If the resistance has no capacitance $C_1=0$ and equation (16) reduces to

$$\frac{E_2}{E}=\frac{1}{\sqrt{\left[\dfrac{R_1}{R_2}+1\right]^2+[\omega C_2R_1]^2}} \tag{17}$$

If $C_1R_1=C_2R_2$, equation (16) becomes independent of frequency since it reduces to

$$\frac{E_2}{E}=\frac{1}{\dfrac{R_1}{R_2}+1}=\frac{R_2}{R_1+R_2} \tag{18}$$

These equations show that whether $\frac{E_2}{E}$ will increase, decrease, or not change with frequency depends upon the values of R_1, R_2, C_1 and C_2. Putting $r=\frac{C_1R_1}{C_2R_2}$, $R_1=8\times10^5$ ohms, $R_2=2\times10^5$ ohms, $C_2=20$ $\mu\mu f$, and assigning to C_1 the values of 0, 5, and 10 $\mu\mu f$ so that r takes the corresponding values of 0, 1, and 2 the curves shown in Figure 5 were obtained. In these curves (a) was plotted from equation (17), showing that the ratio decreases very rapidly with increase in frequency. As ω increases without limit $\frac{E_2}{E}$ approaches 0. Curve (b) is a plot of equation (18) which shows that the voltage divider is independent of frequency when $r=1$. Curve (c) is a plot of equation (16) and shows that the ratio $\frac{E_2}{E}$ increases with an increase in ω. As ω approaches ∞, $\frac{E_2}{E}$ approaches the limiting value $\frac{C_1}{C_1+C_2}$.

If the capacitance C_1 is assumed to be so small it may be neglected, computations from equation (17) show that in order that $\frac{E_2}{E}=0.2$ shall not diminish by more than 5 per cent (or not be less than 0.19), $\omega^2C^2R_1^2$ must not be greater than 2.56. Since $C_2=20\times10^{-12}f$ (which includes the leads as well as the deflection plates), $\omega^2R_1^2=2.56\times\frac{10^{22}}{4}$ $=6.4\times10^{21}$. If $\omega=10^7$ or $\eta=\frac{10^7}{2\pi}$, $R_1^2=\frac{6.4\times10^{21}}{10^{14}}=6.4\times10^7$. Therefore, $R_1=8{,}000$ ohms, $R_2=2{,}000$ ohms and $R_1+R_2=10{,}000$ ohms, which is the maximum resistance which may be used at a frequency of $\frac{10^7}{2\pi}$ or approximately 1,600 kc. Such a resistance across the gap would prevent sparking. Silsbee[2] has shown that a resistance of 5×10^4 ohms is so low as to seriously affect the character of the discharge and might actually prevent the occurrence of a spark. For high-compression engines such as are in use to-day the resistance must be much greater than this. Such low resistances are objectionable in this work because they affect the character of the spark. At times it may happen that fouling of plugs will reduce the resistance across a spark plug to 5×10^4 ohms, but this is a special condition, and while an interesting one, should not be a limiting condition of the problem.

The remainder of this report is devoted to an experimental study of the theory developed in this and the preceding sections, together with a discussion of oscillograph technique and the calibration of the voltage divider.

IV. DESCRIPTION OF APPARATUS

The cathode ray oscillograph was of the high-voltage cold-cathode type. The cathode was operated at approximately 60,000 volts, the supply being the secondary of a high tension transformer. The primary was connected through rotary switches to a 60-cycle 110-volt

[2] Silsbee, N. A. C. A. Report No. 241, Electrical Characteristics of Spark Generators for Automotive Ignition, p. 27.

supply, the switches being operated by a synchronous motor driven from the same source. The switches were constructed so that the 60,000 volts was applied to the cathode on the negative half cycle, either once in 20 cycles or once in 100 cycles. For the present investigation the slower rate of excitation was used.

The cathode tube (*ED*, fig. 6) was modified so that the cathode could be removed and polished. This was made possible by fusing the tungsten rod supporting the cathode to the movable portion of the ground joint as shown in the figure. The diaphragm *D* was mounted in the glass tube so that both the cathode and diaphragm moved together.

The deflection tube has two pairs of deflection plates, one pair horizontal and the other pair vertical. They are shown at *A* and *B* in Figure 6. *C* is a coil which produces a magnetic field deflecting the cathode beam in a horizontal direction. If observations are to be made at low frequencies the voltage is applied to plates *A*, producing a vertical deflection. If, at the same time, the cathode beam is swept across the field by the magnetic sweep *C*, a record is obtained which

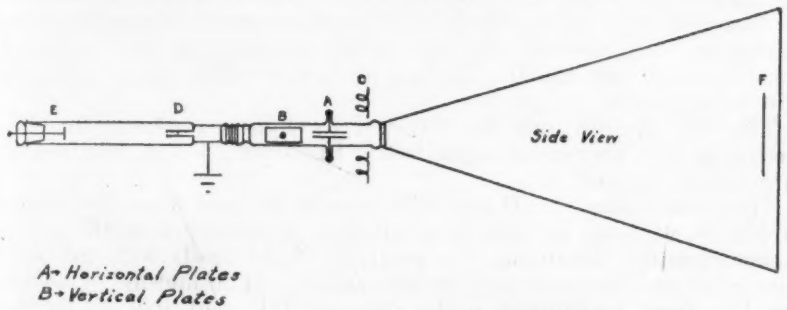

FIGURE 6.—*Diagram of cathode ray oscillograph*

shows the variation with time of the voltage across the deflection plates. An oscillator with a range of 20 to 1,000 kc was supplied with the oscillograph. If this oscillator is connected to plates *A* and the sweep actuated, a sine wave is obtained. For high frequencies the voltage to be measured is connected to plates *B*, and superimposes upon the sine wave a horizontal deflection proportional to the voltage across the plates. The sine wave then gives the time coordinate.

With 60,000 volts applied to the cathode the deflection of the beam at the photographic plate is approximately 1 cm for each 250 volts applied to the horizontal deflection plates. The maximum cathode beam deflection which can be photographed is 5.6 cm, thus limiting the useful voltage across the deflection plates to about 1,400.

The longest time required to sweep the beam across the photographic plate is 1,200 microseconds, and when necessary a faster sweep is used. If the spark discharge is to be photographed in the center of the film the magneto has to be timed accurately. This is accomplished by driving the magneto with the synchronous motor through a set of gears. Adjustment of the gears allows for approximate timing, and the final adjustment is made with the timing device on the magneto. The magneto is radio shielded and was designed for use with 12-cylinder aircraft engines.

Figure 7 is a photograph showing the arrangement of the five capacitors C_1, C_1', C_2, C_2', and C_3'. C_1 and C_1' are two high-voltage radio transmitting capacitors. The range of capacitance is from 10 to 80 $\mu\mu$f. C_2 and C_2' are two high-voltage radio transmitting capacitors having a range of capacitance from 40 to 300 $\mu\mu$f. Since the maximum voltage across C_2 and C_2' is 1,400, it is not necessary to use high-voltage capacitors. It is necessary to keep the leakage of the portion of the circuit called C_2 and C_2' in Section III small, and this requires that the capacitors in the circuit have a high insulation resistance. Since the high-voltage capacitors had a much higher insulation resistance than the low-voltage capacitors which were available, the former were used. C_3' was made by removing alternate plates from a low-voltage capacitor and supporting as shown in the photograph. The range of capacitance was 10 to 80 $\mu\mu$f.

To further reduce leakage the bakelite binding posts were removed and the lead wires brought to the oscillograph through 1-inch holes in the case. This at first seemed an unnecessary precaution, but it was found that the resistance of the binding posts to ground was much less than that of the remainder of the insulated circuit. In magneto discharges a small potential difference remains across the gap between discharges, and although the discharges alternate in sign, this additional leakage through the binding posts was sufficient to noticeably affect the results.

The five circuits may be obtained by simply removing or short circuiting the necessary capacitors. In circuit 5 the resistors are inserted at (a) and (a').

The leads shown at AD and $A'D'$ should be fixed when the voltage divider is adjusted so that they will not be disturbed while making measurements. Changing the position of the leads will unbalance the circuit and the results will be misleading. The method of balancing has been mentioned under Section III, and will be further discussed in Section V.

Figure 8 is a sketch of another arrangement used for circuit 3. The brass cylinder B was threaded and screwed to the binding post protruding through the bakelite bushing BH. This bushing passed through the case of the oscillograph. A is another brass cylinder larger than B, and the capacitance between A and B was changed by sliding the brass rod C through the bakelite bushing E. F was a grounded brass cylinder surrounding the capacitor. Leakage to ground through BH is objectionable for reasons previously given.

A better arrangement is to place the brass cylinder B, together with the other parts of the capacitor inside of the oscillograph case. The small leakage through the bakelite bushing will cause very little change in the spark discharge.

The resistance type of voltage divider was made of a number of resistances connected in series. The advantage of using a number of low resistances in series rather than a single high resistance is that a breakdown is less likely to occur and the capacitance of the unit is less, provided the same type is used for both the high and low resistance. However, this increases the capacitance to ground. This capacitance to ground may be reduced by suspending the resistors away from all metal by means of silk threads.

The spark gap used in most of the preliminary work consisted of two spheres in air. The spheres were 2 cm in diameter with a screw

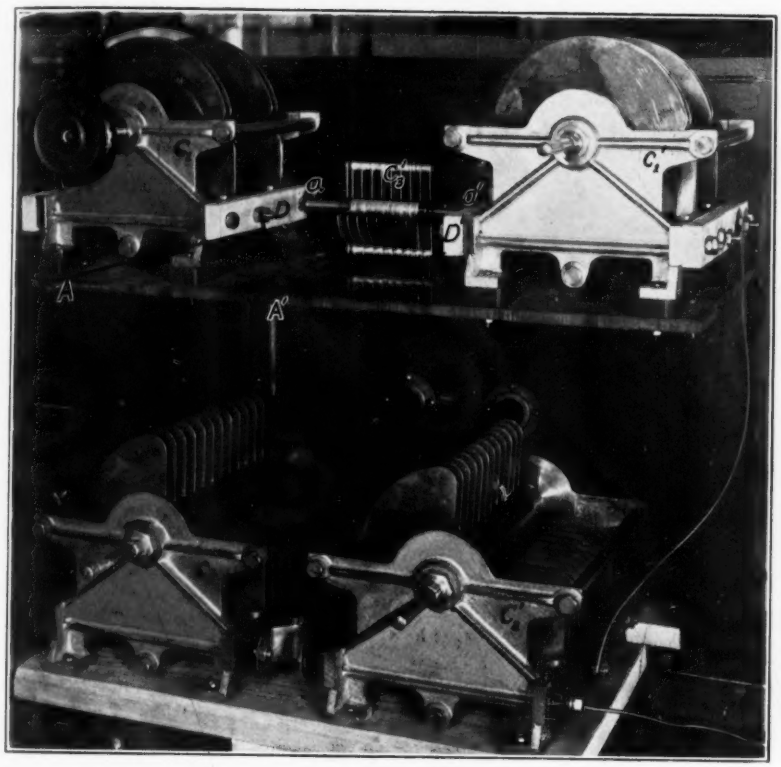

FIGURE 7.—*Arrangement of capacitors for voltage divider*

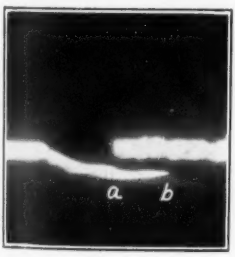

FIGURE 9

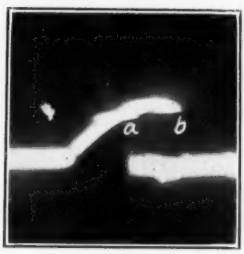

FIGURE 10

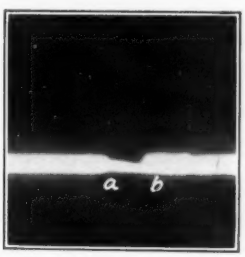

FIGURE 11

Oscillograms showing effect of unbalanced voltage divider.

FIGURE 13.—*Slope of traces shows the reduction ratio of circuit 4 is the same at 20 and 1,000 kc*

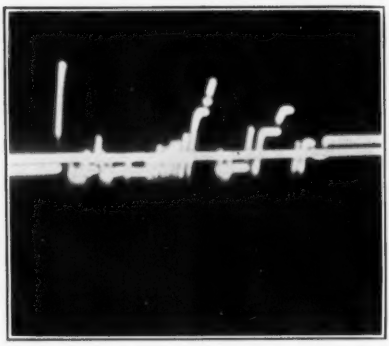

FIGURE 14.—*Magneto spark discharge in CO_2 at 75 pounds pressure (circuit 1)*

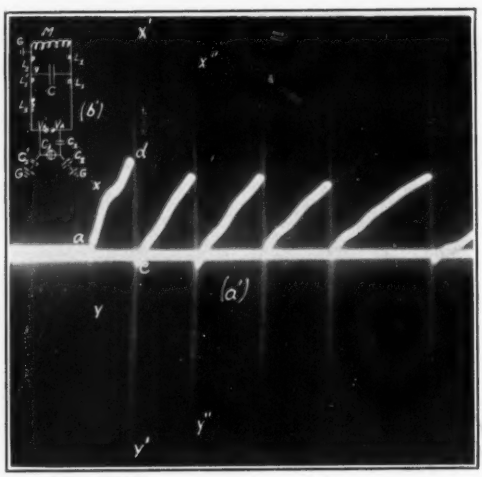

FIGURE 15.—*a', Magneto spark discharges in CO_2 at 15 pounds pressure; b', circuit arrangement used in obtaining oscillogram*

adjustment to change the gap opening. Later, measurements were made using an aviation spark plug in an atmosphere of CO_2 at pressures of 15, 75, and 135 lbs./in.^{2} (absolute). The spark plug was screwed into the end of a brass cylinder about 4 inches long and 2 inches in diameter which was provided with a quartz window for the purpose of observing the spark.

Measurements of the high voltages used in calibrating the oscillograph were made with an electrostatic voltmeter having a range of 0 to 10 kv. A kenotron with an upper range of 30,000 volts was placed in series with the spark gap and voltmeter to ground.

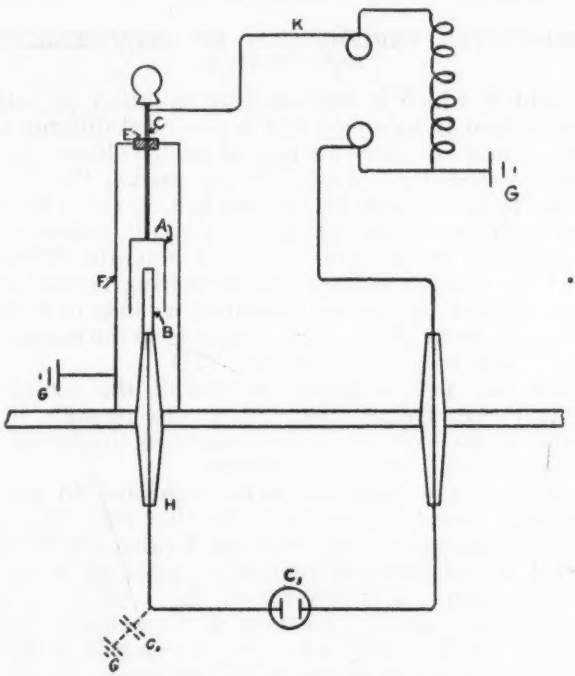

FIGURE 8.—*Arrangement for circuit 2*

V. EXPERIMENTAL RESULTS WITH CIRCUITS 1 TO 5

1. METHOD OF BALANCING VOLTAGE DIVIDER TO SATISFY EQUATION (5)

Before oscillograms showing the variation in voltage are taken it is necessary to balance the capacitance voltage divider as previously explained, so that the condition $\frac{C_2}{C_1}=\frac{C_2'}{C_1'}$ is satisfied. Since the method of balancing is the same for circuits 1, 3, 4, and 5 only one set of oscillograms showing the circuit unbalanced and balanced will be given.

With the two lead wires from the divider (fig. 1) connected to the insulated side of the sphere gap, and the horizontal deflection plates in use, the oscillogram shown in Figure 9 was obtained for circuit 4.

For correct adjustment of the position of the tube there would be no overlap of the beam as shown at (*a*, *b*). This adjustment will be discussed later.

Figure 10 is an oscillogram showing the apparent difference in potential between the two lead wires when C_1 is considerably greater than C_1'. Figure 11 shows the result when the condition $\frac{C_2}{C_1}=\frac{C_2'}{C_1'}$ is satisfied.

It will be understood that subsequent oscillograms pertaining to these four circuits were taken after the circuits had been balanced. It is not necessary to balance circuit 2.

2. EXPERIMENTAL VERIFICATION OF REQUIREMENT 2 AND EQUATION (6)

Requirement 2, which is expressed by equation (6), states that if the voltage divider is balanced and a potential difference is applied to the leads A and A' (fig. 1) a plot of peak voltage versus cathode beam deflection should give a straight line passing through the origin. This is shown to be the case for circuits 1, 3, 4, and 5 by the straight lines shown in Figure 12, at (*a*), (*b*), (*c*), and (*d*), respectively. These lines were obtained by applying a known potential difference to the terminals of the voltage divider and measuring the deflection. The voltage was supplied by the magneto over a range of 2,000 to 10,000 at a frequency of about 20 kc. The details as to the manner of making the calibration will be given in Section VIII.

Equipment was not available to extend the measurements of Figure 12 to higher frequencies, but it was possible to determine that the ratio of the voltages was constant in this range by the use of the oscillator. The procedure follows:

The leads from the oscillator were connected to the horizontal plates, to give a vertical deflection. Another pair of leads was connected from the oscillator to the voltage divider, the divided voltage being applied to the vertical deflection plates so as to produce a horizontal deflection. If the ratio of the applied voltage to the reduced voltage is constant, the trace of the cathode beam must be a straight line. If the ratio is to be independent of frequency the slope of the line must not change with frequency. In Figure 13 are shown two traces of the cathode beam. The straight line (*a*) was photographed at 20 kc. and (*b*) was photographed at 1,000 kc. As closely as measurements can be made these lines are parallel. These traces were photographed with circuit 4, but similar results were obtained for circuits 1, 3, and 5. Circuit 2 was not tested.

In each of these four circuits, C_1 and C_1' were selected so that the voltage divider did not materially change the characteristics of the circuit (requirement 1). Figures 12 and 13 show that the deflections of the cathode beam are proportional to the applied voltage and that this proportionally does not change with frequency (requirement 2). By proper selection of C_2 and C_2' the potentials of the deflection plates to ground were kept within the required limits (requirement 3). The absence of oscillations in the circuit (requirement 4) may best be determined by examining oscillograms of the spark discharge.

3. OSCILLOGRAMS SHOWING THE VARIATION OF VOLTAGE IN MAGNETO SPARK DISCHARGES

In Figure 12 straight lines were drawn showing the relation between $V_A - V_A'$ and the corresponding deflection of the cathode beam. These calibrations were made before the oscillograms shown in the

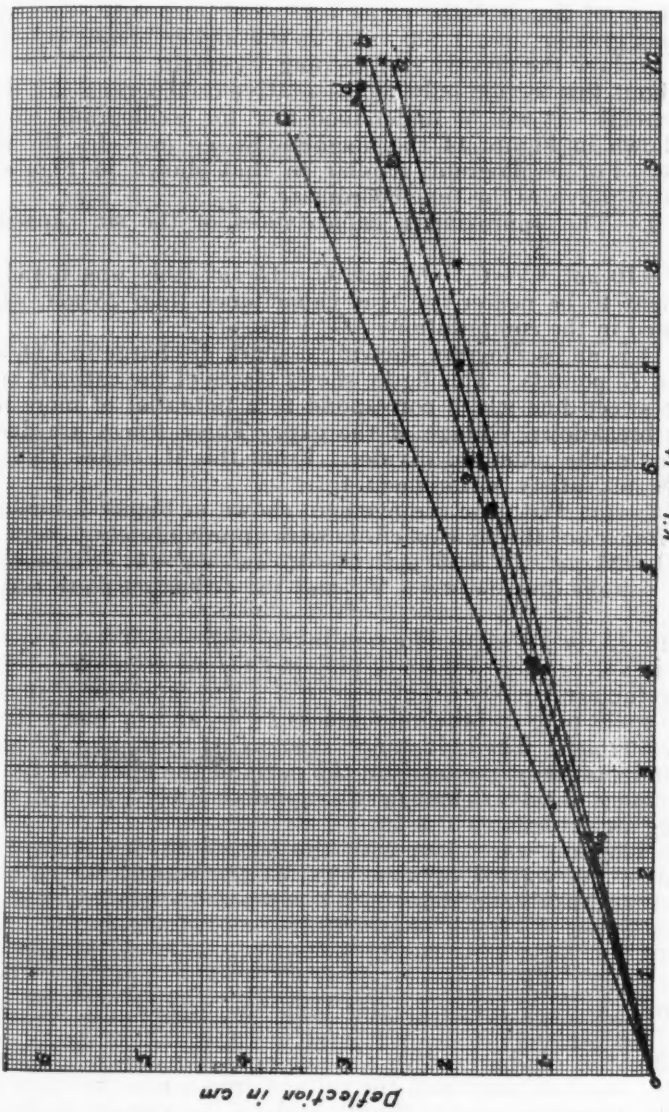

FIGURE 12
Straight lines show deflection is proportional to applied voltage when $\frac{C_2}{C_1}\frac{C_4'}{C_3'}$

remainder of this section were taken. For this reason values of K computed from Figure 12 may not agree with those which follow, since in the latter they were selected so as to give a large deflection when the spark discharge took place at a pressure of 135 pounds. With this setting of the capacitors, oscillograms were taken with

circuits 1, 3, 4, and 5, to show the variation of voltage across a spark plug in CO_2 gas during discharge. Pressures of 15, 75, and 135 pounds were used. All pressures are expressed in pounds per square inch absolute. The oscillograms for circuit 2 were taken with the spark plug in CO_2 gas at 15 pounds pressure as well as with a sphere gap in air at atmospheric pressure.

In the case of circuit 4 the capacitors were purposely selected so that V_B was greater than 1,400 volts at the higher pressures. This was done to show the necessity of keeping V_B small.

Throughout this section only representative oscillograms are given for each circuit. It will be understood that for oscillograms similar to that shown in Figure 14 the magnetic sweep provides the time coordinate. For oscillograms similar to that shown in Figure 17 the oscillator provides the time coordinate.

Circuit 1.—The approximate capacitances of the six capacitors follow:

$C_1 = C_1' = 10$ $\mu\mu$f, $C_2 = C_2' = 65$ $\mu\mu$f, $C_3 = 15$ $\mu\mu$f (this was found by measurement to be nearer the true capacitance than 25 $\mu\mu$f, which was assumed in the computations), $C_3' = 10$ $\mu\mu$f.

Figure 14 is an oscillogram showing a spark discharge in CO_2 at a pressure of 75 pounds. This figure shows traces of the cathode beam below the sweep line which correspond to a potential of more than twice the breakdown voltage of the gap. These traces are due to oscillations in the potential divider. From this it follows that circuit 1 does not satisfy requirement 4.

Circuit 2.—(*a*) With the arrangement shown in Figure 2, circuit 2, the capacitances of the six capacitors were approximately $C_1 = 10$ $\mu\mu$f, $C_1 = \infty$, $C_2 = 25$ $\mu\mu$f, $C_2' = 15$ $\mu\mu$f, $C_3 = 15$ $\mu\mu$f, $C_3' = 0$. Since C_2' is small the voltage drop between V_A' and the deflection plate may be neglected.

In Figure 15, (*a'*) is an oscillogram taken with circuit 2 to show the variation in voltage across a spark plug in CO_2 gas at 15 pounds pressure using the arrangement shown at (*b'*). The capacitor C shunted across the spark plug and the inductances L_1, L_3, and L_1' had a capacitance of 2,800 $\mu\mu$f. The inductances designated by L_1 and L_1' represent the inductance of the leads in the parts of the circuit indicated. The inductance of each L_1 and L_1' was approximately 1 μh. L_3 was a coil having an inductance of 3 μh.

This oscillogram was taken with the horizontal deflection plates connected to the voltage divider. At (*a*) the voltage began to increase and continued to increase until it reached (*d*), where a discharge took place across the spark plug. During the discharge the voltage drop across the spark plug should be small because the resistance of the gap is small. The fainter traces at (x', y') etc., indicate a voltage drop across the plug much greater than the breakdown voltage of the gap. An explanation of these large deflections follows.

If during the discharge $V_A - V_A'$ is small the traces shown by (x', y') etc., can not come from the voltage drop across the spark gap, and should, therefore, appear if both leads of the voltage divider are connected to the same side of the spark gap. Figure 16 (*b'*) shows diagrammatically the circuit arrangement used in obtaining the oscillogram shown in Figure 16 (*a'*). The traces (x', y') etc., are present, and while measurements show that they are slightly larger in Figure 15 (*a'*) than in Figure 16 (*a'*) this is to be expected because in the first

case V_A differs by a small amount from V_A' and in the second $V_A = V_A'$. That this is so becomes apparent from equation (15),

$$V_B - V_B' = \frac{V_A C_1 - V_A'(C_1 + C_2)}{C_1 + C_2 + C_3 + C_3'}$$

for if $V_A = V_A'$ the voltage $V_B - V_B'$ across the deflection plates will be greater or less than

$$\frac{V_A' C_2}{C_1 + C_2 + C_3 + C_3'}$$

which is the value resulting from equation (15) when $V_A = V_A'$.

An inspection of the circuit diagram shows that during the discharge of the capacitor C, the drop in $(L_1' + L_3)$ will make V_A' different from ground potential. V_A' has been measured and found to be 2,300 volts. Substituting this value of V_A' in equation (15) for the circuit arrangement shown in Figure 16 (b')

$$V_B - V_B' = \frac{-V_A' C_2}{C_1 + C_2 + C_3 + C_3'} = \frac{-2{,}300 \times 25}{50} = -1{,}150 \text{ volts.}$$

This corresponds to a deflection of $\frac{1{,}150}{250} = 4.6$ cm, which agrees with the measured value of 4.7 cm for (y'). The measured length of (x') is 4.5 cm.

The faint trace (x, y) is attributed to conditions arising from the breakdown of the gap in the distributor. Figure 15 (a') shows that when the gap breaks down the potential of the circuit increases so rapidly that the cathode beam leaves only a faint trace. This is shown by the separation at (a). This sudden application of voltage causes an appreciable difference of potential between ground and V_A'. The measured deflection of the cathode beam is 2.0 cm (fig. 16 (a')), which corresponds to a voltage across the deflection plates of $2.0 \times 250 = 500$. Substituting in equation (15), $500 = \frac{-V_A' \times 25}{500}$ or $V_A' = -1{,}000$ volts at the instant the distributor gap breaks down.

Figure 16 (a') shows that (a, d) is horizontal, and indicates that V_A' is zero before the spark gap breaks down. Equation (12) may then be used to compute $V_A - V_A'$ from Figure 15 (b').

Figure 17 is an oscillogram showing the traces (x', y') etc., spread out to show the nature of the oscillations. The oscillator operating at 20 kc was used to provide a time coordinate. The oscillogram was taken by connecting the deflection plates directly across a small portion of the lead L_1'. The average frequency obtained from measurements made on this and similar oscillograms was 1.1×10^3 kc. Neglecting the effect of the magneto the computed frequency of the circuit

$$(C,\ V_A,\ V_A',\ L_3,\ L_1) \text{ is } \eta = \frac{1}{2\pi\sqrt{C(L_1 + L_1' + L_3)}} = \frac{10^8}{6.28\sqrt{28 \times 5}}$$
$$= 1.25 \times 10^3 \text{ kc}$$

which agrees with the measured value since the inductors L_1, L_1',

and L_3 were only approximately determined. The maximum current in the circuit is

$$I=E\sqrt{\frac{C}{(L_1+L_1'+L_3)}}=3{,}000\sqrt{\frac{2{,}800\times10^{-12}}{5\times10^{-6}}}=71 \text{ amperes}$$

where E is taken as 3,000 volts, since it is the peak potential difference across the spark plug.

The drop in voltage between (g) and A_4' using the computed frequency (since the computed current was also used) is

$$V_4'-V_g=\omega LI=2\pi\times1.25\times10^6\times4\times10^{-6}\times71=2{,}230 \text{ volts}$$

which agrees with the measured value of 2,300 volts if (g) is assumed to be at ground potential.

It may be well to mention at this time that the portion of the circuit shown grounded, is the magneto. During the discharge of the capacitor the magneto base may not remain at ground potential although grounded to a water pipe with a copper strip. This departure from ground potential becomes more pronounced as the capacitance and inductance of the circuit are decreased. With circuit constants sufficiently small, so that $\eta=10^4$ kc, the maximum potential of the magneto to ground was found to be 750 volts. No measurements were made of the potential difference between the magneto base and ground, or between (g) and ground, with the circuit shown in Figures 15 (b') and 16 (b'). At this relatively low frequency, 1.25×10^3 kc, the drop in voltage between the magneto base and ground, or (g) and ground would be much less.

If better agreement were desired between the computed and measured values of V_4', the potential of (g) to ground would have to be determined and the result added to 2,230 volts.

(b) The capacitance of the arrangement shown in Figure 8 measured from A to B was approximately 20 $\mu\mu$f. The measurement included C_1 as well as the capacitance to ground which in this type of capacitor is relatively large as compared to C_1. Figure 18 is an oscillogram taken with the same circuit arrangement as shown in Figure 15 (b'), except a sphere gap was used instead of a spark plug. It will be noted that the deflections (x', y') are not vertical. This will be discussed later.

Circuit 3.—The approximate capacitances of the six capacitors used in circuit 3 are: $C_1=10$ $\mu\mu$f, $C_1'=70$ $\mu\mu$f, $C_2=25$ $\mu\mu$f, $C_2'=175$ $\mu\mu$f, $C_3=15$ $\mu\mu$f, and $C_3'=25$ $\mu\mu$f.

The oscillogram shown in Figure 19 represents a spark discharge in CO_2 at a pressure of 135 pounds. It shows very clearly just what is taking place between the secondary of the magneto, the gap in the distributor, the lead from the magneto distributor, and the spark plug.

The sweep line KL was taken with the four deflection plates grounded. The horizontal deflection plates were then connected to the voltage divider and the cathode beam swept across the photographic plate until it reached (a) where the contact in the primary circuit was broken.

After the contact was broken the series gap in the distributor of the magneto broke down, and this raised the potential difference across the gap to the voltage indicated at (b). This increase was so

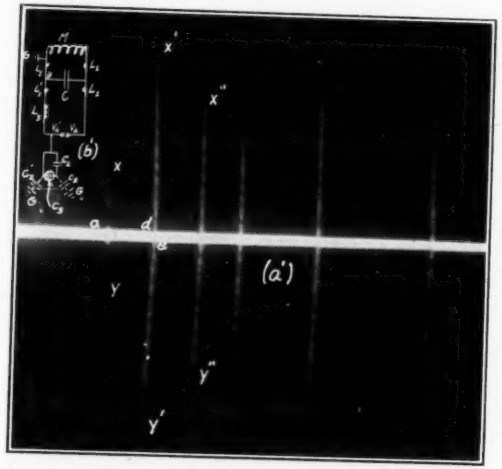

FIGURE 16.—*a', Magneto spark discharge in CO_2 at 15 pounds pressure; b', circuit arrangement used in obtaining oscillogram*

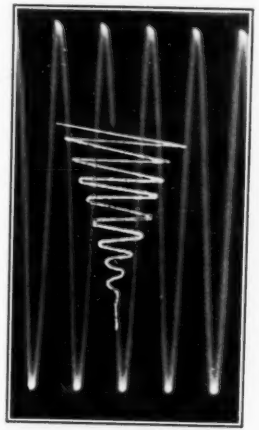

FIGURE 17.—*Waveform of the superimposed oscillations shown at xy, x'y', etc. (Figs. 15 and 16)*

FIGURE 18.—*Magneto circuit arrangement similar to that used in Figure 15 with sphere gap in air replacing spark plug in CO_2*

The sloping lines indicate improper adjustment of the cathode tube.

UNIV. OF CAL.

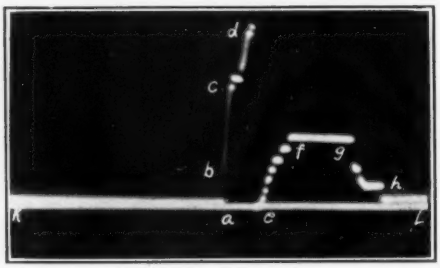

FIGURE 19.—*Magneto spark discharge in CO_2 at 135 pounds pressure (circuit 3)*

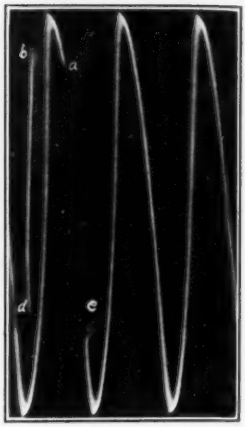

FIGURE 20.—*Magneto spark discharge in CO_2 at 15 pounds pressure (circuit 4)*

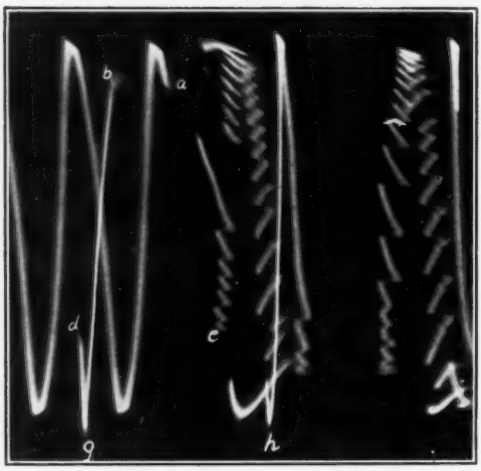

FIGURE 21.—*Magneto spark discharge in CO_2 at 75 pounds pressure (circuit 4)*

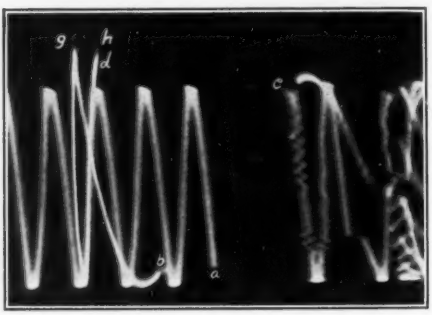

FIGURE 22.—*Magneto spark discharge in CO_2 at 135 pounds pressure (circuit 4)*

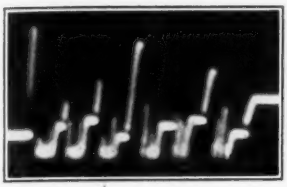

FIGURE 23.—*Magneto spark discharge in CO_2 at 75 pounds pressure (circuit 5)*

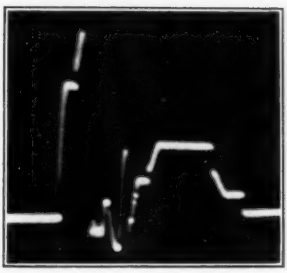

FIGURE 24.—*Magneto spark discharge in CO_2 at 135 pounds pressure (circuit 5)*

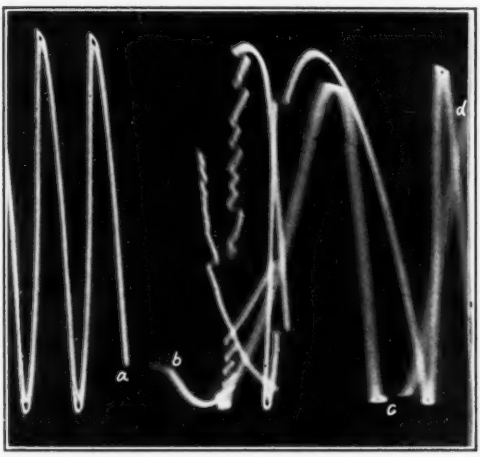

FIGURE 25.—*Magneto spark discharge in CO_2 at 135 pounds pressure (circuit 5)*

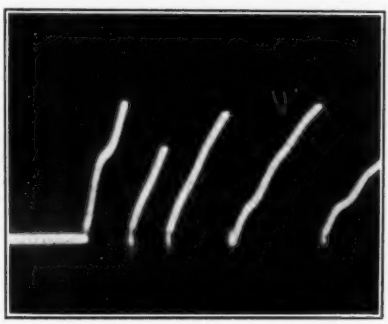

FIGURE 26.—*Magneto spark discharge in CO_2 at 15 pounds pressure (circuit 5)*

UNIV. OF MICH.

FIGURE 27

FIGURE 28

Change in reduction ratio and phase of applied voltage to the divided voltage using resistance voltage divider.

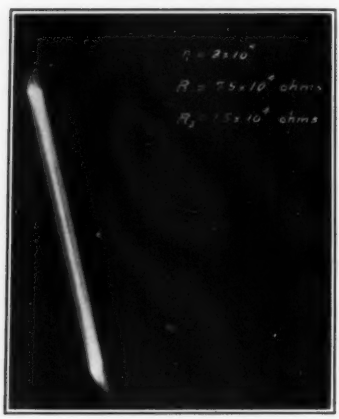

FIGURE 29

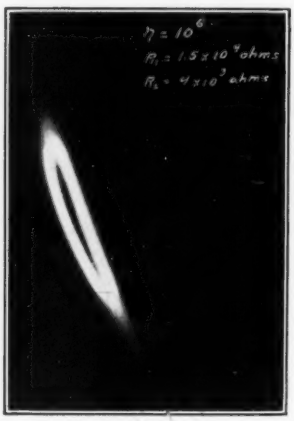

FIGURE 30

Change in reduction ratio and phase of applied voltage to the divided voltage using resistance voltage divider.

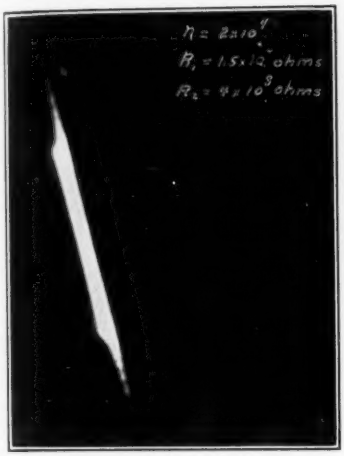

FIGURE 31

FIGURE 32

Change in reduction ratio and phase of applied voltage to the divided voltage using resistance voltage divider.

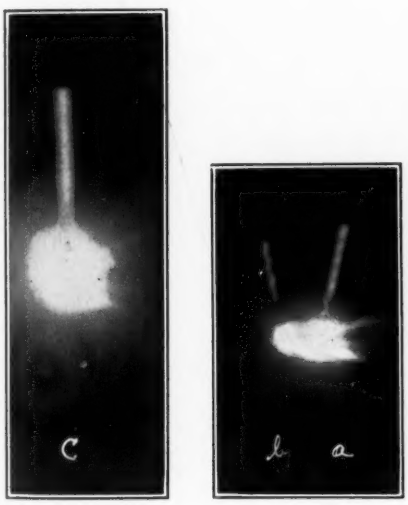

FIGURE 33

Deflections (*a*) and (*b*) show the effect of improper cathode tube alignment. The vertical deflection at (*c*) indicates a correct alignment.

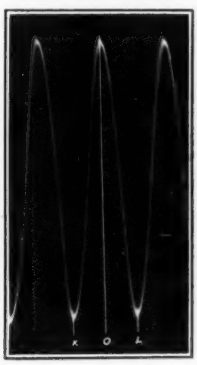

FIGURE 34.—*Symmetrical wave form resulting from proper cathode tube alignment*

UNIV OF MICH.

rapid that the cathode beam left no trace. The gap remained broken and the voltage increased to (*c*) when the series gap broke down, healed, and broke down again until the voltage across the gap was indicated by (*d*), where it healed again. The series gap again broke down and with this small increase in voltage the spark plug gap broke down. The voltage then dropped so rapidly that again the cathode beam did not leave a trace. At (*e*) there is an indication below the sweep line of a small voltage. The spark gap in the magneto broke, and a series of discharges took place across the gap until the voltage indicated at (*f*) was reached. The voltage in the magneto probably increased slightly, but not enough to break down the gap in the magneto. The voltage across the spark plug remained constant until finally the magneto voltage began to fall, and a discharge took place from the spark plug circuit to the magneto. This continued until (*h*) was reached where the potential difference between the magneto and the spark plug circuit was too small to further break down the gap and the potential at (*h*) remained on the spark plug. This voltage is also shown to exist across the spark gap when the sweep first appears on the left side of the oscillogram.

Circuit 3 shows no oscillation, so it satisfies requirement 4. It may be used where the large capacitances C_1' and C_2' are not objectionable.

Circuit 4.—The approximate capacitance of the six capacitors are $C_1 = C_1' = 20$ $\mu\mu$f, $C_2 = C_2' = 25$ $\mu\mu$f, $C_3 = 15$ $\mu\mu$f, $C_3' = 75$ $\mu\mu$f.

The capacitances of C_1 and C_1' were increased to 20 $\mu\mu$f to bring out the effect of increasing V_s and V_s'.

Figures 20, 21, and 22 are oscillograms representing spark discharges at pressures of 15, 75, and 135 pounds, respectively, in CO_2 gas. For these photographs the oscillator provided a time axis. The voltage to be measured was applied to the vertical plates. The photographs are lettered in the same manner as in Figure 19. These photographs show that oscillations are set up in the voltage divider and requirement 4 is not satisfied.

In Figure 21 the peak potential of V_s is approximtely 1,770 volts and in Figure 22 it is approximately 2,750 volts. The effect of this increased voltage is shown at (*g*) and (*h*). These traces indicate voltages on the deflection plates connected to the oscillator greater than the voltage of the oscillator. They are similar to those which appeared in Figures 9, 10, and 11 on the horizontal plates. These deflections are spurious, and are probably due to a potential field set up between the deflection plates *B* and their surroundings.

Circuit 5.—The approximate capacitances of the six capacitors used in circuit 5 were: $C_1 = C_1' = 10$ $\mu\mu$f, $C_2 = C_2' = 65$ $\mu\mu$f, $C_3 = 15$ $\mu\mu$f, $C_3' = 0$. Five hundred ohm resistors were inserted at (*a*) and (*a'*).

Figure 23 is an oscillogram showing the variation in voltage, the discharge taking place in CO_2 gas at 75 pounds pressure. The long faint traces which appear in Figure 14 are not present in this photograph. The faint traces appearing below the heavy traces are probably due to slow electrons, since similar faint traces may be found at maximum voltage of the oscillator. (See fig. 25.)

Figures 24 and 25 are oscillograms representing spark discharges at 135 pounds pressure. Faint traces due to oscillations in the voltage divider are absent in these photographs. Figure 26 is an oscillogram taken with circuit 5 under the same sparking conditions as the os-

cillogram shown in Figure 15 with circuit 2. The oscillations in the voltage divider which are pronounced with circuit 2 are not present with circuit 5. The faint traces appearing at peak voltage are due to the slow electrons in the cathode beam.

Figure 25 shows a progressive shortening of the oscillator amplitude as the voltage across the vertical deflection plates increases. This will be discussed in Section VII.

VI. EXPERIMENTAL RESULTS WITH RESISTANCE VOLTAGE DIVIDERS

It was shown theoretically in Section III that on account of the effective capacitance of resistors and their supports at high frequencies, the reduction ratio of a resistance divider, in general, changes with the frequency. Oscillograms to illustrate the change in reduction ratio as the frequency is varied are shown in Figures 27 to 32. The oscillator voltage was applied directly to the horizontal plates and the reduced voltage to the vertical plates. In each case the total resistance was R_1+R_2, and the vertical deflection plates were connected across R_2.

With R_1 consisting of two 500,000-ohm grid leaks in series and R_2 of two 150,000-ohm grid leaks in series, the oscillogram shown in Figure 27 was taken at 20 kc and that in Figure 28 at 850 kc. The reduction ratio measured from Figure 27 is 0.35 while from Figure 28 it is 0.47. The low frequency reduction ratio, $\frac{R_2}{R_1+R_2}$, is 0.23.

The oscillograms shown in Figures 29 and 30 were taken at 20 and 1,000 kc, respectively, with $R_1=15{,}000$ ohms (a 10,000-ohm and a 5,000-ohm grid leak in series) and $R_2=4{,}000$ ohms (two 2,000-ohm grid leaks in series). $\frac{R_2}{R_1+R_2}=0.21$. The reduction ratios measured from the oscillograms are 0.20 and 0.30, respectively.

The oscillograms shown in Figures 31 and 32 were taken with wire-wound resistors, with $R_1=75{,}000$ ohms (a single resistor) and $R_2=15{,}000$ ohms (a 10,000-ohm resistor in series with one of 5,000 ohms). $\frac{R_2}{R_1+R_2}=0.17$. The measured reduction ratios are 0.17 at 20 kc and 0.29 at 1,000 kc.

It is generally impossible to arrive at these reduction ratios by using equation (16), since neither C_1 nor C_2 are accurately known. Furthermore, equation (16) does not take into account capacitances to ground. It is sufficient for the purposes of this discussion to show on the theoretical side that the ratio $\frac{E_2}{E}$ may either increase or decrease with increase in frequency of the applied voltage and to show on the experimental side that this ratio does vary with the frequency.

VII. OSCILLOGRAPH TECHNIQUE

In connection with the study of voltage dividers, certain details in the technique of cathode-ray oscillograph operation were found to be important. Some of these are mentioned in the literature of the cathode-ray oscillograph, but because of their importance it seems desirable to consider them more in detail at this time.

1. ALIGNMENT OF THE CATHODE TUBE

The usual method of aligning the cathode tube is to place the bright spot in the center of the photographic plate. This means that the active spot on the electrode, the small opening or diaphragm through which the electrons enter the deflection tube and the center of the photographic plate are in a straight line. In the deflection tube the cathode beam must travel between two sets of deflection plates. When a voltage is applied to the plates an electrostatic field exists with respect to the surroundings. If the deflection plates and surroundings are symmetrical with respect to the cathode beam, the electrostatic field will have a kind of symmetry that will produce no deflection of the ray except that which is normal to, and caused by, the difference of potential between each pair of plates. If the field is not symmetrical, the voltage applied to each pair of deflection plates will produce a deflection made up of two components, one normal and one parallel to the plates.

If the two vertical deflection plates B and one horizontal plate A shown in Figure 6 are connected to ground and a voltage applied to the second horizontal plate shown at A, the deflection with the usual adjustment of the cathode tube will generally show a negligible horizontal component. If plates A are used with a voltage divider, such as circuit 4, the difference of potential between the plates may be small in comparison with the difference of the potential between the plates and ground. In this case, the horizontal component may be as great as, or greater than, the vertical component. This effect is shown in Figures 9 and 10, where the tip of the deflection is not vertically above or below the break in the sweep. Figure 11 shows a horizontal deflection although the indicated potential difference between the plates is zero. By swinging the cathode tube horizontally a position was found where the tip of the deflection did not extend more than 1 mm beyond the break in the sweep line. With circuit 4 it was impossible to eliminate this effect entirely when V_B and V_B' were large.

Another example of incorrect alignment of the cathode tube is shown in Figure 18. The lines (x', y') etc., may be made normal to the horizontal deflection plates by swinging the cathode tube horizontally. The traces (x', y') etc., in Figure 15 (a') shows the tube alignment greatly improved. To determine whether or not the cathode tube is correctly aligned for a particular set of conditions the following procedure may be used.

With the four deflection plates at ground potential and the sweep demagnetized the cathode tube is adjusted until the spot appears in the center of the fluorescent screen. The horizontal plates are connected to the voltage divider and the divider balanced as previously described, after which the leads to the divider are connected across the spark gap. If now a spark discharge takes place across the gap the electrostatic field between the deflection plates and the surroundings is that which will exist during the photographing of the discharge. By swinging the cathode tube horizontally, a position will be found where the deflection is vertical. In Figure 33, (a) and (b) show the tube out of alignment while (c) shows the tube aligned horizontally. The oscillograms were taken with circuit 4. A corresponding procedure is followed for the vertical alignment. It is well to check both alignments after the adjustments are completed.

Figure 34 was taken after alignment of the tube by this method. It will be noted that point (*O*) falls midway between (*K*) and (*L*). This method of alignment may not always be the most desirable, because if the horizontal plates are not parallel to the trace produced by the magnetic sweep, or the vertical plates not perpendicular to this trace, the adjustment will displace the cathode tube so that the bright spot is considerably displaced from the center of the photographic plate. For measuring potential differences a small slope is not objectionable unless it is desired to determine a relation between the rate of increase and decrease of the voltage. In most cases it is possible to correct for the small slope. When it is desired to determine the instantaneous relation between current and voltage, using one pair of plates to measure the voltage and the other pair to measure the potential difference across some reactance, the pattern photographed is usually so complicated that it is difficult to make corrections for both pairs of plates. It is this latter problem that led to the method given above for the adjustment of the cathode tube. In Figure 34 the bright spot is above and to the left of the center of the photographic plate.

2. SENSITIVITY OF THE CATHODE BEAM

It is well known that the sensitivity of the cathode beam to either an electrostatic or an electromagnetic field changes with the cathode voltage. The maximum voltage which may be applied to the cathode before a discharge takes place is limited by the pressure and composition of the gases in the cathode tube. Indirectly, then, the sensitivity of the cathode beam depends upon the pressure and composition of gases. In measuring voltages it is therefore necessary to know that the electrostatic sensitivity at the time of photographing the phenomena is the same as at the time of calibration, or else to have available a ready means of determining the sensitivity.

Measurements made with a hot-wire pressure gauge can not be relied upon to determine sensitivity if the photographic film has not been thoroughly out gassed. Unless this out gassing is carried out in a separate container before the film is placed in the oscillograph a great deal of time is lost. The procedure generally followed until this portion of the work was undertaken was for the observer to reduce the pressure until the sweep line appeared dotted and then allow the pressure to increase until the line appeared solid. At this time the photographs were taken. Working in this manner with a film which had not been out gassed the sweep first appeared dotted with a gauge reading of 54 on film 1 and a few minutes later the sweep first appeared dotted with a gauge reading of 42 on film 6. In common with other investigators the practice was adopted of photographing the sweep with a known voltage across the horizontal plates immediately after photographing the phenomena, and using this line as a measure of sensitivity.

This same idea was used to indicate visually the sensitivity before photographing. The deflection plates, oscillator, and a source of known voltage were connected to a double-pole double-throw switch so that either the oscillator or known voltage could be applied to the deflection plates. About 1 centimeter below the top of the fluorescent screen a narrow line was drawn with willemite. When a vacuum was obtained which gave a good solid sweep the known voltage was

adjusted until the sweep passed through the willemite line. This line appeared green against a bluish background.

To control the sensitivity it is only necessary to apply this voltage to the deflection plates and adjust the vacuum until the sweep passes

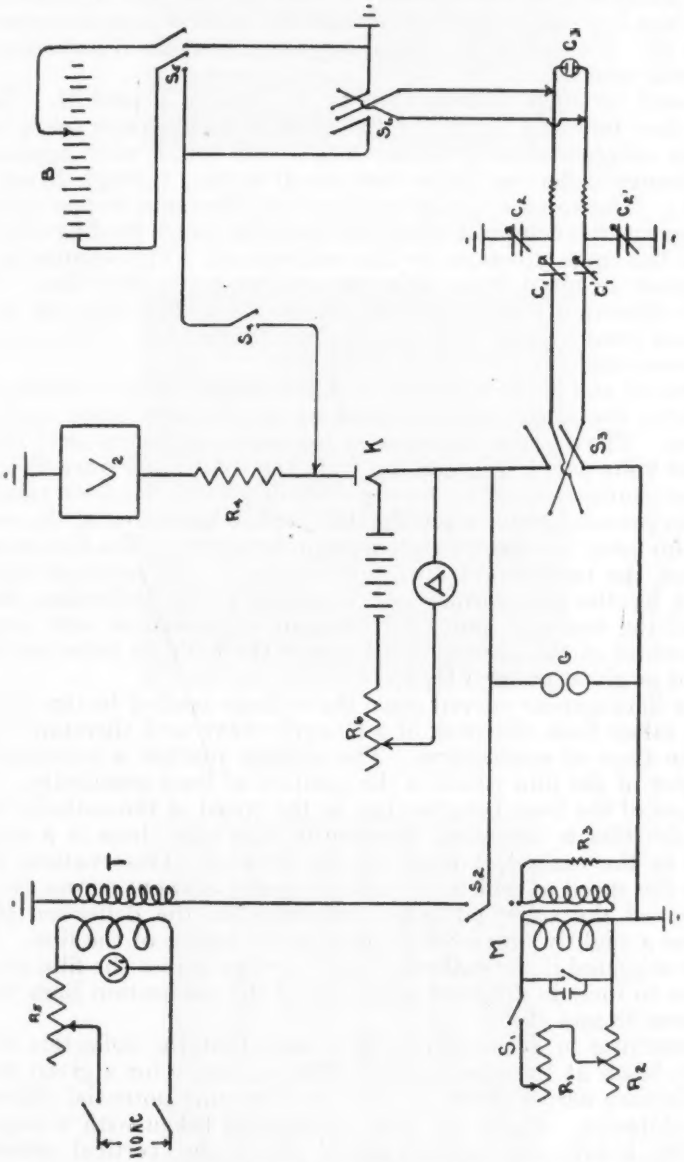

FIGURE 35.—*Circuit diagram for calibration and sensitivity measurements*

through the willemite line. The voltage was supplied by a small transformer T and rectified by the kenotron K as shown in Figure 35. The double-throw switch S_2 was arranged so that the transformer or magneto could be connected to the kenotron. V_1 is an alternating current voltmeter used to indicate the voltage drop across the primary

of the transformer. By changing the resistance R_5 to compensate for changes in the 110-volt supply a constant voltage was supplied to the primary. It was assumed this maintained a constant secondary voltage. The voltmeter V_2 was not sensitive enough for this work, since it was graduated in kilovolts. With S_5 open and S_4 closed, the voltage was applied to the deflection plates, and its polarity reversed, through S_6. Unless the line voltage is constant radio B batteries will give better results.

The need for such control is shown by Figures 36 and 37. These figures show only the left and right halves of oscillograms taken with potential differences of 0, ±218, ±437, and ±692 volts applied to the horizontal deflection plates from the B battery through S_5 and S_6. (Fig. 35.) The hot-wire gauge readings were the same, but on account of changes in the composition of the gases the gauge readings did not indicate the same pressures in the oscillograph. This change in gas composition resulted from different out-gassing of the films. The average deflection computed from Figure 36 is 275 volts per centimeter and from Figure 37 is 215 volts per centimeter. The measurements were made at the center of the film.

Figures 38 and 39 show the left and right halves of two oscillograms taken after the sensitivity indicated by the cathode beam appeared the same. The average deflection computed from the center of Figure 38 is 250 volts per centimeter and from the center of Figure 39 is 255 volts per centimeter. The average rounded value has been taken as 250 volts per centimeter when the deflection is measured at the center of the film using the slowest electromagnetic sweep. The two extreme traces on the oscillogram are photographs of the constant voltage supplied by the transformer and kenotron to the deflection plates. None of the constant potential lines are symmetrical with respect to the center of the photograph because the cathode tube had been adjusted as given under VII, 1.

These lines appear curved since the voltage applied to the cathode tube is taken from the peak of a 60-cycle wave and therefore varies with the time of application. The voltage reaches a maximum at the center of the film which is the position of least sensitivity. The curvature of the lines becomes less as the speed of the cathode beam across the film is increased, because in this case there is a smaller change in the cathode voltage in the interval. Observations show that as the speed at which the cathode beam is swept across the film is increased the same potential difference on the deflection plates produces a slightly greater deflection at the center of the film. This is to be expected if the cathode beam is swept across the film at such times as to include different segments of the calibration lines shown in Figures 38 and 39.

By referring to Figure 6 it will be seen that the deflection of the cathode beam at the photographic film is greater for a given potential difference across plates B than for the same potential difference across plates A. Figure 40 is an oscillogram taken with voltages of 0, ±218, ±437, and ±692 applied across the vertical deflection plates. The vertical deflection was obtained by applying the oscillator voltage to the horizontal deflection plates. The alignment of the cathode tube was the same as for Figures 38 and 39. Measurements made between the sharp edges starting from the far central ruled lines gave an average deflection of 195 volts per centimeter.

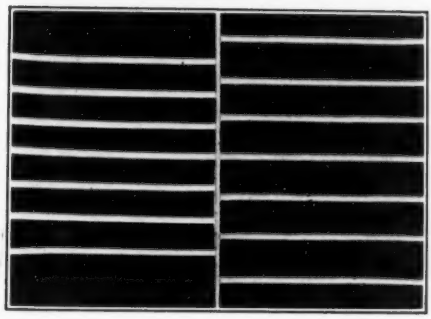

FIGURE 36 FIGURE 37

Two sets of calibration lines with sensitivity matched with thermocouple pressure gauge.

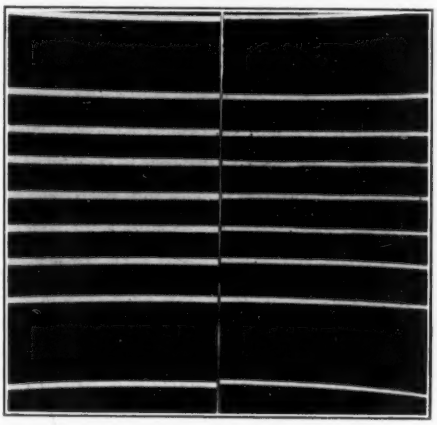

FIGURE 38 FIGURE 39

Two sets of calibration lines with sensitivity matched with known voltage and willemite mark.

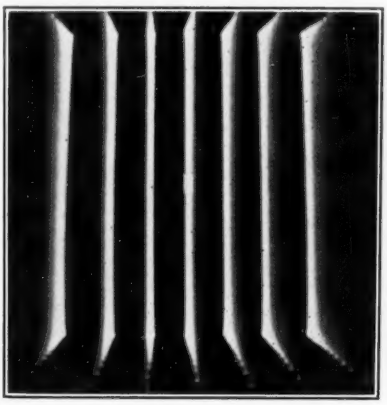

FIGURE 40.—*Calibration lines using vertical plates*

UNIV OF MICH.

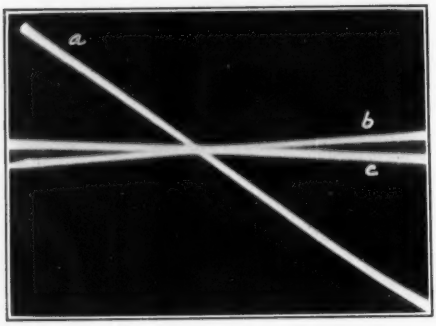

FIGURE 41

Line *a* indicates the ratio of the sensitivity between the horizontal and vertical deflecting plates.

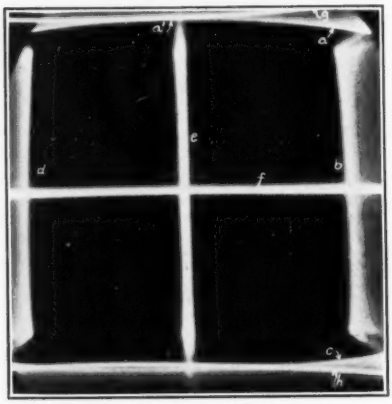

FIGURE 42.—*Effect of nonuniform electrostatic fields*

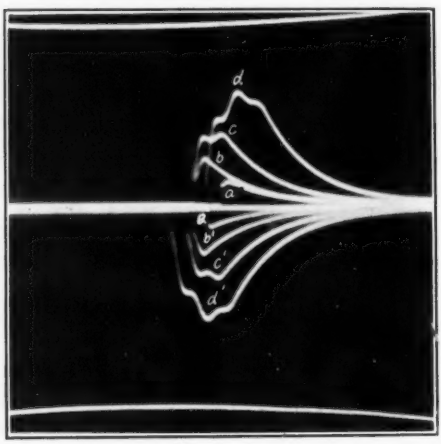

FIGURE 43.—*Magneto impulses used for the calibration of voltage dividers*

A 1-megohm resistor was shunted across the magneto terminals.

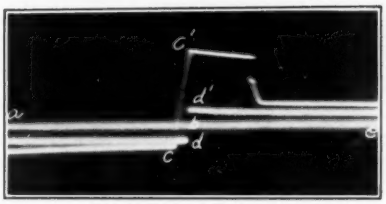

FIGURE 44.—*Magneto impulses used for calibration of voltage divider without resistor shunted across magneto terminals*

FIGURE 46.—*Oscillogram used for determining the reduction ratio of voltage divider using oscillator*

UNIV OF

At the time this calibration was made precautions had not been taken to control the sensitivity of the cathode beam.

A second method of determining the sensitivity of the vertical deflection plates is to determine the ratio of the sensitivity of the two pairs of deflection plates and multiply the sensitivity of the horizontal deflection plates by this ratio. If s_1 be the sensitivity of the cathode beam to plates A (volts/cm) and s_2 that to plates B, then the ratio $v=\frac{s_1}{s_2}$ must be constant. This ratio is independent of the voltage applied to the cathode tube as well as the composition and pressure of the gases in the oscillograph. This ratio is conveniently found by applying the oscillator voltage directly to both pairs of plates. The slope of the resulting line, shown at (a) in Figure 41, is the ratio v, which is thus found to have the constant value 1.39 for this deflection tube. Only the straight portion of this line near the center was used because as will be shown presently a small distortion may take place with large deflections of the cathode beam. Thus if s_1 is known, s_2 is found from $s_2=\frac{s_1}{v}$. For $s_1=250$ volts per centimeter, $s_2=180$ volts per centimeter.

To explain the slight curvature at the extremities of line (a) in Figure 41 as well as the progressive shortening of the oscillator amplitude in Figure 25 it is necessary to consider the space variation of electrostatic field intensity transversely across the field between the deflection plates. This variation is indicated in Figure 42. The traces (g) and (h) were obtained in the same manner as the two extreme calibration traces shown in Figures 38 and 39. The trace (a) was obtained by applying a constant voltage across the horizontal plates (fig. 6) and the oscillator voltage across the vertical plates. Between the vertical plates the cathode beam oscillated in a horizontal central plane at a frequency of 20 kc. The constant voltage deflected the oscillating cathode beam toward one of the horizontal deflection plates, depending upon the polarity. If the field traversed by the cathode beam is uniform the trace on the photographic film will be parallel to the plates, and if not, it will travel along a path showing the variation in field intensity. The inner edge of (a) was recorded at maximum cathode voltage, which may be considered constant in this very short interval of 2.5×10^{-5} seconds. The lighter portion above this dark line is the record of many oscillations at lower cathode voltage. The trace (c) was obtained by reversing the polarity of the constant voltage. Trace (f) was obtained in a similar manner after grounding the horizontal deflection plates.

The traces (b) and (d) were obtained by applying the constant voltage across the vertical deflection plates and the oscillating voltage across the horizontal plates. The cathode beam is first deflected to the right or left by the vertical plates, depending on the polarity of the applied voltage. The cathode beam, deflected away from the central axis horizontally, then enters the oscillating field of the horizontal plates, and oscillates at a frequency of 20 kc. With the constant voltage deflecting the beam to the right the trace (b) was photographed, and with voltage reversed, (d) was photographed. Trace (e) was taken in a similar manner with the vertical plates grounded. The most intense portion, of the traces, which are the inner edges of (b) and (d), were recorded at maximum cathode voltage.

If it is assumed that the maximum oscillator voltage remains constant during the photographing of (*b*), (*e*), and (*d*), as well as the sensitivity as determined by the pressure and gas composition, lines joining the ends should show the change in sensitivity with transverse distance from the center of the horizontal plates. These lines would be parallel to (*a*) and (*c*), respectively. They would be difficult to draw because the slow electrons striking the middle of the photograhpic film fall in the same vertical plane as the fast electrons, whereas at (*b*) and (*d*) they are deflected to the side.

The curvature of lines (*a*), (*b*), (*c*), and (*d*) can be attributed to the existence of potential fields whose intensities are not uniform throughout.

It has been shown that an oscillogram taken with the oscillator voltage deflecting the cathode beam vertically and the slow magnetic sweep deflecting it horizontally, with the vertical plates grounded, would show a variation of oscillator amplitude depicted by the lines (*g*) and (*h*) of Figure 42. The amount of this variation diminishes as the speed of the sweep is increased. If at the same time a voltage is applied to the vertical deflection plates, rapidly increasing to an amount sufficient to cause the horizontal deflection (*e*) to (*b*), the path of the beam between the horizontal plates is suddenly transferred from a field of maximum intensity (*a'*) to a field of less than maximum intensity (*a*). If now the combined action of the electrostatic field of the vertical plates and the electromagnetic field of the sweep has not caused the beam to be deflected entirely off the photographic film, the resulting oscillogram will show a change in the amplitude of the oscillation. This change in amplitude will depend upon the horizontal displacement of the cathode beam by the voltage across the vertical deflection plates as well as the instantaneous cathode voltage. These two effects may either counteract or reinforce each other. Effects of this kind are believed to be the cause of the progressive shortening of the amplitude of the oscillation at (*a*), (*b*), (*c*), and (*d*) shown in Figure 25. In order that the shortening in Figure 25 be explained quantitatively by Figure 42 it is necessary to assume that the cathode beam in the former is displaced more to the right than the displacement shown in the latter figure.

While it is possible to explain qualitatively, at least, the lengthening of (*g*) and (*h*) in Figures 21 and 22 in the same manner, it is believed that these spurious effects were caused by V_B and V_B' becoming large. This seems all the more reasonable since a lengthening appeared in Figure 11 with no potential difference between the deflection plates. It is also now apparent why the extremities of line (*a*) in Figure 41 are slightly curved.

It is not intended to discuss these effects in detail or make a study of the variation of voltage throughout the whole field, but peculiar effects were obtained and their interpretation was difficult until the oscillogram shown in Figure 42 was taken.

VIII. CALIBRATION OF THE CAPACITANCE VOLTAGE DIVIDER

If the capacitance of each capacitor and lead wire were accurately known, the quantity represented by K, which has been called the reduction factor of the voltage divider, could be calculated. If this

method is followed, care must be taken in measuring the capacitances of the six capacitors as well as the leads between the capacitors. The disadvantage of this method is that it requires a series of careful measurements with each change in the settings of the capacitors.

It is more feasible, therefore, to calibrate experimentally, and this may be done in two ways: (1) By applying a known alternating voltage across the divider and photographing the resulting cathode beam deflection, and (2) by determining the ratio between the cathode beam deflection when an alternating voltage is applied directly to one pair of plates and the reduced voltage to the other pair.

1. CALIBRATION BY APPLICATION OF KNOWN VOLTAGES

The leakage which takes place through the insulation of the capacitors prevents the use of a constant voltage for calibrating a capacitance voltage divider. A convenient source of alternating voltage is found in the magneto, since the polarities of consecutive impulses are of opposite sign. The circuit connections for calibrating are shown in Figure 35. The electrodes G were separated to prevent a spark discharge across the gap. The voltage induced in the secondary of the magneto M was controlled by shunting variable resistances R_1 and R_2 across the primary breaker contacts. This voltage was applied to the divider through switches S_2 and S_3, the latter switch controlling the polarity applied to the deflection plates. The kenotron K acted as a check valve and allowed the voltmeter V_2 to indicate the peak voltage. The magneto, which was synchronized with the oscillograph, generated 36 surges per second, 18 positive and 18 negative with respect to ground.

Figures 43 and 44 are oscillograms showing the application of this method with and without the resistor R_3 shunted across the secondary of the magneto. Voltage divider circuit 5 was used. In Figure 44 the peak voltages indicated by the voltmeter were 2,000 and 6,000, and are, respectively, represented by (bd') and (bc'), where (b) lies on the line of zero potential difference. The corresponding voltages of opposite polarity remaining from the previous surge are (db) and (cb).

The advantage of using the 1-megohm grid leak R_3 is shown by Figure 43. In this case the potential difference across the gap is quickly brought to zero. The surges were all of the same polarity with respect to the magneto, but their polarity with respect to the deflection plates was reversed on each voltage by switch S_3. (Fig. 35.) The peak voltages represented by (a) and (a'), (b) and (b'), (c) and (c'), and (d) and (d') are, respectively, $\pm 2{,}350$, $\pm 4{,}075$, $+5{,}900$ and $-6{,}075$, and $+9{,}600$ and $-9{,}750$. These deflections determine the lines (a) and (b) shown in Figure 45. Since no two surges are exactly alike and the voltmeter indicates the average of 18 surges per second, a variation between observations is to be expected. Before photographing the surges shown in Figure 43, the sensitivity was checked in the manner described in Section VII.

With a smaller reduction ratio the straight line (d) in Figure 45 was determined. The plotted points represent the average of six independent observations. They were taken to show that the reduction factor of circuit 5 is constant, and that the deviations of the

plotted points in Figure 12 become less as a greater number of observations are averaged. These deviations are caused by the magneto since the peak voltages of two sparks are not necessarily the same.

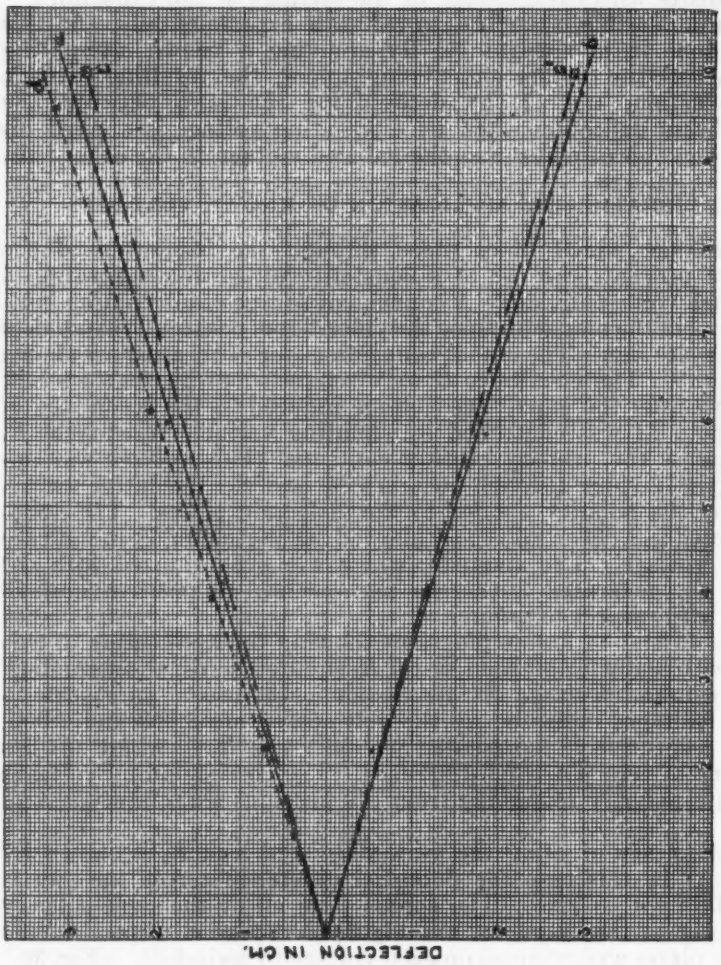

FIGURE 45

a and b are calibration lines for circuit 5 using known voltages. c and c' are calibration lines for circuit 5 using the oscillator. d is a calibration line similar to a and b, but with slightly increased reflection ratio.

2. CALIBRATION BY USE OF THE OSCILLATOR

A method for using the oscillator supplied with the oscillograph to determine the relative sensitivity of the two pairs of deflection plates has already been discussed. This method, which consists simply in applying the undivided oscillator voltage to one pair of plates and the divided voltage to the other pair, is also useful for calibration. The slope of the resulting line, of which Figures 13 and 46 are examples, determines the ratio

$$\frac{V_B - V_B'}{V_A - V_A'}$$

after the ratio of sensitivity between the two pairs of plates has been determined.

In Figure 46 the straight line (*a*) was obtained by applying the oscillator voltage directly to the vertical deflection plates and the divided voltage (using circuit 5) to the horizontal plates. The same capacitor settings were used as for Figure 43, the reversal of slope being obtained by reversing the leads to the voltage divider. The exposures shown at (*b*) and (*c*) in Figure 41 were made after making a small change in the capacitor settings. With the divided voltage applied to the horizontal plates, as in this instance, the reduction factor K is equal to $\frac{v\delta_2}{\delta_1}$, where δ_1 is the mean of two deflections measured along two vertical ruled lines, δ_2 is the total horizontal deflection measured between these lines, and $v=\frac{s_1}{s_2}$ = the ratio of sensitivity for plates A (horizontal) in volts per centimeter to that for plates B (vertical). The constant v is 1.39. Measurements made on Figure 46 gives $\delta_1=0.55$ cm and $\delta_2=10.75$ cm. Hence, $\frac{1}{K}=0.071$.

On account of the small slope produced, when K becomes greater than 15 or 20 the method just described may not be found practicable. In such cases it will be necessary to calibrate by the method of applying known voltages. But the convenience of using the auxiliary equipment supplied with the oscillograph makes the second method preferable when the reduction ratio is of such magnitude as to allow its use. It is then unnecessary to obtain a source of high alternating voltage or high-voltage measuring instruments. (The term "high voltage" is relative. The maximum voltage used in this investigation was 10,300.)

It is interesting to note that method (2) gives

$$\frac{1}{K}=\frac{V_B-V_B'}{V_A-V_A'}$$

absolutely, without regard to the sensitivity of the cathode beam.

To compare the results obtained by the two methods of calibration it is only necessary to substitute this value of K in the expression,

$$D=\frac{V}{Ks}$$

where D is the deflection in centimeters, V is an arbitrary applied voltage and s is sensitivity in volts per centimeter. Let $V=10{,}000$. From the previous sensitivity measurements (Sec. VII) it is known that

$$s_1=250 \text{ volts per centimeter}$$

and

$$s_2=180 \text{ volts per centimeter}$$

and for the same capacitor settings $\frac{1}{K}$ was found above to be 0.0712. Therefore

$$D_1=0.071\times\frac{10{,}000}{250}=2.85 \text{ cm for plates A}$$

and

$$D_2=0.071\times\frac{10{,}000}{180}=3.95 \text{ cm for plates B}$$

The deflection D_1 is indicated on Figure 45 by the lines (*c*) and (*c'*), and agrees closely with the calibration by the method of known potentials. If the leads had been reversed and another straight line obtained the average of the two would give a better value for r than was obtained from the single line (*a*) in Figure 41. This should lead to a better agreement between the two methods.

IX. CONCLUSION

The results of this investigation show that if it is desired to measure voltages in spark discharges whose peak voltages lie within the range found in the average automotive engine ignition system, voltage divider circuit 5 will probably be found satisfactory for use with a cathode ray oscillograph of the type described. However, it is well to call attention to the fact that some of the other circuits may be equally satisfactory for other types of measurements. The faint traces which were observed in oscillograms due to oscillations in the voltage divider circuit can probably be eliminated by inserting resistances as was done in circuit 5. One of the chief merits of the capacitance voltage divider is its adaptability to a wide range of conditions of voltage measurement.

Resistance voltage dividers are unsatisfactory for frequencies commonly found in spark discharges unless special care is taken to balance the capacitance and inductance of the resistance. In the development of the equation for resistance voltage dividers only the simplest assumptions were made as to capacitance, and the inductance of the resistors was completely neglected. This equation, therefore, represents only in a very rough way what actually occurs. The oscillograms obtained in testing the resistance divider are evidence in themselves of the unsuitability of this type of divider for high-frequency work.

In the literature of cathode ray oscillography there has been a disappointing lack of detail regarding the theory and technique of measurements. It is hoped that the details set forth in this paper will be of value to those who are using the instrument in work of a similar nature.

Another point that can hardly be overemphasized is the fact that in this work no phenomena have been recorded by the oscillograph that have not been susceptible of rational explanation. It has been the repeated experience of the authors that recorded phenomena which are most baffling when first observed on an oscillogram can usually be interpreted after careful study and experimental investigation.

X. ACKNOWLEDGMENTS

This work was supported by the Bureau of Aeronautics of the Navy Department and the National Advisory Committee for Aeronautics.

The authors wish to thank Doctors Mueller, Silsbee, and Brickwedde for their many helpful suggestions.

WASHINGTON, April 8, 1932.